Removal or Immobilization of Radionuclides and Trace-metals in Water, Soil and Poultry Litter Using Stabilized Nanoparticles

by

Wenbo Xie

A dissertation submitted to the Graduate Faculty of
Auburn University
in partial fulfillment of the
requirements for the Degree of
Doctor of Philosophy

Auburn, Alabama
August 1, 2015

Keywords: Fe-Mn, ZVI, Stabilized Nanoparticles,
Soil remediation, Metal contaminants

Approved by

Dongye Zhao, Huff Professor of Environmental Engineering (Major advisor)
Mark Barnett, Malcolm Pirnie Professor of Environmental Engineering
Clifford Lange, Associate Professor of Environmental Engineering
Virginia Davis, Alumni Professor of Chemical Engineering
Anne Gorden, Associate Professor of Chemistry and Biochemistry

Abstract

Two kinds of stabilized nanoparticles were synthesized and tested for the *in situ* immobilization of metals and radionuclides in soil and groundwater, namely Fe-Mn binary oxide nanoparticles for adsorptive immobilization and zero valent iron (ZVI) nanoparticles for reductive immobilization. A water-soluble starch or food-grade carboxymethyl cellulose (CMC) was used as a stabilizer to facilitate the *in situ* delivery of the particles into the contaminated soil. The Fe-Mn nanoparticles showed rapid sorption kinetics and high sorption capacities toward trace metals such as selenium, arsenic and phosphate. The Langmuir maximum capacity was determined to be 110 and 95 mg-Se/g-Fe, and 310 and 300 mg-P/g-Fe for starch- and CMC-stabilized nanoparticles, respectively, and this high uptake was observed over the typical groundwater pH range of 5-8. Column breakthrough tests indicated that both stabilized Fe-Mn and ZVI nanoparticles were deliverable in a model sandy soil while non-stabilized particles were not. When Se(IV)-spiked soil was treated *in situ* with the Fe-Mn nanoparticles, >92% water leachable Se(IV) was transferred to the nanoparticle phase and immobilized as the particles were retained in the downstream soil matrix. When applied to poultry litter (PL), the stabilized Fe-Mn nanoparticles reduced the water soluble P from 66% (for untreated PL) to 4.4% and peak soluble P concentration from 300 to <20 mg/L under simulated land application conditions, while at the same time reducing the water soluble As from 79% to 5%. By transferring the peak soluble P to nanoparticle-bound P, the Fe-Mn nanoparticles therefore not only greatly reduce the potential runoff loss of P from PL, but also provide a long-term slow-releasing nutrient source.

The ZVI nanoparticles converted soluble U(VI) to its immobile form U(IV) very effectively, thereby greatly reducing the mobility and bioavailability of the uranium. Batch experiments indicated that the U(VI) leachability of the contaminated soil was reduced by nearly 99% when a U(VI) spiked sandy soil (395 mg-U/kg-soil) was amended with the CMC-nZVI (0.1 g/L) at a soil-to-liquid ratio of 1 g/50 mL at pH 6.0. When subjected to remobilization tests, <1% of the immobilized U(IV) was released into the aqueous phase under anoxic conditions. There were no inhibition effects of the natural microbial activity on the U immobilization and CMC-nZVI also effectively reduced the bio-toxicity of U(VI). When the soil column was treated with 50 pore volumes of the nanoparticle suspension at pH 6.0, water soluble U was reduced by 93%. In all cases, the nanoparticle amendment reduced the leachability of the contaminant in soil. This technology holds the potential to fill a major technology gap in the remediation of metal-contaminated soil and groundwater.

Acknowledgments

I would never have been able to finish my dissertation without the guidance of my committee members, support from my family, and help from my friends.

In the first place, I would like to express my greatest gratitude to Dr. Dongye Zhao for his excellent guidance, caring, and patience. He has consistently provided me with an excellent atmosphere for doing research and his outstanding scientific intuition has made him a constant oasis of new ideas and passion for science, inspiring and enriching my growth as a student, a researcher and an engineer. I am indebted to him more than he knows.

I gratefully acknowledge the enlightened guidance from my committee members Drs. Mark Barnett, Clifford Lange, Virginia Davis and Anne Gorden for their encouraging words, thoughtful criticism, and the time and attention they have devoted to me in their busy schedules. I would also like to thank Dr. Michael Bozack, who help me to complete the XPS analysis.

I would like to thank Jinling Zhuang for providing analytical and mechanical assistance. It is also a pleasure to pay tribute to my fellow students in the environmental engineering program here at AU for their research advice and for creating a supportive environment. It would have been a lonely and uncreative lab without them.

Finally, I would like to thank my wife and parents for their support and encouragement throughout the last five years. I have experienced happiness, loneliness and sickness during the long march towards my Ph.D. and I could not have won through without my wife's companionship, sympathy and support.

Table of Contents

List of Tables

List of Figures

List of Abbreviations

As   Arsenic

CMC   Carboxymethyl Cellulose

CSC   Critical Stabilization Concentration

EPA   Environmental Protect Agency

FDA   Food and Drug Administration

Fe-Mn   Iron Manganese Oxides

FTIR   Fourier Transform Infrared Spectroscopy

MCL   Maximum Contaminant Level

NPDES   National Pollutant Discharge Elimination System

nZVI   Zero Valent Iron Nanoparticles

P   Phosphorus

PBET   Physiologically Based Extraction Test

PL   Poultry Litter

PRB   Permeable Reactive Barriers

PV   Pore Volume

Se   Selenium

TBN   Total Bacteria Number

TCLP   Toxicity Characteristic Leaching Procedure

TEM   Transmission Electron Microscope

U   Uranium

UNSC   United Nations Scientific Committee

USDA   U.S. Department of Agriculture

WET   Waste Extraction Test

XPS   X-ray Photoelectron Spectroscopy

ZVI   Zero Valent Iron

Chapter 1. General Introduction

1.1 Se and U contamination in soil and groundwater

Environmental contamination caused by metals and radionuclides such as selenium and uranium has been a serious problem worldwide for decades. This is a special concern because soil and groundwater contamination may lead to long term harmful effects on human health, either directly through water intake or indirectly by contaminating growing plants and animals. This contamination is primarily caused by human activities such as mining, chemical industries, fuel manufacturing, and nuclear weapon tests (in the case of radioactive elements such as U), among others (Szlachta et al., 2012; Torres et al., 2010).

Selenium has been detected in a wide range of soils and groundwater sources. The worldwide average Se content in non-seleniferous soil is about 0.4 mg/kg, with a range of 0.2-5 mg/kg, but in seleniferous soil the Se range can vary from 1 to 80 mg/kg and levels as high as 1200 mg/kg have been observed (Haudin et al., 2007; Mclean and Bledsoe, 1992). In the U.S., Se levels of 0.1-5.3 mg/kg have been reported (USGS, 2008). While Se is an essential trace nutrient for both humans and animals, the intake of excessive Se can lead to adverse health effects such as gastrointestinal disorders, hair and nail loss, irritability and fatigue, and in extreme cases may result in liver cirrhosis and pulmonary edema (Hamilton, 2004). Bioaccumulation of Se in the food chain has been associated with fish kills, bird deformities, and the loss of aquatic resources (Hamilton, 2004; Loyo et al., 2008; Spallholz and Hoffman, 2002). Harmful effects on fish and wildlife have been reported when exposed to levels as low as 2 to 4 μg/L Se in water and 4 μg/g in soil (Rowland et al., 2003). Interestingly, the window between Se deficiency and toxic effects is very narrow; a

daily consumption of <0.1 mg Se/kg of body weight leads to Se deficiency, but an intake of >1 mg has toxic effects (Gonzalez et al., 2012). To mitigate the adverse impact of human exposure, the U.S. EPA (Environmental Protect Agency) has set a MCL of 0.05 mg/L for total Se in drinking water (USEPA, 2009). To our knowledge, there has been no similar regulatory limit defined for Se in soil, though the EPA has set a TCLP (Toxicity Characteristic Leaching Procedure) limit of 1 mg/L for Se in solid wastes.

Uranium (U^{238}) is a common radioactive element in nature that is often found at low levels in soil and rock formations worldwide. In the U.S., at least 7 states have an average U concentration above 3 mg/L equivalent uranium (Duval et al., 2005). Various anthropogenic activities can cause uranium contamination of soil and groundwater, including mining and refining nuclear materials, nuclear fuel manufacturing, nuclear weapon tests or nuclear power plant accidents, and radioactive waste disposal (Choy et al., 2006; Gavrilescu et al., 2009). In 2013, the world's total uranium production of U_3O_8 was 70,015 tonnes, 64% of which was contributed by Kazakhstan, Canada and Australia (WNA, 2014). In the U.S., the total uranium concentrate production from mines was 1792 tonnes in 2013 and 1888 tonnes in 2014, mainly produced in Utah, Wyoming, Texas and Nebraska (USEIA, 2014). The average concentration of uranium in U.S. groundwater is ~3 µg/L (i.e., 2 pCi/L), and the MCL of uranium in drinking water is set at 30 µg/L (i.e., 20 pCi/L) by the U.S. EPA (USEPA, 2011). However, the concentration of uranium in soil varies over a wide range from 0.3 to 11.7 mg/kg according to a UNSC report on the effects of atomic radiation (UNSC, 1993). The general daily maximum intake of soluble uranium salts for an individual is 0.5 µg per kg of body weight and was established by the World Health Organization. Overintake of uranium may lead to renal dysfunction and even kidney failure (Choy et al., 2006).

The most commonly used techniques for selenium remediation in soils involve either *ex situ* treatment such as soil washing/extraction or excavation and landfill, or *in situ* treatment such as permeable reactive barriers (PRBs), soil flushing and phytoremediation (Mulligan et al., 2001). Compared to the *ex situ* technologies, *in situ* remediation is generally less costly and causes less disruption to the environment. Based on the technologies developed for removing Se from water, which include adsorption, biological reduction (Mishra et al., 2011), enhanced coagulation, membranes (Mavrov et al., 2006), chemical reduction (El-Shafey, 2007) and reverse osmosis (Gonzalez et al., 2012), high capacity adsorbents offer considerable promise as a method for *in situ* treatment (e.g., PRBs); however, current *in situ* remediation practices face some serious limitations, the most serious of which may be their inability to cope effectively with contaminants buried deep in the subsurface or contained in contaminated aquifers located under existing surface structures. Therefore, the *in situ* adsorptive immobilization of toxic metals by injecting engineered nanoparticles into contaminated source zones may be one promising alternative approach that mitigates the related environmental and health impacts. The research reported in the papers presented in this dissertation focuses on measuring the adsorptive immobilization effectiveness for Se(IV) of stabilized Fe-Mn nanoparticles specifically developed and synthesized for this project and the soil deliverability of the nanoparticles.

It is important to note that adsorptive immobilization is not the best option for U remediation since the solubility and mobility of U in the soil are both greatly affected by factors such as the oxidation states involved, the geochemical properties of the soil (e.g., pH, dissolved oxygen (DO), Natural organic matter (NOM), carbonate), its microbial activity and any physical effects (e.g., soil texture, hydraulic regimes) (Gavrilescu et al., 2009; Wang et al., 2013). Generally, the oxidized form, U(VI), is soluble in natural water as the uranyl form (UO_2^+) and

commonly forms complexes with both inorganic and organic ligands, while the reduced form, U(IV), exists in insoluble oxides as uraninite (UO_2) and is less mobile in groundwater than U(VI) (Chang et al., 2014; Jackson et al., 2005; Wersin et al., 1994). Thus, U(VI) and its complexes are considered the predominant contaminant species posing the highest risks to human and ecological health via processes such as migrating into soil water, being adsorbed by plants or microorganisms, and contaminating groundwater (Igwe et al., 2005).

Due to the considerations outlined above, most soil remediation technologies for U contaminated sites have focused on the reductive precipitation of U(VI) to U(IV) by way of either chemical or biological mechanisms (Fiedor et al., 1998; Lovely et al., 1991; Scott et al., 2005; Wu et al., 2006). Conventional remediation technologies for U contaminated soil generally involve two steps: i) extraction, where U is extracted from the contaminated soil via various methods (e.g., citrate acid, bicarbonate) (Choy et al., 2006; Gavrilescu et al., 2009); and ii) reduction, where the main options are biodegradation, chemical reduction or photodegradation (Francis and Dodge, 1998; Gu et al., 2005). Compared to *ex situ* techniques, PRBs can be very cost-effective in spite of their limitations related to the depth of the contamination (being restricted to shallow surface contamination or shallow groundwater), and the continuous need to replace reactant and dispose of used reactant. To achieve a highly effective and low-cost *in situ* reductive immobilization of U(VI), we have synthesized a stabilized nZVI that can be injected into soils and is thus delivered to the contaminated zone under external pressure. This research is described in detail in Chapter 2 and 4.

1.2 P and As leaching from poultry litter

Phosphorus (P) is an essential nutrient for the growth of organisms in natural ecosystems, and yet, excessive discharges of phosphate into the water bodies often result in eutrophication (taking the form of algal blooms), especially in confined lakes, reservoirs and coastal areas (Zhao and Sengupta, 1998). To limit the discharge of P in wastewater into the environment, levels of effluent P in municipal and industrial wastewater are rigorously regulated and the National Pollutant Discharge Elimination System (NPDES) enforces a general P permit limit of 1 mg/L for all discharges to surface waters; however, P released from agricultural wastes such as poultry litter and animal manure receives much less attention than that from wastewater, even though agricultural waste is known to contain large amounts of P. For example, Felton et al. (2007) observed that the average P concentration reached as high as 10.8 mg/L in simulated runoff water from poultry litter stockpiles. However, while eutrophication due to excessive nutrients is known to be one of the primary water contamination issues in agriculture-intensive regions worldwide, P is also itself a valuable resource. As a mineral, P has been listed as one of the 20 critical raw materials that are being consumed at an alarming rate (EC, 2014).

Arsenic contamination produced by agricultural applications has been a health concern for decades (Onken and Hossner, 1996). In 2011, the U.S. FDA approved four arsenic-based drugs for use in poultry and swine production, namely roxarsone, nitarsone, arsanilic acid and carbarsone. Of these, roxarsone (3-Nitro®), or 3-nitro-4-hydroxybenzenearsonic acid, is the first and most commonly used arsenical animal drug (USFDA, 2011). In the poultry industry, roxarsone has been extensively used as an organoarsenical feed additive to control the protozoan parasitic disease coccidiosis, enhance weight gain and improve feed efficiency (Garbarino et al., 2003; Jackson and Bertsch, 2001).

Generally, roxarsone is added to poultry feed at the rate of 22.7 to 45.4 grams per ton, which corresponds to 0.0025 to 0.005% of the animal's body weight (Bellows, 2005). Garbarino et al. (2003) measured a concentration of 9×10^5 kg roxarsone in manure if 70% of the broiler chickens in the U.S. were fed by chicken feed containing roxarsone in 2000, with this amount climbing to approximately one million kilograms in 2006 (Hileman, 2007). Most of the roxarsone in the feed is not retained by the broilers but instead excreted unchanged in the litter (Morrison, 1967), creating a source of arsenic pollutant in the environment if the manure is applied to fertilizer or the animal wastewater is discharged (Jackson et al., 2006). Each broiler excretes about 150 milligrams of roxarsone during the 42-day growth period in which it is administered (Bellows, 2005) and the litter can contain from 15 to 48 mg/kg of the resulting organoarsenical contamination (Arai et al., 2003; Jackson et al., 2006). In addition, the arsenic content increases considerably during composting since the litter volume reduces by 25 to 50% and the litter weight by 40 to 80% due to the loss of water and carbon dioxide involved, so poultry litter that contains 30 ppm arsenic before composting will contain 50 to 150 ppm arsenic afterwards (Bellows, 2005). The degradation of roxarsone under different photo- or bio- chemical conditions can produce inorganic forms of arsenic that are both more mobile and more toxic than roxarsone, with the already rapid degradation rate potentially being accelerated depending on various environmental conditions such as sunlight, bacteria, moisture, temperature, etc. (Bednar et al., 2003; Hu et al., 2012; Stolz et al., 2007). Recently, the US FDA (food and drug agency) announced that the sale of roxarsone in U.S. was being suspended by the supplier, Zoetis, Inc, a former subsidiary of Pfizer, Inc, because the levels of inorganic arsenic in chicken livers had been shown to increase when treated with roxarsone using a new detection method (FDA, 2015). This is expected to lead to a significant

drop in the arsenic content in poultry litter in the future, but major chicken-producing states such as Alabama, Georgia and Kansas are still using this type of organoarsenical feed additive.

Based on the latest poultry production statistics reported by the U.S. Department of Agriculture (USDA), more than 8.54 billion broiler chickens were raised in U.S. in 2014. Eighteen states in the eastern and central parts of the country (including GA, AL, AR, NC, MS, and TX) produced 8.0 billion birds (i.e., 93.6% of the total), of which Alabama and Georgia alone each produced more than 1 billion (USDA, 2014). Typically, approximately 90% of the resulting PL is disposed of through local land applications as a fertilizer and source of organic matter for soil (Stolz et al., 2007). Consequently, large amounts of nutrients (P and N) and some organic arsenic (As) compounds (e.g., roxarsone) are released into the environment, either through land applications or directly from litter stockpiles (Cortinas et al., 2006; Felton et al., 2007; Wood et al., 1996). Currently, there are no state or federal regulations limiting annual total metal inputs on agricultural lands via PL amendments. There is thus an urgent need to control the level of release of P and As from agricultural wastes to prevent water contamination and support sustainable agricultural practices.

To date, adsorption and chemical precipitation have been the most common methods used to remove and recover P and As from wastewater or streams (Zhao and Sengupta, 1998). A wide variety of materials have been tested for such applications, including fly ash (Chen et al., 2007), blast furnace slag (Oguz, 2004), oxide tailings (Zeng et al., 2004), zeolite (D. Wu et al., 2006), clay materials (Rao and Mishra, 2005; L. Yan et al., 2010) and iron-based adsorbents (Genz et al., 2004). These absorbents are prepared as granular or powder aggregates that are not readily dispersible in porous media and are hence not convenient for treating solid/hazardous wastes such as poultry litter or for *in situ* soil application. Taking advantage of the high sorption capacity and

good soil-deliverability of stabilized Fe-Mn nanoparticles, we therefore applied stabilized nanoparticles to control the leaching of P and, fortuitously, As from poultry litter (or other animal wastes) by amending the wastes with the stabilized nanoparticles. This research is reported in Chapter 3.

1.3 Synthesis of polysaccharide bridged or stabilized nanoparticles

Nanoscale materials have elicited considerable interest for the removal of metal or/and radionuclide contaminants including Se, As, P, and U, among others. Conventional techniques including aggregated nanoparticles are not readily deliverable into contaminated soil, and can thus only be used in *ex-situ* configurations or in PRBs. If they are to be suitable for applications such as *in situ* soil and groundwater remediation, the nanoparticles are required to: 1) be deliverable in soil under moderate external pressure; 2) offer decent immobilization effectiveness for the target contaminants; and 3) remain in a confined area without spreading once the external pressure is removed. To enhance the soil deliverability of the nanoparticles, our group has developed a number of polysaccharide-stabilized nanoparticles (e.g., ZVI, $Fe_3(PO_4)_2$, FeS, Fe_3O_4 and Fe-Mn) using starch or CMC as a stabilizer (An and Zhao, 2012; Gong et al., 2012; He and Zhao, 2005; Liang et al., 2012; Liu and Zhao, 2007a; Xie et al., 2015; Xu and Zhao, 2007). In this case, a stabilizer is a chemical that can be adsorbed onto the surfaces of the nanoparticles and prevent their aggregation through various steric and/or electrostatic stabilization mechanisms. The proper use of a stabilizer during the particle preparation process facilitates nucleation, crystallization and particle growth, and controls the particle size and, possibly, the morphology. By preventing the particles from aggregating, an appropriate particle stabilization strategy can be utilized to create soil-deliverable nanoparticles that can be used for *in situ* remediation applications.

Step 1: Mix 120 mL of a starch or CMC (0 ~ 0.1 wt.%) solution and 10 mL of 13.9 g/L Fe^{2+} solution

System under N_2 purging/mixing

⇩

Step 2: Add 10 mL of 2.65 g/L of $KMnO_4$

System under vigorous magnetic stirring

⇩

Step 3: Adjust pH to ~7.5 using 4M NaOH and grow for 1 h

Figure 1-1. Procedures for synthesizing starch- or CMC-stabilized Fe-Mn nanoparticles.

In the study, stabilized Fe-Mn and ZVI nanoparticles were synthesized and tested for adsorptive and reductive immobilization, respectively. The stabilized ZVI nanoparticles were prepared following the method described by He and Zhao (2005). **Figure 1-1** shows the modified procedure used for preparing the polysaccharide bridged or fully stabilized Fe-Mn nanoparticles. First, prepare a 1 wt.% stock solution of starch or a 1 wt.% CMC stock solution (proper heating is needed to dissolve the starch in water). Then, take a desired volume (from 0 to 28 mL) of the starch or CMC solution and dilute with deionized water to 120 mL, and mix for 10 min. Prepare an $FeSO_4 \cdot 7H_2O$ solution of 13.9 g/L and another solution of 2.65 g/L of $KMnO_4$ in deionized (DI) water, and then add 10 mL of the $FeSO_4 \cdot 7H_2O$ solution into 120 mL of a stabilizer solution and mix for 15 min under N_2 purging. The redox reaction is then initiated by adding 10 mL of the

9

KMnO$_4$ solution into the mixture of iron sulfate and the chosen stabilizer under vigorous magnetic stirring. Immediately increase the pH of the mixture to ~7.5 using 4 M NaOH, and shake the mixture on a platform shaker at 200 rpm for 1 h. Fe–Mn nanoparticles are then obtained as either non-stabilized aggregates or a fully stabilized suspension, depending on the concentration and type of the stabilizers present. The Fe–Mn particles are then tested or analyzed within 1 h of preparation. The cost of the Fe-Mn particles for industrial application is estimated to be $1.8/kg-Fe (bare), $2.2/kg-Fe (starch stabilized) and $2.8/kg-Fe (CMC stabilized) based on current industrial grade chemical prices (e.g., $250/ton for FeCl$_2$·4H$_2$O, $1,200/ton for KMnO$_4$, $400/ton for starch, $1,000/ton for CMC).

1.4 Objectives

The overall goal of this work is to test the feasibility of nanoparticle application for the remediation of groundwater and soils contaminated with metals or radionuclides. The specific objectives are to:

1. Synthesize fully stabilized nano-scale Fe-Mn and ZVI particles for adsorptive and reductive immobilization, respectively, using two "green" polysaccharides as the stabilizer, namely a water soluble starch and CMC. Characterize the resulting Fe-Mn nanoparticles using TEM (Transmission Electron Microscope), DLS (Dynamic Light Scattering), FTIR (Fourier Transform Infrared Spectroscopy), zeta potential, and UV-visible spectroscopy.

2. Investigate the effects of stabilizers and water chemistry (e.g., pH, competing ions) on Se(IV) sorption by the stabilized Fe-Mn nanoparticles. Probe the transport behavior of the stabilized nanoparticles in a model soil and determine the maximum transport distance of the

stabilized Fe-Mn nanoparticles using column breakthrough tests and transport modeling. Examine the efficacy of the stabilized Fe-Mn nanoparticles for immobilizing Se(IV) in a contaminated soil.

3. Study the phosphate sorption by Fe-Mn nanoparticles, focusing on the water chemistry and the mechanism involved. Test the effectiveness of Fe-Mn nanoparticles amendment for reducing phosphate and arsenic leachability from poultry litter through batch and column experiments.

4. Conduct batch and column experiments to examine the effectiveness of stabilized ZVI nanoparticles for the reductive immobilization of U(VI) in U-contaminated soil. Test the remobilization of immobilized U in soil and the effects of bio-activity.

1.5 Organization

This dissertation consists of five chapters and is formatted in the style specified by the journal *Water Research* except for Chapter 1 (General Introduction) and Chapter 5 (Conclusions and Suggestions for Future Research). Chapter 1 introduces the background and objectives of this dissertation. Chapter 2 presents the synthesis of the stabilized Fe-Mn nanoparticles and their characterization by TEM, DLS, zeta potential and UV-visible spectra and then goes on to test the effectiveness of stabilized Fe-Mn nanoparticles for selenite immobilization in water and soil and investigate the soil deliverability of the nanoparticles. This chapter is based on a paper previously published in the journal *Water Research* (Xie et al., 2015). Chapter 3 investigates the effectiveness of Fe-Mn nanoparticle amendment for reducing P and As leachability from poultry litter. This chapter is based on two papers, one of which has been submitted to the journal *Science of the Total Environment* and other of which is about to be submitted to *Frontiers of Environmental Science & Engineering*. Chapter 4 reports the synthesis of the stabilized ZVI nanoparticle and the tests

conducted on the reductive immobilization of U(VI) in soil and groundwater. This chapter is based on a paper that has been submitted to the journal *Water Research*. Chapter 5 summarizes the major conclusions of this research and makes suggestions for future work.

Chapter 2. Immobilization of Selenite in Soil and Groundwater using Stabilized Fe-Mn Binary Oxide Nanoparticles

This chapter introduces Fe-Mn binary oxide nanoparticles, which were successfully synthesized with starch and sodium CMC as a stabilizer, and the synthesized nanoparticles were characterized with TEM and DLS. Batch tests were conducted to investigate the Se(IV) sorption kinetics and isotherms, and effects of starch/CMC concentrations and pH on Se(IV) sorption capacity. Se(IV) immobilization effectiveness by stabilized Fe-Mn nanoparticles was evaluated through a series of batch and column tests. The Se leachability of immobilized Se-laden soil and untreated soil were compared by TCLP and WET (Waste Extraction Test). The travel distance of stabilized Fe-Mn nanoparticles was estimated by model through column breakthrough tests and transport modeling. Copyright permission was obtained from Elsevier (Appendix 3).

2.1 Introduction

Se has been widely detected in soil and groundwater. The worldwide average Se content in non-seleniferous soil is about 0.4 mg/kg, with a range of 0.2-5 mg/kg, while in seleniferous soil, the Se range varies from 1 to 80 mg/kg and may reach 1200 mg/kg (Haudin et al., 2007; Mclean and Bledsoe, 1992). For U.S. soil, Se at 0.1-5.3 mg/kg has been reported (USGS, 2008). In addition to natural dissolution, many human activities such as mining, agriculture, chemical and petrochemical industries have been cited as the major anthropogenic sources of Se (Szlachta et al., 2012; Torres et al., 2010).

While Se is an essential trace nutrient to human and animals, intake of excessive Se can lead to adverse health effects such as gastrointestinal disorders, hair and nail loss, irritability and fatigue, and may result in liver cirrhosis, pulmonary edema in extreme cases (Hamilton, 2004). In addition, bioaccumulation of Se in the food chain has been associated with fish kills, bird deformities, and loss of aquatic resources (Hamilton, 2004; Loyo et al., 2008; Spallholz and Hoffman, 2002). Harmful effects on fish and wildlife have been reported when exposed to 2 to 4 μg/L Se in water and 4 μg/g in soil (Rowland et al., 2003). Interestingly, the window between Se deficiency and toxic effects is very narrow. While a daily consumption of <0.1 mg Se/kg of body weight leads to Se deficiency, an intake of >1 mg Se/kg results in toxic effects (Gonzalez et al., 2012). To mitigate the human exposure, the US EPA has set a Maximum Contaminant Level of 0.05 mg/L for total Se in drinking water (USEPA, 2009). To our knowledge, there has been no similar regulatory limit for Se in soil, though EPA has set a TCLP limit of 1 mg/L for Se in solid wastes.

Generally, there are two predominant oxidation states of inorganic Se in water and soil: Se(IV) in the form of SeO_3^{2-} (selenite) and Se(VI) in SeO_4^{2-} (selenate) (Das et al., 2002). While both oxyanions are highly mobile and transportable in soil and groundwater, the adsorption affinity towards metal oxides differs, i.e., Se(IV) interacts with oxide surfaces much more strongly than Se(VI) (Das et al., 2002; Parida et al., 1997). Therefore, the mobility and transport of selenium are redox dependent. In general, moderately anoxic groundwater conditions favor reduction and immobilization of Se. In terms of toxicity, Se(IV) is more toxic than Se(VI), especially for aquatic organisms and fish, and is more prone to uptake by plants (Hamilton, 2004; Maier et al., 1993; Skorupa, 1998).

A number of technologies have been reported for removal of Se from water, including adsorption, biological reduction (Mishra et al., 2011), enhanced coagulation, membrane (Mavrov et al., 2006), chemical reduction (El-Shafey, 2007) and reverse osmosis (Gonzalez et al., 2012). Various adsorbents, such as activated aluminum, iron and silica oxides, zero valent iron (ZVI), ion exchange resins and metal oxides/hydroxides (Al-Fe), have been found effective for Se removal (Chan et al., 2009; Duc et al., 2003; Liang et al., 2013; Martínez et al., 2006; Missana et al., 2009). Trussell et al. (1980) reported that activated alumina removed Se(IV) ten times more than Se(VI) under identical conditions. Gonzalez et al. (2010) reported that the adsorption capacities of synthetic magnetite for Se(IV) and Se(VI) were 1.923 and 1.428 mg-Se/g, respectively. In terms of adsorption mechanisms, Peak (2006) and Elzinga et al. (2009) observed a hybrid of outer-sphere and inner-sphere surface complexes on the Al_2O_3 surface for Se(IV), while primarily outer-sphere surface complexes for Se(VI). Liang et al. (2013) reported Se(IV) is first adsorbed on ZVI surface and then reduced to Se(0), resulting in a Se(0)-Fe(III) shell surrounding the iron core.

The most commonly used techniques for selenium remediation in soils include *ex situ* treatment (e.g., soil washing/extraction or excavation and landfill) and *in situ* treatment (e.g., permeable reactive barriers (PRBs), soil flushing and phytoremediation) (Mulligan et al., 2001). Compared to the *ex situ* technologies, *in situ* remediation is often less costly and less disruptive to the environment. Current *in situ* remediation practices bear with some serious limitations. For instance, the technologies are less effective for contaminants deep in the subsurface or contaminated aquifers located under existing surface structures. Therefore, *in situ* immobilization of toxic metals by injecting engineered nanoparticles into the contaminated source zone offers a promising alternative to mitigate the related environmental and health impacts.

Binary oxides/hydroxides are widely found in the natural environment, such as Al(III)/Fe(III) oxides mixed with SiO_2 (Chan et al., 2009), Mn/Al hydrotalcite (Liu et al., 2009), and Fe-Mn hydrous oxide (Szlachta et al., 2012). In general, these adsorbents offer higher anion adsorption capacities compared to the single oxide minerals due to increased specific surface area, concurrent redox reactions and/or anion exchange of the oxyanions (Goh et al., 2008).

Nanoscale adsorbents have elicited great interests for removal of trace contaminants including Se from water (An et al., 2011). Reports on research into removal or *in situ* immobilization of selenium in soil and groundwater has been rare. Conventional adsorbents including aggregated nanoparticles are not deliverable into contaminated soil, and thus, can only be used in *ex situ* configurations or in PRBs. To facilitate soil deliverability of the nanoparticles, our group has developed a number of polysaccharide-stabilized nanoparticles (e.g., ZVI, $Fe_3(PO_4)_2$, FeS, Fe_3O_4 and Fe-Mn) with starch or CMC as a stabilizer (An and Zhao, 2012; Gong et al., 2012; He and Zhao, 2005; Liang et al., 2012; Liu and Zhao, 2007a, 2007b; Xu and Zhao, 2007). In addition to much improved soil deliverability, the stabilized nanoparticles were found highly effective for *in situ* reductive and/or adsorptive immobilization of toxic metals such as Cr(VI), Pb(II), Cu(II), Hg(II) and As(V) and As(III) in soil and groundwater. The use of the stabilizers during the particle synthesis facilitates the nucleation, crystallization and particle growth, thereby preventing the nanoparticles from aggregating.

The overall goal of this work is to test the efficacy of stabilized Fe-Mn binary oxide nanoparticles for removal/immobilization of Se(IV) in water and soil. The specific objectives were to: 1) prepare and characterize the desired Fe-Mn nanoparticles using a water-soluble starch or CMC as a stabilizer, 2) investigate the effects of the stabilizers on Se(IV) removal by the nanoparticles, 3) test the effects of particle dosage and pH, 4) probe the transport behavior of the

stabilized nanoparticles in a model soil, and 5) examine the effectiveness of the stabilized

nanoparticles for immobilizing Se(IV) in a contaminated soil.

2.2 Materials and Methods

2.2.1 Materials

$FeSO_4 \cdot 7H_2O$, $FeCl_2 \cdot 4H_2O$, $KMnO_4$, Na_2SeO_3, CMC (sodium salt, MW = 90,000), and a

hydrolyzed potato starch were purchased from Acros Organics (Morris Plains, NJ, USA). $FeCl_3$,

NaOH, citric acid and acetic acid were acquired from Fisher Scientific (Pittsburgh, PA, USA).

Hydrochloric acid and nitric acid were obtained from Mallinckrodt Chemicals (St. Louis, MO,

USA). All the chemicals were of analytical grade or higher, and all solutions were prepared with

ultrapure deionized (DI) water (18.2 Ωcm^{-1}).

2.2.2 Preparation of Se(IV)-spiked soil and soil analysis

A sandy soil was taken from the Smith Research Field (Tallassee, AL, USA). The soil was

pre-washed with tap water to remove soluble compounds and suspended solids. The soil was then

air-dried, sieved through a 2-mm screen and stored in a sealed glass bottle (An and Zhao, 2012).

The key soil properties include: OM (organic matter) = 0.1%, CEC = 0.5 meq/100g, and Fe = 4

mg/kg.

Soil analyses were performed by the Soil Testing Laboratory at Auburn University. **Table**

2-1 provides salient physical and chemical properties of the soil. Elemental analysis of the soils

was conducted following EPA method 3050B and using an inductively coupled plasma optical

emission spectrometer (Vista-MPX, Varian Inc., Palo Alto, CA, USA). The content of sand, silt

and clay was determined following the pipette method (Gee, 2002). Soil organic matter (SOM)

was measured per the Dumas method with a LECO CN-2000 combustion unit (LECO Corp., Joseph, MI, USA) at 1050 ℃ after the soils were treated with 4N H_2SO_4 to dissolve free carbonates before the dry combustion.

The hydraulic conductivity was measured to be 6.3 ± 0.5 cm/day by the Darcy equation following the constant head method,

$$q = \frac{V}{A \cdot t} = -K \frac{\Delta H}{\Delta Z} \tag{2-1}$$

where q is the Darcy velocity (m/s), V is the volume of water (m^3) passing through a cross-sectional area of porous medium A (m^2) during time t (s), K is the hydraulic conductivity (m/s), ΔH is the hydraulic head difference between the top and bottom of the sample, and ΔZ is the height of the soil bed (0.12 m). Water was continuously fed to the column at $q = 3.6 \times 10^{-6}$ m/s to maintain a constant hydraulic head between the top and bottom of the soil, i.e., $\Delta H = 0.6$ m.

Se(IV)-spiked soil samples were prepared by mixing 200 g of the air-dried soil with 300 mL of a Se(IV) solution containing 100 mg/L of Se(IV) in a batch reactor at pH 6.5. After 2 weeks of equilibration, the supernatant was decanted and the Se(IV)-laden soil was rinsed twice with DI water. The final Se(IV) loading on the soil was determined to be 40.5 mg of Se(IV)/kg-dry-soil by measuring aqueous-phase Se concentrations, which was confirmed by measuring the solid-phase Se via EPA Method 3050B (USEPA, 1996).

Table 2-1. Physicochemical characteristics of the sandy soil used in this study.

Textural Class	pH	H₂O	CEC meq/100g	O.M.	Ca ppm	K ppm	Mg ppm	P ppm	S ppm	Al ppm	As ppm	B ppm
Sand	6.77	0	0.5	0.1%	59	6	14	<0.1	1	12	<0.1	2

Ba ppm	Cd ppm	Cr Ppm	Cu Ppm	Fe ppm	Mn ppm	Mo ppm	Na ppm	Ni ppm	Pb ppm	Zn ppm
2	<0.1	<0.1	4	4	2	<0.1	18	<0.1	<0.1	4

2.2.3 Synthesis of stabilized Fe-Mn nanoparticles

Starch- or CMC-stabilized Fe-Mn oxide nanoparticles were prepared based on the method described by An and Zhao (2012). In each batch, 200 mL of the nanoparticle suspension was prepared in a 250 mL glass flask. First, prepare the following solutions: 1.12 mM $FeCl_2$, 5.95 mM $KMnO_4$, 1 wt.% starch, and 1 wt.% CMC. Then, various volumes (0 to 20 mL) of the starch or CMC solution was added to 160 mL of the $FeCl_2$ solution and mixed for 20 min. Then, 10 mL of the $KMnO_4$ solution was added into the mixtures of starch-$FeCl_2$ or CMC-$FeCl_2$ under vigorous magnetic stirring to complete the redox reaction:

$$3Fe^{2+} + Mn^{7+} \rightarrow 3Fe^{3+} + Mn^{4+} \tag{2-2}$$
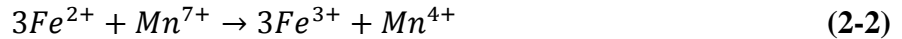
The pH of the mixture was kept at ~7.5 using 1 M NaOH, and the total volume of the mixture was maintained at 200 mL by adding DI water (0-10 mL) or a Se(IV) working solution (0-10 mL). The resultant nanoparticle suspensions contained 0.05 g/L Fe and 0.017 g/L Mn with a stabilizer concentration of 0-0.1 wt.%. The nanoparticles were allowed to grow for 1 h under shaking at 200 rpm then used for the subsequent experiments. For comparison, starch- or CMC-stabilized magnetite nanoparticles were also prepared following the method by Liang et al. (2012).

2.2.4 Physical characterization of Fe-Mn nanoparticles

A Zeiss EM10 transmission electron microscope (TEM) (Zeiss, Thornwood, NJ, USA) operated at 31.5 and 50 kV was used to obtain the TEM images. To this end, the nanoparticle suspensions were prepared at 0.1 g/L as Fe with 0-0.1 wt.% of starch or CMC. Then, a single drop of a suspension was placed on a 300 mesh copper specimen grid and air-dried for 24 h before imaging. The images were then processed using the Image-J (He and Zhao, 2005) to obtain the size distribution of the particles.

A Zetasizer nano ZS (Malvern Instruments, UK) was used to measure the zeta (ζ) potential and hydrodynamic diameter of the nanoparticles. Suspensions of bare, 0.10 wt.% starch- or CMC-stabilized Fe-Mn nanoparticles (Fe= 0.1 g/L) were prepared and then adjusted to a pH of 3 to 11. All the samples were sonicated with a sonicator (550 Sonic Dismembrator, Fisher Scientific, USA) before each measurement. Measurements were obtained with a folded-capillary cell containing 0.75 mL of a nanoparticle suspension at 25 °C. The viscosity of each suspension was measured with a Gilmont viscometer (Barnant Co., Barrington, IL, USA) to correct the ζ potential values.

2.2.5 Selenite removal from water: Batch tests

A series of batch kinetic experiments were carried out to test the effectiveness of the nanoparticles for selenite removal from water. Batch kinetic tests were conducted using 250 mL glass flasks with rubber stoppers, and were initiated by adding known volumes of a Se(IV) solution (100 mg/L) into each nanoparticle suspension to give the following initial conditions: suspension volume = 200 mL, particle concentration = 0.05 g/L as Fe, CMC or starch = 0.05 wt.%, Se(IV) = 5 mg/L and pH = 7.0. The pH was kept at 7.0±0.2 during the tests through intermittent adjustment using 0.1 M HCl and 0.1 M NaOH. The mixtures were continuously shaken on a platform shaker at 200 rpm. At predetermined times, the suspensions were sampled at 3 mL each and filtered through a 25 nm mixed cellulose esters membrane (MF-Millipore Corp., Billerica, MA, USA). The filtration was able to completely remove the particles, but no soluble Se. All the tests were conducted in duplicate and control tests were carried out with DI water or a dispersant solution in parallel.

Sorption equilibrium experiments were also carried out to test the effects of the stabilizers and pH on the Se(IV) uptake. The same test protocol was followed except the initial Se(IV)

concentration was fixed at 5 mg/L and the nanoparticles were prepared at a fixed iron concentration of 0.05 g/L with various concentrations of starch or CMC (0.02, 0.03, 0.04, 0.05, and 0.06 wt.%). To test the pH effects, batch equilibrium tests were conducted over a pH range from 4 to 11 under otherwise identical conditions. To test the effects of competing ions, sulfate (1 mM) or phosphate (1 mM) was introduced in the batch equilibrium tests at pH 7 under otherwise identical conditions.

2.2.6 Immobilization of soil-laden Se(IV): Batch kinetic tests

A series of batch kinetic tests were conducted to investigate the effectiveness of the nanoparticles for reducing the Se leachability from the Se-laden soil. The tests were initiated by mixing 2 g of the Se(IV)-laden soil with 20 mL of a nanoparticle suspension in plastic centrifuge tubes at pH 7.0±0.2. The mixtures were rotated on an end-to-end rotator at 30 rpm. At predetermined times, the suspensions were centrifuged at 6500 rpm (5857 g of RCF), and the supernatants were filtered using the membrane and then analyzed for Se in the aqueous phase. Control experiments were carried out with Se-laden soil in the absence of the nanoparticles.

2.2.7 Particle transportability and *in situ* Se(IV) immobilization: Column tests

Column breakthrough experiments were carried out to evaluate the soil mobility of CMC-stabilized Fe-Mn nanoparticles in soil. The column setup included a Harvard Apparatus PHD 2000 syringe pump (Plymouth Meeting, PA, USA), a plastic column (DxL = 1.27x20 cm, D = inner diameter and L = length), and a fraction collector (Eldex Laboratories, Napa, CA). Approximately 21 g of the sandy soil was packed in the column, giving a soil porosity of 0.34, a unit pore volume of 3.9 mL and a soil bed length of 12 cm. The nanoparticle suspension (0.1 g/L as Fe with 0.1 wt.% CMC) was pumped through the soil bed in the down-flow mode at a flow rate of 0.15 mL/min

(i.e., a pore velocity of 5.8×10^{-3} cm/s). To investigate the effects of hydrodynamic conditions, the breakthrough tests were also carried out at a pore velocity of 3.9×10^{-3}, 1.9×10^{-3}, 7.7×10^{-4} and 3.9×10^{-5} cm/s. The nanoparticle concentration in the effluent was quantified by measuring the total Fe concentration. To probe the hydrodynamic characteristics of the column system, tracer tests were conducted with a KBr solution (50 mg/L as Br$^-$) under identical operating conditions.

   In situ Se immobilization tests were carried out in the same column configuration by treating the Se-laden soil using the stabilized nanoparticles. First, 21 g of the Se(IV)-laden sandy soil was packed in the column. Then, the contaminated soil was treated with 16 pore volumes (PVs) of a nanoparticle suspension (0.1 g/L as Fe and 0.10 wt.% CMC) at a pore velocity of 5.8×10^{-3} cm/s. Se in the effluent was determined as soluble Se and total Se. To determine soluble Se, the effluent samples were first filtered through the 25-nm membrane to remove all the particles; the filtrate was then analyzed for soluble Se. To determine the total Se, which includes both soluble and nanoparticle-sorbed Se, the samples were first treated with HNO_3 (5 M) to completely dissolve the nanoparticles, and then analyzed for Se. For comparison, parallel elution tests of the Se-laden soil were carried out using DI water under otherwise identical conditions.

2.2.8 Leachability tests of Se(IV) in soil

   To further gauge the immobilization effectiveness, the untreated and column-treated soil samples were subjected to the TCLP (EPA Method 1311) and WET (California HML Method 910) procedures. For TCLP tests, the nanoparticle treated soil samples were air-dried and then subjected to the TCLP fluid No. 1 (0.57% glacial acetic acid + 0.64 N NaOH, pH 4.93±0.05) at a solid-to-solution ratio of 1 g to 20 mL. The mixtures were rotated at 30 rpm for 19 h. For WET tests, the air-dried soil samples were mixed with the extraction fluid (0.2 M citric acid solution, pH 5.0) at

a solid-to-solution ratio of 1 g to 10 mL for 48 h. Following the equilibration, the samples were centrifuged at 6500 rpm for 20 min. Then, the supernatants were filtered with the 25 nm membrane, and the filtrates were analyzed for Se. The Se leachability was quantified by,

$$\text{Leachability of Se} = \frac{C_{Se} \times V}{M_{Se}} \tag{2-3}$$

where C_{Se} is the Se concentration in the solution (mg/L), V is the volume of the solution, and M_{Se} is the initial mass of Se in the soil before the extraction.

2.2.9 Chemical analyses

Selenium, iron and manganese were analyzed using a Varian 710-ES ICP Optical Emission Spectrometer (OES), which has a detection limit (DL) of 4.0, 0.2, 0.05 µg/L, respectively. Bromide was analyzed using a Dionex Ion Chromatograph (Model DX-20) equipped with an AS14 column (DL<0.05 mg/L).

2.3 Results and Discussion

2.3.1 Characterization of Fe–Mn nanoparticles

Figure 2-1 shows representative TEM images of bare, starch- or CMC-stabilized Fe-Mn particles. Fully stable Fe-Mn nanoparticles (0.1 g/L Fe) were obtained in the presence of 0.10 wt.% of starch or CMC. Based on measurements of ~500 particles, the mean diameter of the CMC-stabilized nanoparticles was estimated to be 38±9 (±standard deviation) nm, whereas the starch-stabilized nanoparticles appeared bridged aggregates, and the primary particle size was roughly estimated at 47±11 nm. The bare particles were present as more poly-dispersed aggregates with a mean diameter of 78±16 nm, while aggregates of >250 nm were observed. CMC offered better particle stabilization and gave smaller particle size and more uniform size distribution. It is also

noteworthy that the degree of aggregation for bare Fe-Mn nanoparticles was much less than other iron-based nanoparticles such as ZVI (He and Zhao, 2007; Zhang et al., 2007b) and magnetite (An et al., 2011), which can be attributed to the weakened intermolecular and magnetic interactions among the nuclei due to the blending of manganese in the iron oxide matrix. The DLS-measured hydrodynamic diameter was 286±27 nm and 198±13 nm for CMC and starch-stabilized nanoparticles, respectively.
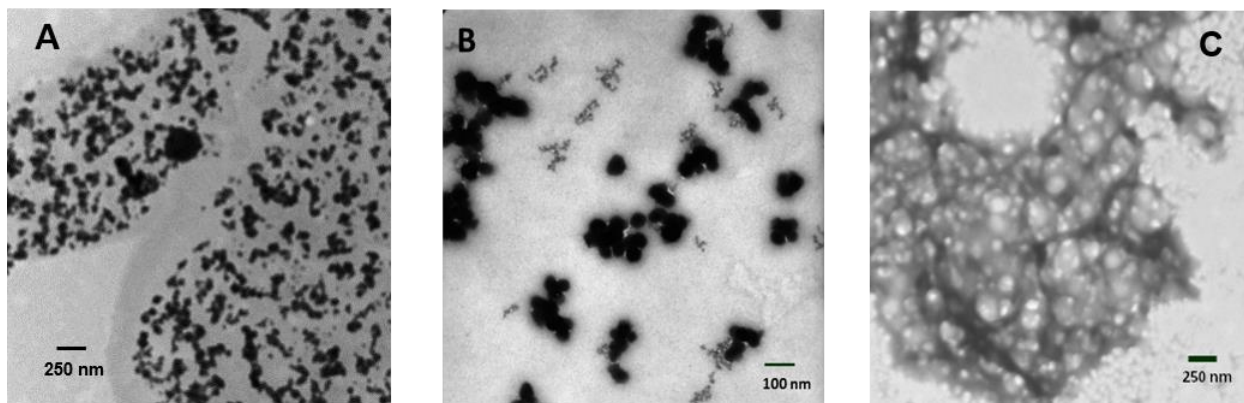
Figure 2-1. TEM images of Fe-Mn binary oxide nanoparticles prepared at 0.1 g/L as Fe with: (A) no stabilizer, (B) 0.10 wt.% CMC, and (C) 0.10 wt.% starch.

The ζ potential affects the stability, interparticle electrostatic interactions and sorption behavior of the nanoparticles in water. **Figure 2-2** shows the ζ values as a function of pH for bare and stabilized Fe-Mn nanoparticles. Evidently, the nature of the stabilizer greatly influences the surface potential. For bare Fe-Mn particles, the ζ value varied from +4 mV at pH 3.5 to -38 mV at pH 10, with the pH of the point of zero charge (pH$_{PZC}$) being 6.2. Zhang et al. (2007b) reported a pH$_{PZC}$ of 5.9 for a bare Fe-Mn material prepared in a similar manner, and they observed that the predominant oxidation states of Fe and Mn were +3 and +4, respectively. The pH$_{PZC}$ value coincided with that (6.1) for synthetic magnetite (Fe_3O_4) particles reported by Liang et al. (2012), but was much greater than that (4.2) for β-MnO$_2$ (Zhao et al., 2010) and that (2.5) of δ-MnO$_2$

(birnessite) (Allard et al., 2009). The comparison suggests that the surface potential of the Fe-Mn particles is likely dominated by that of the iron oxides.
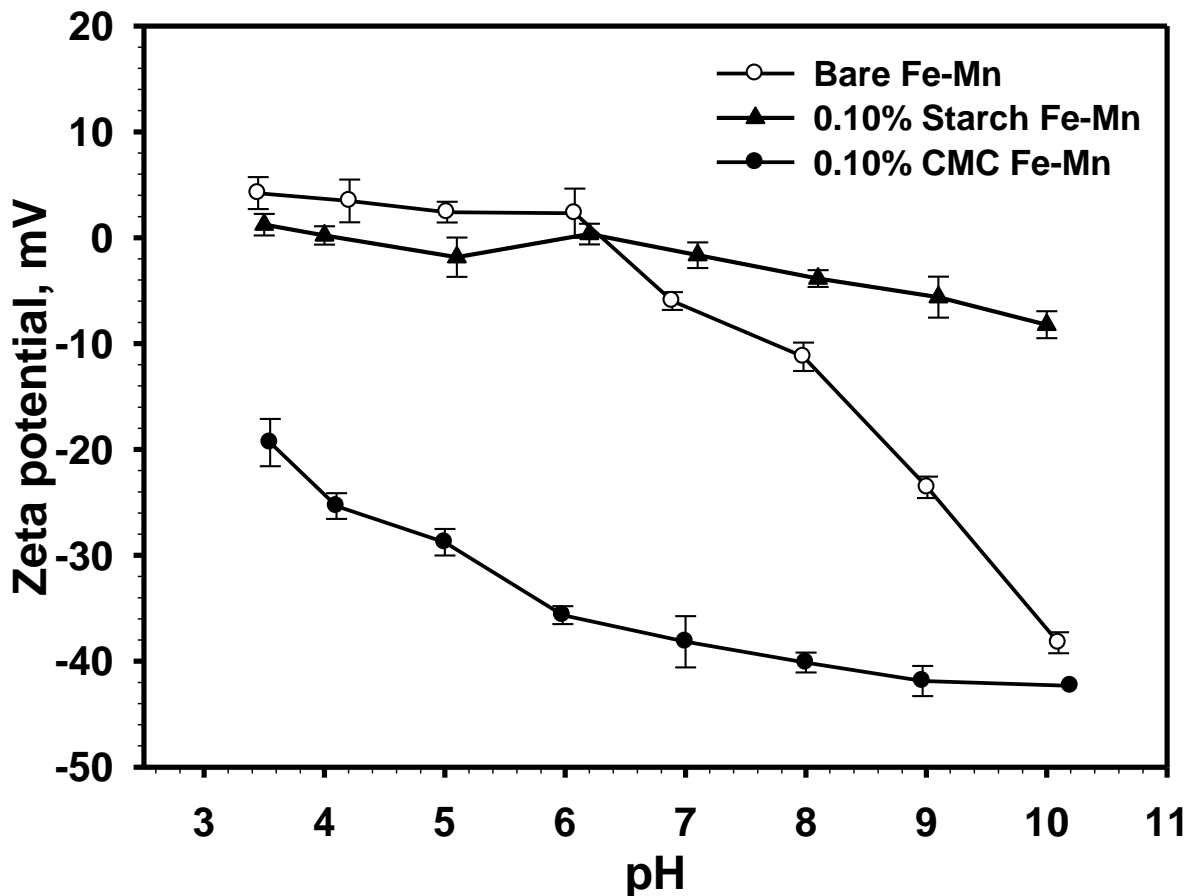
Figure 2-2. Zeta potential (ζ) as a function of pH for bare and stabilized Fe-Mn nanoparticles.

Fe = 0.1 g/L, Mn = 0.03 g/L, CMC or starch = 0.10 wt.% the for stabilized nanoparticles. Data are plotted as mean of duplicate, error bars are calculated as standard deviations.

In the presence of starch, the surface potential was nearly neutral over the pH range of 3.5-7.1, and turned to slightly negative thereafter to around −8 mV at pH 10. In contrast, the coating of CMC rendered a much more negative surface potential. Increasing pH from 3.5 to 10 increased the ζ value from −19 mV to −42 mV. Starch is a neutral polymer with dense H-bonds and high viscosity. The coating of the starch macromolecules on the particles masked the effect of H^+/OH^- on the surface charge of the core Fe-Mn particles. In contrast, CMC macromolecules ($pK_a = 4.3$) carry a high density of negative charges, and thus, the CMC coating builds up a negatively charged shell. From the standpoint of particle stabilization, starch stabilizes particles per steric exclusion while CMC works through concurrent steric and electrostatic repulsion.

2.3.2 Se(IV) adsorption kinetics and isotherms

Figure 2-3 compares Se(IV) adsorption rates of bare, stabilized Fe-Mn, and stabilized magnetite nanoparticles. The adsorption reached equilibrium in ~10 h for bare and starch-stabilized Fe-Mn particles, but more than 24 h for CMC-stabilized particles. The equilibrium removal follows the sequence of: Starched Fe-Mn (80%) > Bare Fe-Mn (69%) > CMC-stabilized Fe-Mn (65%) > Starched magnetite (60%) > CMC-stabilized magnetite (25%). The much higher Se uptake by Fe-Mn than magnetite particles unveils the important role of Mn in formulating the adsorbent structure and properties. The addition of Mn(VII) during the particle synthesis resulted in more Fe(III) oxide in Fe-Mn than in magnetite. Moreover, the redox reaction between Fe(II) and Mn(VII) and blending of the major reaction products (iron and manganese binary oxides) not only increases the formation of more nanoparticles, but opens up more specific surface area (Zhang et al., 2007a, 2005). The presence of manganese may also delay the Ostwald ripening during the formation and growth of the nanoparticles and result in more and smaller nanoparticles,

like the aluminum effect on Fe(III) oxide formation (Hu et al., 2013). The mean diameter of the starched magnetite was 75 ± 17 nm (Liang et al., 2012), which is 1.6 times larger than that for the starch-stabilized Fe-Mn. While CMC is the most effective stabilizer, the high negative surface potential renders an unfavorable condition for adsorption of like-charged Se(IV) oxyanions ($HSeO_3^-$ or SeO_3^{2-}, $pK_{a1} = 2.32$ and $pK_{a2} = 8.32$). Between the CMC-stabilized Fe-Mn and magnetite, the latter has a much more negative surface (zeta potential $= -140$ mV) (i.e., much more CMC molecules were coated) (Liang et al., 2012), which also accounts for the 40% higher removal rate of CMC-stabilized Fe-Mn. For comparison, the removal of Se(VI) was also tested under the identical conditions. The equilibrium removal of Se(VI) were 8%, 9% and 6% for bare, starch- and CMC-stabilized Fe-Mn, respectively, indicating that the nanoparticles are much more selective for Se(IV) than Se(VI).
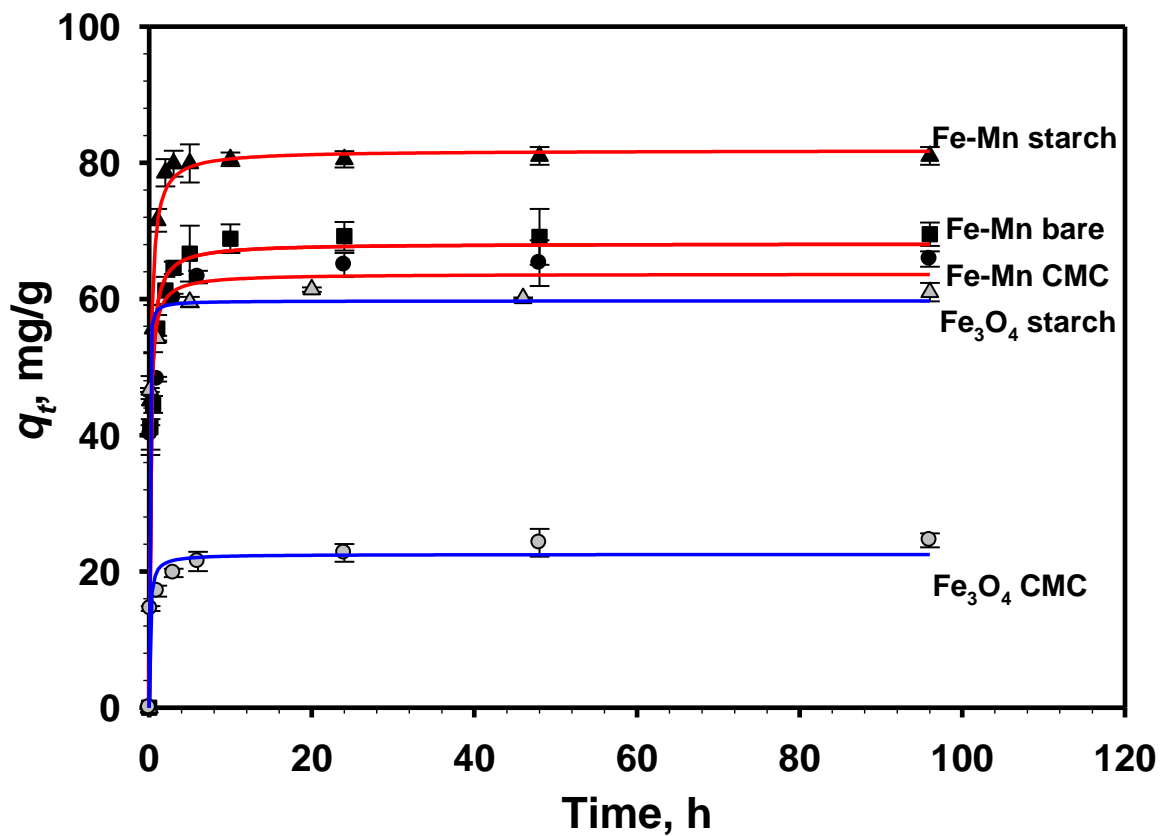
Figure 2-3. Kinetics of selenite uptake using bare or stabilized Fe-Mn or magnetite nanoparticles. Experimental conditions: initial Se(IV) = 5 mg/L, nanoparticles = 0.05 g/L as Fe, CMC or starch = 0.05 wt.%, pH = 7.0±0.1. q_t : Se concentration in solid phase at time t. Symbols: Experimental data; Lines: Pseudo second-order kinetic model simulations.

A pseudo second-order kinetic model (Chen and Huang, 2012) was used to interpret the Se adsorption kinetics:

$$\frac{dq_t}{dt} = K_s(q_e - q_t)^2 \qquad \text{(2-4)}$$

where t is the contact time (h), q_e and q_t are the solid phase Se(IV) concentrations (mg/g) at equilibrium and time t, respectively, and K_s is the adsorption rate constant (g/µg-h). Under the experimental conditions, the solution of the kinetic model gives:

$$q_t = \frac{K_s \times q_e^2 \times t}{1 + K_s \times q_e \times t} \qquad \text{(2-5)}$$

Using SigmaPlot program (version 11.0, Systat Software Inc.), the best-fitted K_s values for bare, starch- or CMC-stabilized Fe-Mn nanoparticles are 90 ± 5, 106 ± 9, and 79 ± 6, respectively ($R^2 = 0.9711, 0.9762, 0.9736$). Evidently, CMC-stabilized Fe-Mn nanoparticles offered the slowest adsorption rate despite their smallest particle size.

From an application viewpoint, bare Fe-Mn particles are likely more suitable for water treatment for their decent Se adsorption capacity and easy settleability by gravity. However, for *in situ* soil remediation, bare particles are not deliverable in soil, thus stabilized nanoparticles become necessary. Between the two stabilizers, CMC gives much smaller particle size (i.e., better particle deliverability) while starch provides ~13% higher capacity. Therefore, the stabilization techniques may be adjusted according to specific site characteristics and particle deliverability.
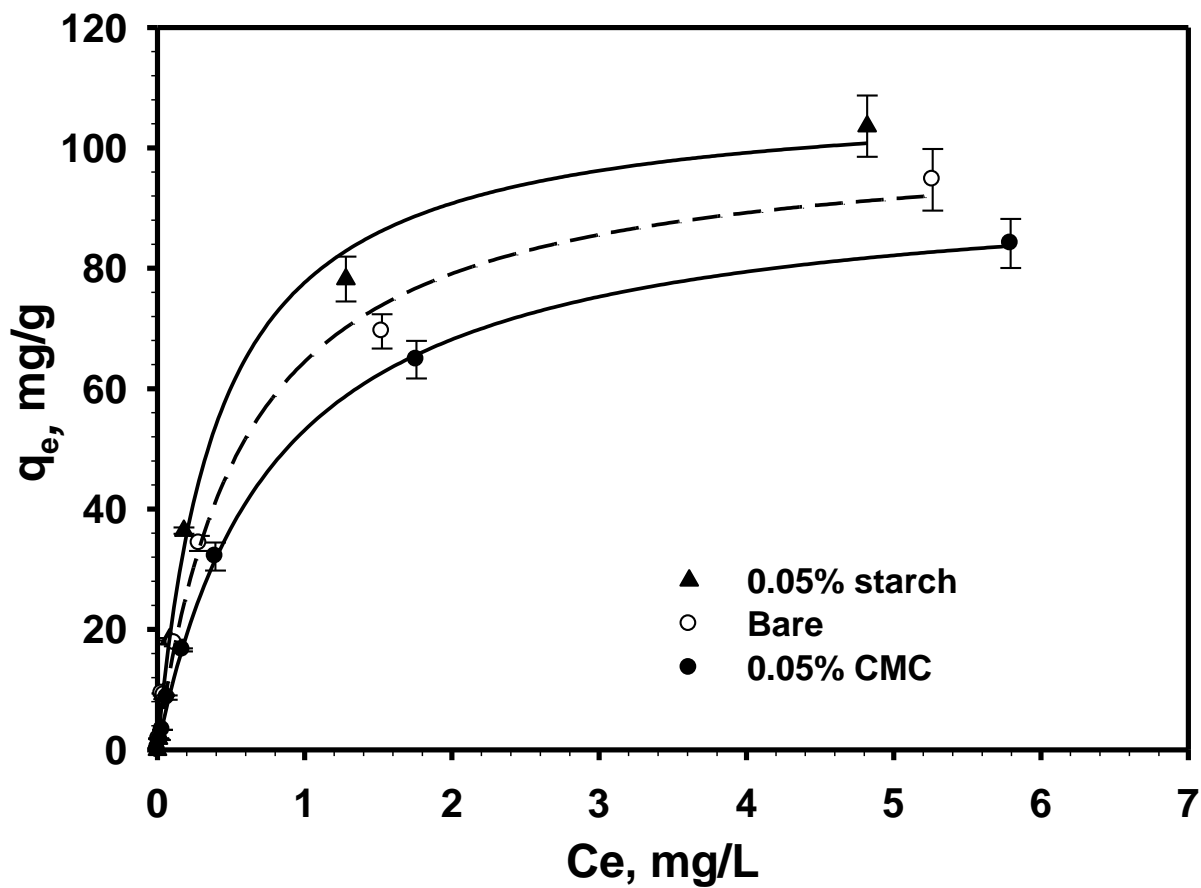
Figure 2-4. Se(IV) sorption isotherms with bare, starch- or CMC-stabilized Fe-Mn nanoparticles. Experimental conditions: Initial Se (IV) = 0.1-10 mg/L, Nanoparticles = 0.05 g/L as Fe, CMC or starch = 0.05 wt.%, pH = 6.8-7.1, Equilibrium time = 48 hrs. Symbols: Experimental data; lines: Langmuir model simulations.

Figure 2-4 shows Se(IV) sorption isotherms for bare, starch- and CMC-stabilized Fe-Mn nanoparticles. The classical Langmuir isotherm model was used to interpret the experimental data,

$$q = \frac{bQC_e}{1+bC_e} \qquad \text{(2-6)}$$

where q is the solid-phase Se(IV) concentration (mg/g), C is the aqueous-phase concentration (mg/L), and b and Q are the Langmuir affinity coefficient (L/mg) and the maximum capacity (mg/g), respectively.

The best-fitted Q values are 100 ± 17, 110 ± 25, and 95 ± 3 (mg/g) for bare, starch- and CMC-stabilized Fe-Mn nanoparticles ($R^2 = 0.9945$, 0.9960, and 0.9995), respectively, and the b values 1.7 ± 0.2, 2.5 ± 0.3 and 1.3 ± 0.1 (L/mg). These capacity values are much greater than those reported, e.g., 32.7 mg/g for Al(III)/SiO$_2$ and 20.4 mg/g for Fe(III)/SiO$_2$ (Chan et al., 2009), and 0.352 (Martínez et al., 2006) and 2.38 mg/g (Gonzalez et al., 2010) for magnetite.

2.3.3 Effects of stabilizers, pH and competing ions

Figure 2-5 presents equilibrium Se(IV) uptake by Fe-Mn nanoparticles with various concentrations of CMC or starch. Based on total Fe in the supernatants, the Fe-Mn nanoparticles were fully stabilized by 0.05 wt.% of starch or 0.04 wt.% of CMC, referred to as the critical stabilization concentration (CSC) (i.e., the minimum stabilizer concentration for complete particle stabilization). For the case of starch, the partially stabilized or flocculated particles (at starch <CSC) offered lower Se uptake than the bare particles, while the capacity steadily increased with increasing starch concentration; at CSC, fully stabilized Fe-Mn sorbed ~20% more Se than bare particles. Compared to bare particles, the partially stabilized particles may have lost some of the reactive sites due to the blocking effect of the stabilizer. In contrast, the fully stabilized particles offer much higher specific surface area (smaller particles) that outweighs the blocking effect. For

CMC, partially stabilized particles sorbed 15% less Se than bare particles, while fully stabilized particles offered comparable Se uptake. In this case, the CMC-induced surface exclusion effect offsets the gain in specific surface area. For both stabilizers, further increasing the stabilizer beyond CSC had little further effect on the Se uptake, suggesting that the gain in adsorption sites due to smaller size is counterbalanced by the formation of a thicker polymer layer on the surface, which slows down the mass transfer and blocks some of the sorption sites.
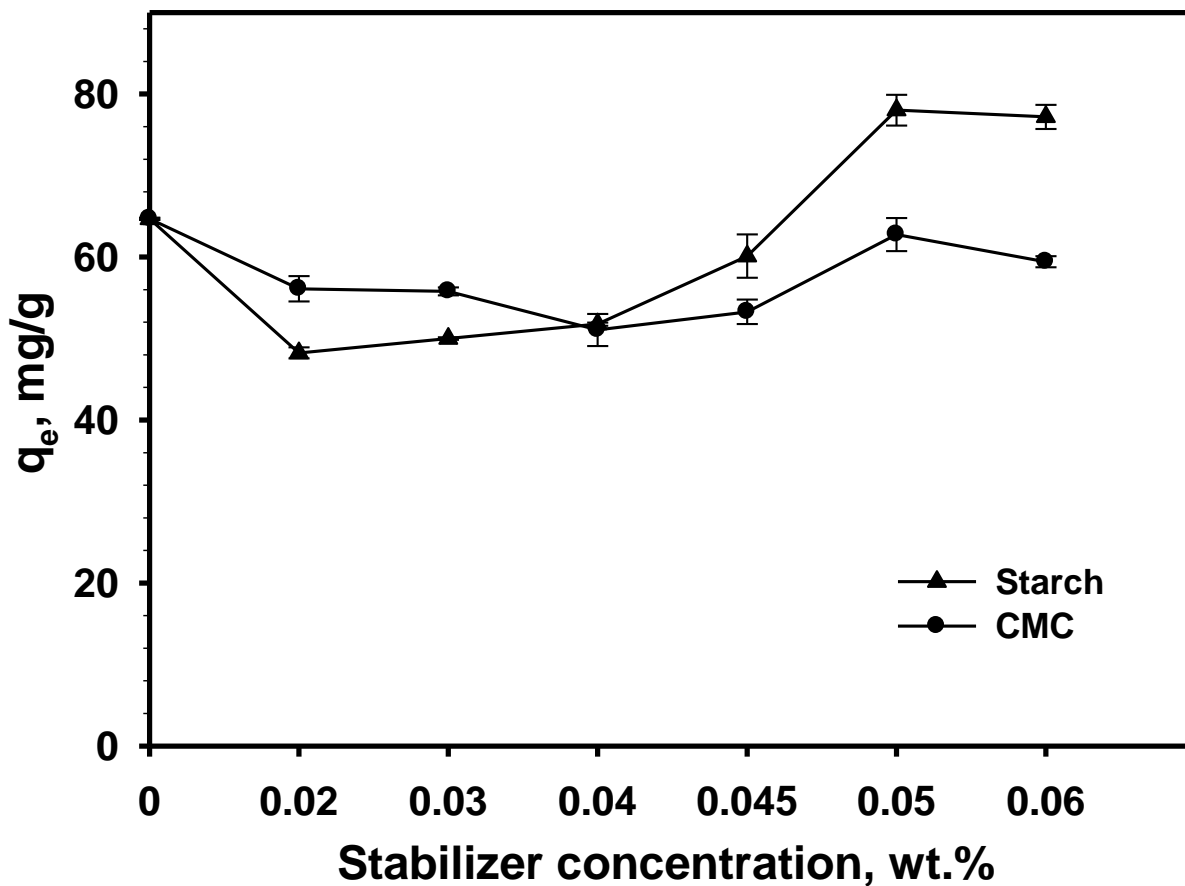
Figure 2-5. Effects of stabilizer type and concentration on uptake of selenite by Fe-Mn nanoparticles. Experimental conditions: Initial Se = 5 mg/L, Nanoparticles = 0.05 g/L as Fe, pH = 6.8-7.1, Equilibrium time = 48 hrs.

Figure 2-6 shows the Se(IV) uptake as a function of equilibrium pH for bare and stabilized Fe-Mn particles. While the starched particles displayed the highest sorption capacity and the greatest buffering ability to resist the pH effect, the sorption was favored in acidic pH for all three cases. The maximum sorption capacity was observed in pH 4-6, though the sorption remained strong in pH 6-8. The uptake dropped sharply at pH >8, and almost no removal was observed at pH 11.

Solution pH affects both surface potential of the particles and selenite speciation. The lower the pH, the less negative (or more positive) the surface potential of the particles, and the more favorable for binding with the Se(IV) oxyanions. At elevated pH, $HSeO_3^-$ becomes the predominant species and the particle surface turns more negative (**Figure 2-2**), which disfavors the Se(IV) sorption. At alkaline pH (pH > 9), OH^- ions become more competitive with selenite (Zhao and Sengupta, 2000), which sharply reduces the selenite uptake. In other words, the particles may be completely regenerated at pH 11 (**Figure 2-6**).

The observed adsorption edge is typical of adsorption of oxyanions. For example, Chan et al. (2009) prepared and tested Al-Si or Fe-Si binary oxides for selenite adsorption, and observed similar pH-dependence profiles, though the stabilized Fe-Mn particles offer >3 times higher sorption capacity.
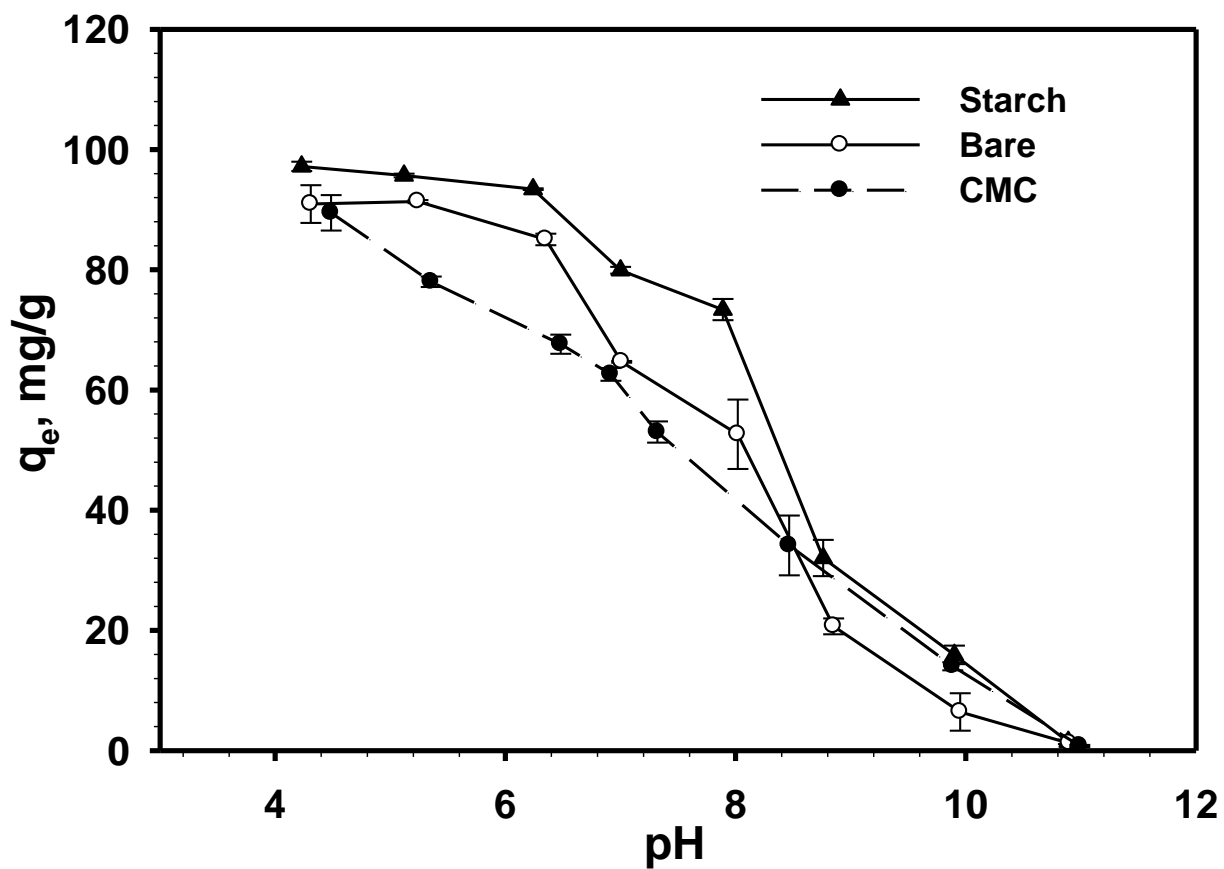
Figure 2-6. Se(IV) uptake as a function of solution pH for bare, starch- or CMC-stabilized Fe-Mn nanoparticles. Experimental conditions: Initial Se (IV) = 5 mg/L, Nanoparticles = 0.05 g/L as Fe, CMC or starch = 0.05 wt.%, Equilibrium time = 48 hrs.

Figure 2-7 shows that the presence of 1 mM sulfate only slightly lowered (by <2.4% in all cases) the equilibrium uptake of Se(IV). The greater selectivity of the nanoparticles toward $HSeO_3^-$ over SO_4^{2-} is attributed to the stronger ligand characteristics of $HSeO_3^-$, and thus, the stronger Lewis-acid base interactions between Fe and the ligand (i.e., formation of Fe-O-Se complexes) (An et al., 2005; An and Zhao, 2012). While phosphate is also a strong ligand, it only suppressed the selenium uptake by <4.6% in all cases despite the unusually high concentration (1 mM). This observation indicates that the nanoparticles were able to offer sufficient sorption sites to accommodate both types of strong ligands.
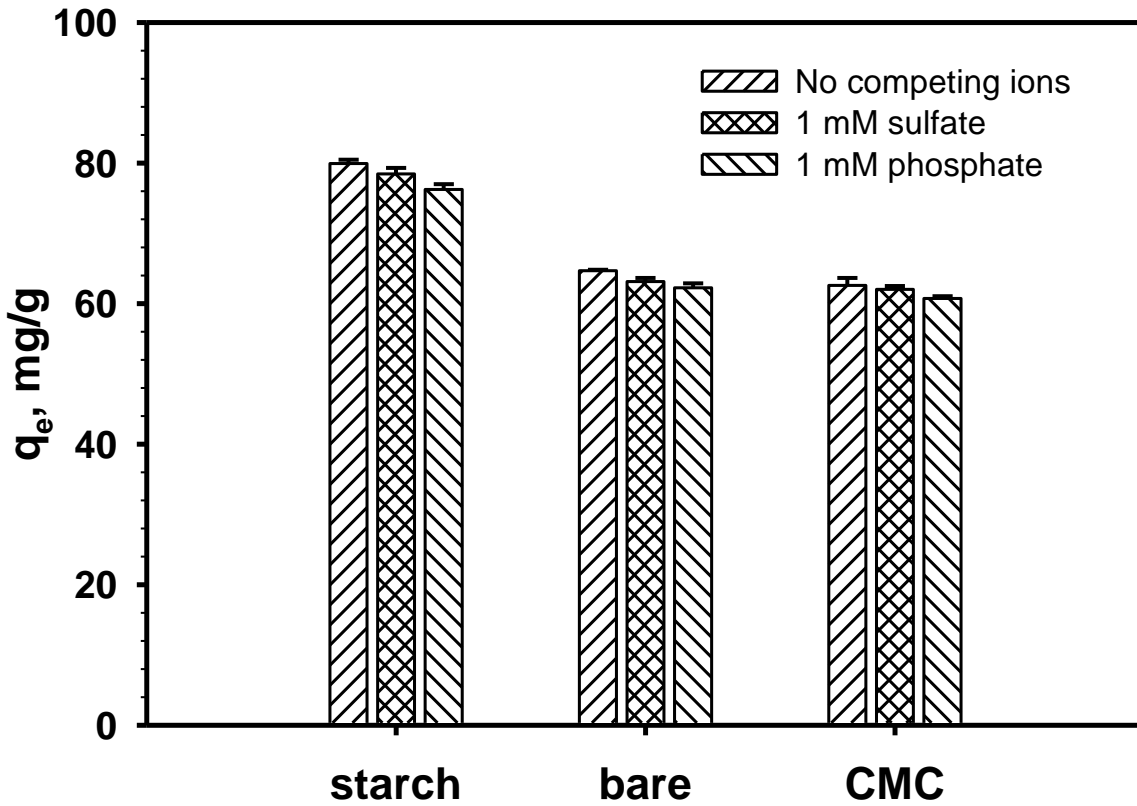
Figure 2-7. Effects of competing ions on uptake of selenite by bare and stabilized Fe-Mn particles. Batch experiment conditions: Initial Se(IV) = 5 mg/L, Nanoparticles = 0.05 g/L as Fe, CMC or starch = 0.05 wt.%, pH = 6.8-7.1, sulfate or phosphate = 1 mM, Equilibrium time = 48 hrs. q_e: Equilibrium uptake of Se(IV).

2.3.4 Enhanced immobilization of Se(IV) in soil: Batch tests

To facilitate *in situ* immobilization, the nanoparticles must meet some critical requirements. First, the nanoparticles must be deliverable in soil under moderate external pressure; second, the nanoparticles should offer decent adsorption capacity and affinity toward target contaminants, and third, the delivered nanoparticles should remain in a confined domain once the external pressure is removed. While both starch and CMC were able to facilitate very high Se uptake, CMC was a more effective stabilizer. Considering that the bottleneck for *in situ* remediation has been the poor deliverability, CMC-stabilized Fe-Mn nanoparticles are likely more suitable, and thus, were further tested for immobilization of Se(IV) in a sandy soil.

Figure 2-8 shows the leaching rates of soluble Se(IV) from the Se-contaminated soil in the absence and presence of CMC-stabilized Fe-Mn nanoparticles. In all cases, desorption equilibrium was reached in ~24 h. At equilibrium, DI water leached ~47% of the pre-loaded Se(IV) (soluble Se concentration = ~2.24 mg/L). The soluble Se was lowered to 0.83 and 0.39 mg/L by 0.05 and 0.10 g/L of CMC-stabilized nanoparticles, i.e., reducing the leachability by 63% and 83%, respectively.
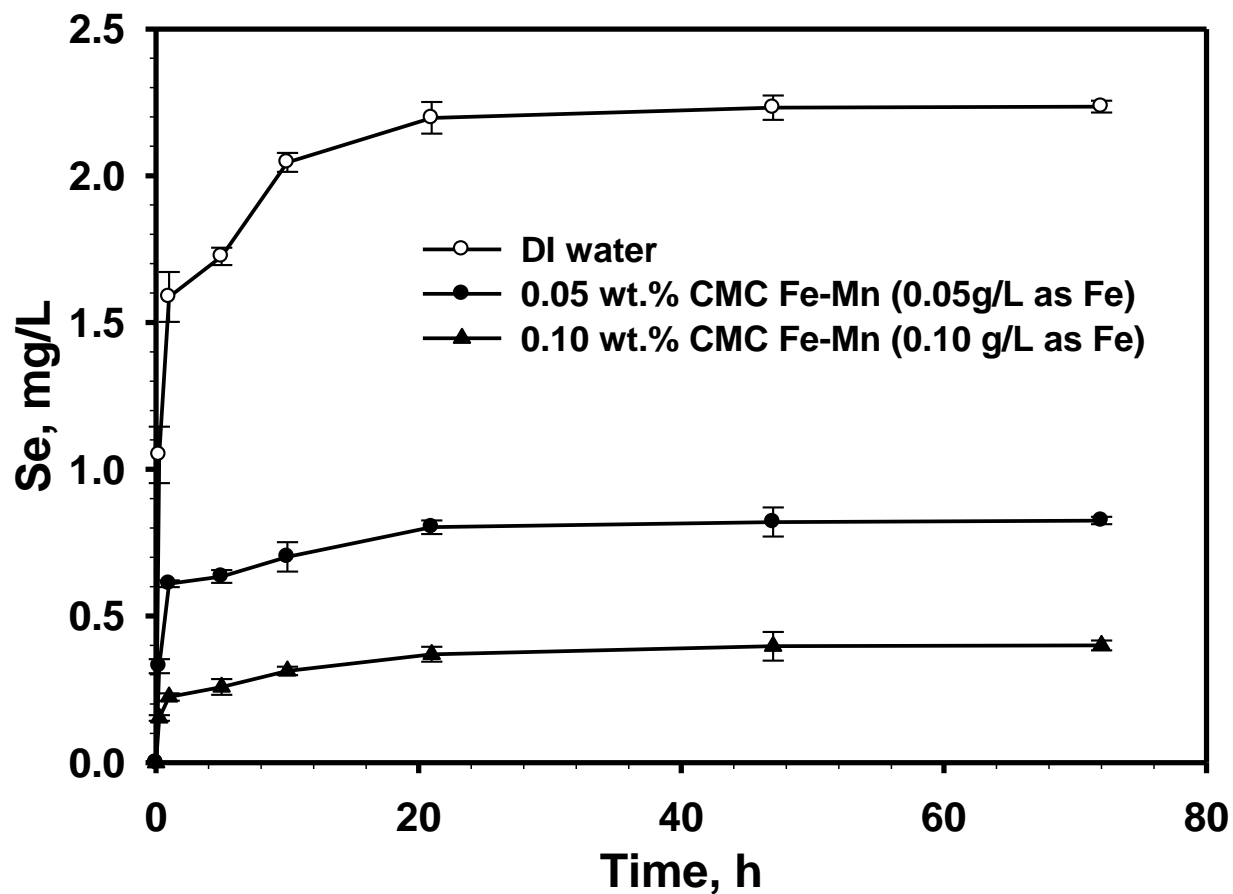
Figure 2-8. Se(IV) desorption rates from a Se-laden sandy soil in the absence or presence of CMC-stabilized Fe-Mn nanoparticles. Experimental conditions: Initial Se in soil = 48 mg/kg; Soil/solution = 1 g/ 10 mL; pH = 6.6-7.2. Data are plotted as mean of duplicate, error bars are calculated as standard deviations.

2.3.5 Mobility of stabilized Fe-Mn nanoparticles in soil

The soil transportability of the nanoparticles was tested through column breakthrough experiments. **Figure 2-9a** shows the breakthrough curves of CMC-stabilized Fe-Mn nanoparticles through the sandy soil at various pore velocities. For comparison, the breakthrough curve of a non-reactive tracer (Br⁻) is superimposed. The software STANMOD with the CXTFIT code for evaluating solute transport in soils and groundwater was employed to model the breakthrough data (Feinstein and Guo, 2004). The CXTFIT code is a modified version for estimating solute transport parameter using a nonlinear least-squares parameter optimization method based on an 1-D convection-dispersion equation as following:

$$R\frac{\partial C}{\partial t} = D\frac{\partial^2 C}{\partial x^2} - v\frac{\partial C}{\partial x}$$ (2-7)

where C is the solution concentration, x is distance, t is time, D is the hydrodynamic dispersion coefficient, v is the average pore water velocity, and R is the retardation factor, defined as:

$$R = 1 + \frac{\rho K}{\theta}$$ (2-8)

where ρ is the soil bulk density, K is an empirical distribution constant, θ is the volumetric water content.

The hydrodynamic dispersion coefficient (D) was obtained by fitting the tracer breakthrough curve, and then applied to simulating the breakthrough curves of the nanoparticles. At the pore velocity of 5.8×10^{-3} cm/s, the full breakthrough of the nanoparticles occurred after ~3.5 PVs with a steady C/C_0 of ~0.9 (i.e., ~10% was consistently retained in the soil), and in comparison, the full breakthrough of the tracer occurred at ~2 PVs ($C/C_0 = 1$). Evidently, the CMC-stabilized nanoparticles were quite mobile in the soil under a hydraulic gradient of 3.6-27.

When the pore velocity was lowered to 7.7×10^{-4} and 3.9×10^{-5} cm/s, the full breakthrough was delayed to 5 PVs and 9 PVs, respectively, though the breakthrough plateau (C/C_o) remained

nearly the same. During the 12-PVs column run, the soil bed retained 21%, 29% and 59% of the nanoparticles, respectively, at the pore velocities of 5.8×10^{-3}, 7.7×10^{-4} and 3.9×10^{-5} cm/s, respectively, indicating the nanoparticle retention can be manipulated by regulating the injection pressure. The soil-retained nanoparticles add strong affinity and capacity for immobilization of selenite. The more gradual breakthrough of the nanoparticles reflects the greater mass transfer resistance, dispersion, and soil filtration effects of the nanoparticles than the tracer (Chen et al., 2006). The subsequently elution tests showed that the deposited nanoparticles were irreversible, i.e., not leachable through water elution (data not shown).

The maximum travel distance of the nanoparticles in soil as a function of the pore flow velocity was calculated by the method by He et al. (2009).

$$L_{max} = -\frac{2}{3}\frac{d_c}{(1-f)\alpha\eta_0}\ln(0.01) \qquad (2\text{-}9)$$

where L_{max} is defined as the maximum travel distance over which 99% removal of the nanoparticles occurs, d_c is the collector grain diameter, f is the bed porosity, α is the attachment efficiency representing the fraction of collisions between particles and collectors that result in an attachment, η_0 is the overall single collector removal efficiency.

$$\alpha = \frac{\eta}{\eta_0} = -\frac{2}{3}\frac{d_c}{(1-f)L\eta_0}\ln(\frac{C}{C_0}) \qquad (2\text{-}10)$$

where L is the porous medium bed height (m), $\frac{C}{C_0}$ is the outlet normalized particle concentration at the full breakthrough. The overall single collector removal efficiency can be broken down into three components (Tufenkji and Elimelech, 2004),

$$\eta_0 = \eta_D + \eta_I + \eta_G \qquad (2\text{-}11)$$

where η_D, η_I, and η_G are single-collector contact efficiencies due to diffusion, interception, and gravitational sedimentation, respectively, which are determined by the following equations:

$$\eta_{\mathrm{D}} = 2.4A_S^{1/3} N_R^{-0.081} N_{Pe}^{-0.715} N_{vdW}^{-0.052} \tag{2-12}$$

$$\eta_{\mathrm{I}} = 0.55A_S N_R^{1.55} N_{Pe}^{-0.125} N_{vdW}^{0.125} \tag{2-13}$$

$$\eta_{\mathrm{G}} = 0.22N_R^{-0.24} N_G^{1.11} N_{vdW}^{0.053} \tag{2-14}$$

$$A_S = \frac{2(1-\gamma^5)}{2-3\gamma+3\gamma^5-2\gamma^6} \tag{2-15}$$

$$N_{Pe} = \frac{Ud_c}{D_\infty} \tag{2-16}$$

$$N_{vdw} = \frac{A}{kT} \tag{2-17}$$

$$N_{\mathrm{G}} = \frac{2}{9}\frac{a_p^2(\rho_p-\rho_f)g}{\mu U} \tag{2-18}$$

where A_s is the porosity-dependent parameter of the Happel's model, f is the porosity of the porous medium (0.34), $\gamma = (1-f)^{1/3}$, N_R is the aspect ratio ($N_R = d_p/d_c$), d_p is the particle diameter (286 nm), d_c is the collector diameter (0.3 mm), N_{Pe} is the Peclet number, U is the flow velocity (m/s), D_∞ is the bulk diffusion coefficient ($D_\infty = kT/(6\pi\mu a_p)$), where k is the Boltzmann constant (1.3805×10^{-23} J/K), T is the absolute temperature (298K), μ is the absolute viscosity of fluid (1.12×10^{-3} kg/(m s)), a_p is the radius of particle (143 nm), N_{vdW} is the van der Waals number, A is the Hamaker constant (1×10^{-20} J), N_G is the gravitational force number, ρ_p is the density of particle (6230 kg/m^3), ρ_f is the density of fluid (999 kg/m^3), and g is the gravitational acceleration (9.81 m/s^2). **Table 2-2** gives the calculated model parameters.

Table 2-2. Experimental conditions and model parameters for simulating the breakthrough curves of the CMC stabilized Fe-Mn nanoparticles.

Porous media	Flow rate (mL/min)	Pore velocity (cm/s)	C/C_0	η_D	$\eta_{I\times10^{-5}}$	$\eta_{G\times10^{-5}}$	η_0	α	L_{max} (m)
Sandy soil	0.15	5.8×10^{-3}	0.91	0.0024	21.18	3.89	0.0027	0.115	4.37
	0.10	3.9×10^{-3}	0.89	0.0033	22.2	6.10	0.0035	0.096	3.95
	0.05	1.9×10^{-3}	0.88	0.0054	24.3	13.21	0.0057	0.065	3.60
	0.02	7.7×10^{-4}	0.88	0.0104	27.26	36.63	0.0110	0.0434	2.83
	0.001	3.9×10^{-5}	0.86	0.0874	39.57	1×10^4	0.0979	0.0067	2.06

Figure 2-9b plots L_{max} as a function of pore velocity. The results indicate that once delivered, the nanoparticles will remain in a confined domain under typical natural flow conditions. For example, at a groundwater velocity of 0.1 m/d, L_{max} of the nanoparticles is 2.1 m. Following the column tests, the hydraulic conductivity of the particle-loaded soil was re-measured to be 6.05±0.9 cm/d, i.e., no significant change from the untreated bed (6.3 ± 0.5 cm/d).
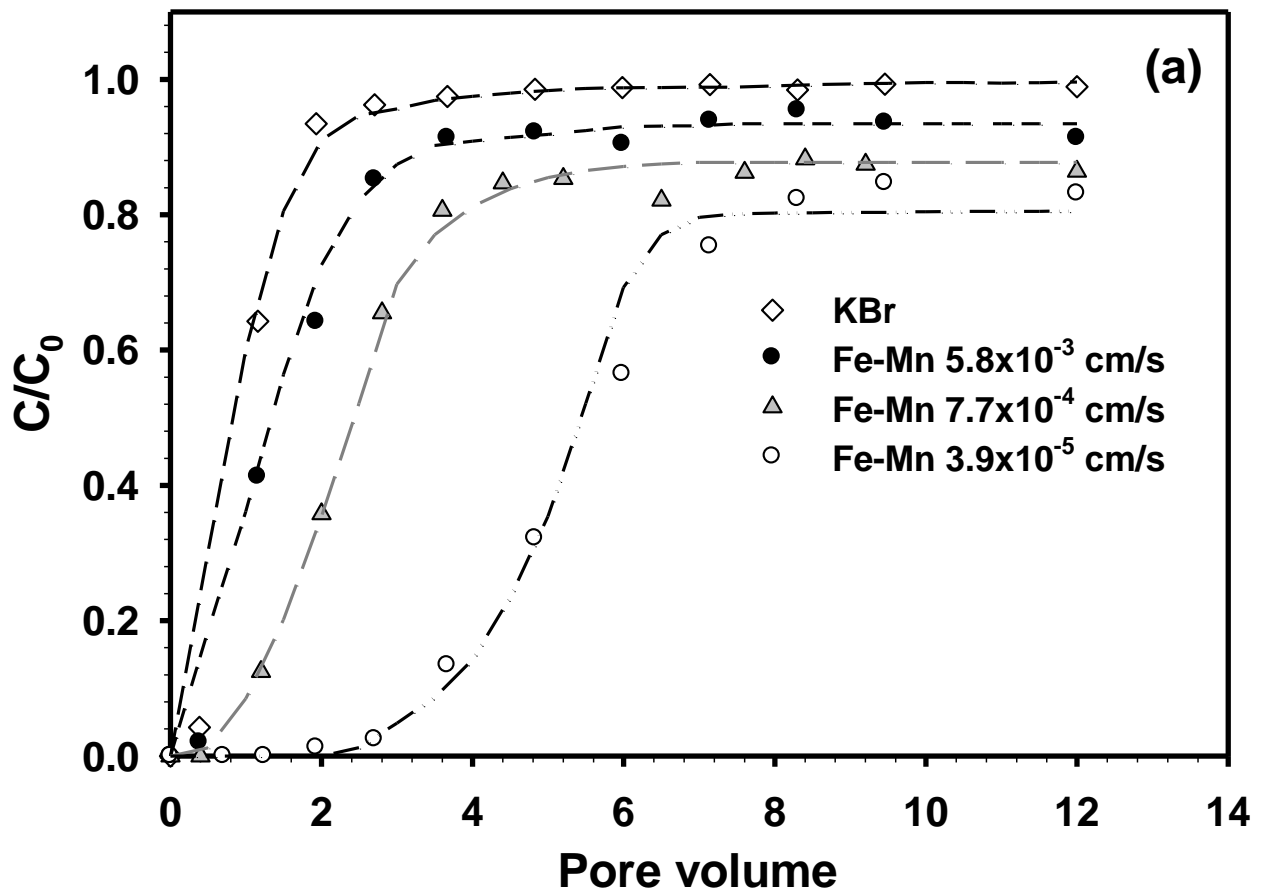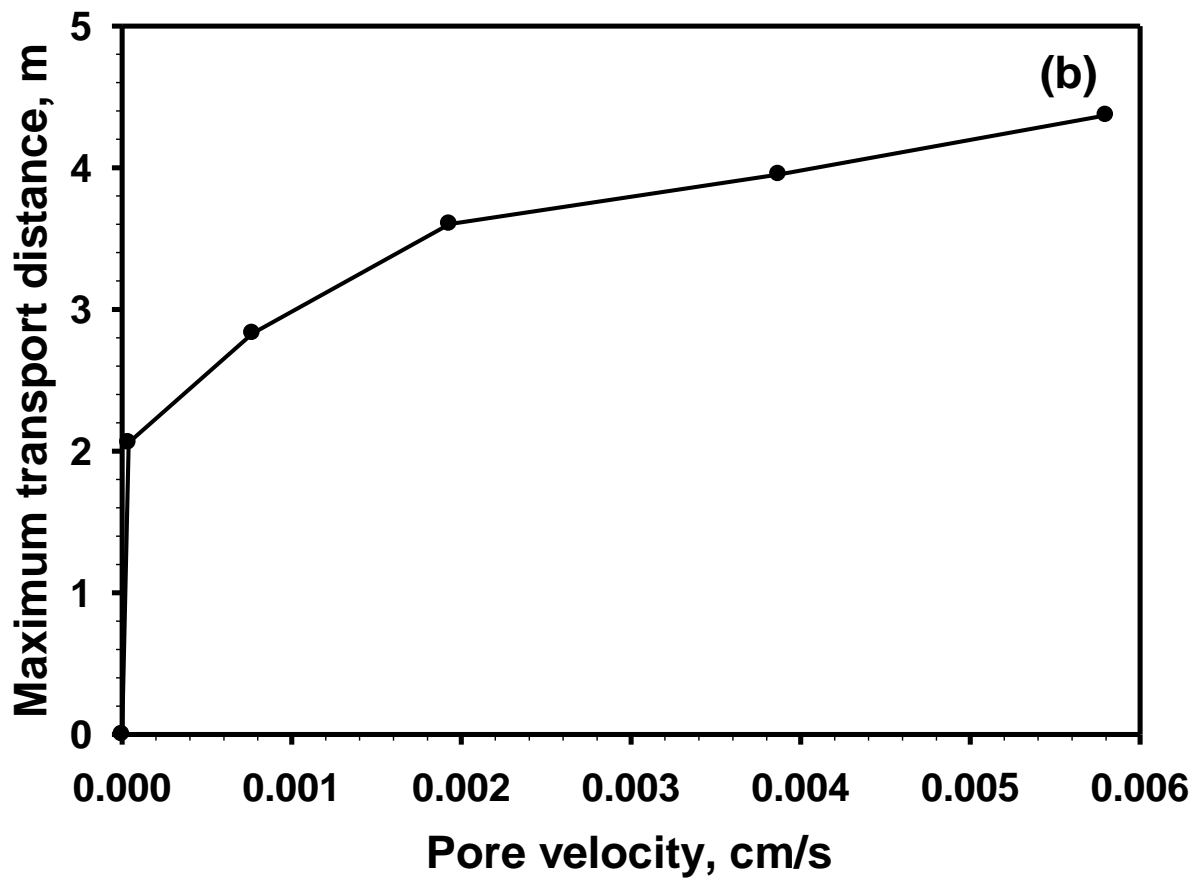
Figure 2-9. (a) Breakthrough curves of bromide and CMC-stabilized Fe-Mn nanoparticles through a sandy soil bed at various pore velocities. (b) Maximum transport distance of CMC-stabilized Fe-Mn nanoparticles in the soil as a function of pore velocity. Br- = 50 mg/L, Nanoparticle = 0.1 g/L as Fe, CMC = 0.10 wt.%, pH = 7.0. Symbols: Experimental data; Lines: Model simulations.

2.3.6 Immobilization of Se(IV) in soil: Column tests

The same fixed-bed column configuration was employed to simulate the application of the nanoparticles for *in situ* immobilization of Se(IV) in the soil. **Figure 2-10a** shows the selenite elution profiles during two parallel column runs, where the Se-laden soil was treated with DI water and the nanoparticle suspension (0.10 g/L as Fe) under otherwise identical conditions. Both elution curves displayed a sharp chromatographic peaking of total Se immediately following the treatment, followed by a gradual tailing profile. Mass balance calculations indicated that DI water leached ~73% of the pre-loaded Se with a peak Se concentration of 35.4 mg/L, while the nanoparticle suspension eluted ~58% of Se with a peak Se of 28.1 mg/L.

It is noteworthy that while DI-water eluted Se is soluble (and thus, more bioavailable and toxic), ~90% of the nanoparticle-eluted Se is associated with the nanoparticles, i.e., the nanoparticles lowered water-soluble Se by >92%. As the eluted nanoparticles are retained by the downstream soil matrix upon release of the external injection pressure, the contaminants sorbed thereon are to be co-immobilized with the nanoparticles.

To test the effects of the nanoparticle treatment on the leachability of Se remaining in the soil, the soil samples from the two column runs in **Figure 2-10a** and untreated Se-laden soil were subjected to the TCLP and WET procedures. **Figure 2-10b** shows that the TCLP-based leachability (**Eq. 2-3**) was 95%, 93% and 19% for the untreated, DI-water eluted and nanoparticle-amended soil samples, respectively, and the WET leachability was 96%, 94% and 25%. The much reduced leachability is attrib2zuted to the strong sink effect of the soil-retained Fe-Mn nanoparticles. When aged for one year at 22±1℃, the leachability was further reduced by ~5% for all cases. Practically, the nanoparticle amendment may facilitate converting hazardous wastes into

non-hazardous wastes by lowering the contaminant leachability, thereby greatly reducing the waste disposal cost.
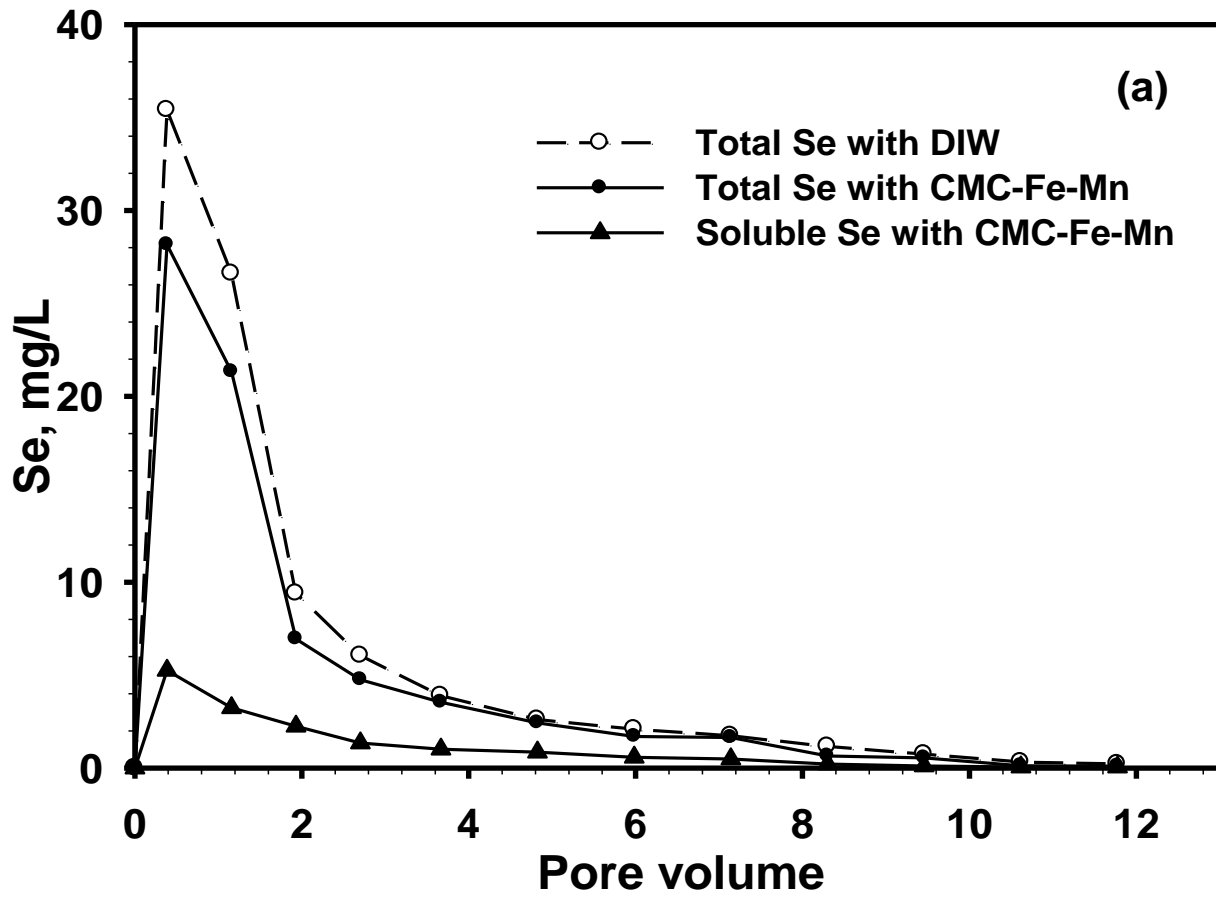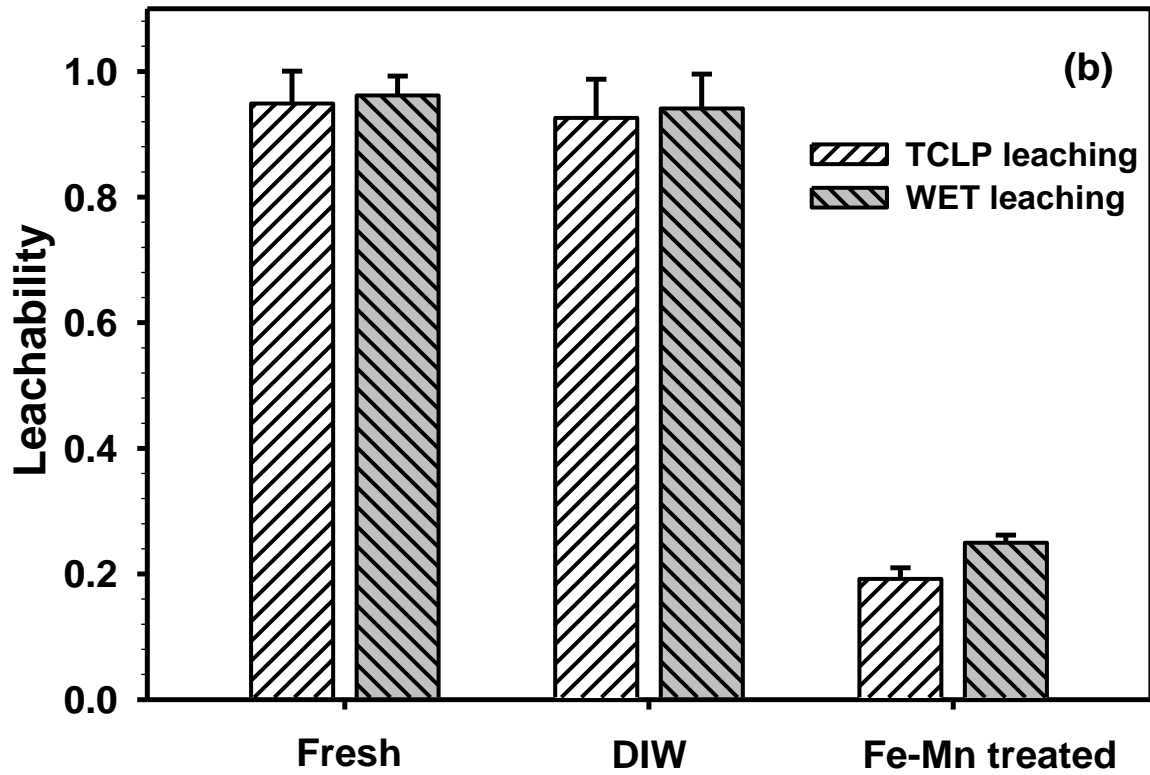
Figure 2-10. (a) Se concentration histories during column elution tests using DI water or a suspension of CMC-stabilized Fe-Mn nanoparticles through a Se-laden sandy soil. Initial Se(IV) = 48 mg/kg-Soil, Nanoparticle = 0.1 g/L as Fe, CMC = 0.10 wt.%, pH = 6.8-7.2, EBCT = 26 min, pore velocity = 5.8×10^{-3} cm/s. **(b) TCLP and WET leachability for Se-laden soil that was untreated or treated in (a).**

2.4 Conclusions

This work investigated the effectiveness of stabilized Fe-Mn binary oxide nanoparticles for *in situ* immobilization of selenite in soil and groundwater. The main findings are summarized as follows:

- Both starch and CMC can act as effective stabilizers to facilitate dispersion of the Fe-Mn nanoparticles. The stabilized nanoparticles showed much higher (> 3 times) Se(IV) sorption capacity than other sorbents reported. The Langmuir maximum capacity was determined to be 100 mg/g, 110 mg/g and 95 mg/g for bare, starch- and CMC-stabilized Fe-Mn nanoparticles, respectively. The nanoparticles are best used at pH<8, and are not suitable for pH above 9.

- Batch desorption tests showed that the presence of 0.1 g/L of CMC-stabilized nanoparticles reduced water leachable Se(IV) by 92%.

- Column breakthrough tests indicated that CMC-stabilized nanoparticles are potentially deliverable in soil, and ~10% of the delivered nanoparticles were retained in the soil after full breakthrough. The delivered nanoparticles remain virtually immobile in soil matrix under natural groundwater conditions and serve as a strong sink for selenite immobilization.

- Column tests demonstrated that amending the Se-laden soil with 12 PVs of CMC-stabilized Fe-Mn (0.1 g/L) reduced the effluent soluble Se by >92%. The nanoparticle amendment also reduced the TCLP and WET leachability of Se(IV) remaining in the soil.

Chapter 3. Controlling Phosphate and Arsenic Releasing from Poultry Litter Using

Stabilized Fe-Mn Oxide Nanoparticles

This chapter presented an application of stabilized Fe-Mn nanoparticles on mitigating the environmental impacts of poultry litter, including the effectiveness of nanoparticles for controlling phosphate and arsenic releasing from poultry litter and the effects of nanoparticles on the performances of poultry litter as a fertilizer. Batch tests were conducted to investigate the phosphate sorption kinetics and isotherms, and the sorption mechanism was investigated by the FTIR tests.

3.1 Introduction

Phosphorus is an essential nutrient for the growth of organisms in natural ecosystems. However, excessive discharge of phosphate into the water bodies often results in eutrophication (algae bloom), especially in confined lakes, reservoirs and coastal areas (Zhao and Sengupta, 1998). Eutrophication leads to accumulation of organic matter and results in taste and odor in water, both of which require costly water treatment processes (Kelleher et al., 2002; Smith et al., 1999). To limit discharge of P from wastewater, effluent P in municipal and industrial wastewater has been well regulated, e.g., the National Pollutant Discharge Elimination System (NPDES) placed a general P permit limit at 1 mg/L for all discharges to surface waters.

However, P released from agricultural wastes such as poultry litter and animal manures has been much less addressed than that from wastewater, though agricultural wastes was known to

49

contain large amounts of P. Based on the reported poultry production statistics from the U.S. Department of Agriculture (USDA), more than 8.52 billion broiler chickens were raised in U.S. in 2013, of which Alabama and Georgia each produced more than 1 billion and 13 other states (such as AR, MS, NC, TX etc.) each produced 168-996 million heads (USDA, 2014). These areas represent primary nutrient contamination concerns due to the long-term high poultry production and land applications of PL as fertilizer (Bednar et al., 2003). Typically, approximately 90% of the PL is disposed of through local land applications (Stolz et al., 2007). In addition, the PL in most areas of US contains organic arsenic due to the extensive uses of organoarsenical feed additive (roxarsone), which is excreted unchanged in the litter by broilers (Garbarino et al., 2003; Jackson and Bertsch, 2001; Morrison, 1967). Consequently, large amounts of nutrients (P and N) and some organic As compounds are released into the environment through either land applications or directly from litter stockpiles (Cortinas et al., 2006; Felton et al., 2007; Wood et al., 1996). Felton et al. (2007) observed that the average P concentration reached as high as 10.8 mg/L in simulated runoff water subjected to PL stockpiles. While eutrophication due to excessive nutrients has been known to be one of the primary water contamination issues in these agriculture-intensive regions, P is also a valuable resource. In fact, P mineral has been listed as one of the 20 critical raw materials that are running out at an alarming rate (EC, 2014). Therefore, there is an urgent need for controlling releases of P from agricultural wastes to prevent water contamination and to facilitate sustainable agricultural practices.

Various chemicals and materials have been applied to amend poultry litter, such as aluminum sulfate, sodium bisulfate, ferrous sulfate, lime, limestone, and zeolite, to control the release N, P and As (Kelleher et al., 2002; Li et al., 2008; Moore et al., 1998). Moore and Miller (1994) reported that the application of alum, lime and ferrous iron was able to reduce the water

soluble P level from >2,000 to <1 mg-P/kg-PL. However, these treatment required fairly high dosages of the chemicals (>2.5 wt.%) and the effective period is usually within 3-4 weeks due to the high solubility of the chemicals (Huff et al., 1984).

Adsorption and chemical precipitation have been the most common practices to remove and recover P from wastewater or streams (Zhao and Sengupta, 1998). A wide variety of materials have been tested in this regard, including fly ash (Chen et al., 2007), blast furnace slag (Oguz, 2004), oxide tailings (Zeng et al., 2004), zeolite (Wu et al., 2006), clay materials (Rao and Mishra, 2005; L. Yan et al., 2010) and iron-based adsorbents (Genz et al., 2004). In recent years, synthetic iron-based adsorbents, especially bimetal oxides and trimetal oxides, have attracted more attention due to the low cost, high adsorption capacity and environmentally friendliness. Borggaard et al. (2005) reported that both ferrihydrite and goethite are effective for phosphate adsorption, with the maximum Langmuir adsorption capacity (Q) being 5.0 and 2.7 μmol/m^2, respectively. Long et al. (2011) synthesized a magnetic Fe–Zr binary oxide, which offered a Q of 13.65 mg-P/g at pH 4 and the advantages of easy magnetic separation and reusability of the spent adsorbent. Zhang et al. (2009) prepared and tested an Fe-Mn binary oxide adsorbent at an Fe:Mn molar ratio of 6:1, and they observed a Langmuir Q of 36 mg-P/g at pH 5.6. Lǚ et al. (2013) synthesized and tested a nanostructured Fe–Al–Mn trimetal oxide adsorbent with an Fe:Al:Mn molar ratio of 3:3:1, and the material offered a Langmuir Q of 48.3 mg-P/g at pH 6.8, which is much higher than that of the single component oxide. However, these absorbents are prepared as granular or powder aggregates that are hardly dispersible in porous media, and thus, are not convenient for treating solid/hazardous wastes (e.g., poultry litter) or for *in situ* soil application.

An and Zhao (2012) prepared a new class of polysaccharide-stabilized Fe-Mn binary oxide nanoparticles using starch or CMC as a stabilizer. Based on DLS measurements, the hydrodynamic

diameter was 350 ± 46 (standard deviation) nm and 247 ± 9 nm for the CMC- and starch-stabilized Fe–Mn nanoparticles, respectively. The stabilized nanoparticle can not only effectively immobilize water soluble As, but also reduce the leachability of the As retained in soil. Moreover, the stabilized nanoparticles, prepared as aqueous suspensions, can be directly injected/delivered into porous materials such as soil to facilitate *in situ* remediation. Given the very similar chemical properties between arsenate and phosphate, and taking advantage of the high sorption capacity as well as the soil-deliverability of the stabilized Fe-Mn nanoparticles, this study aimed to develop a new technology to control the leaching of P and fortuitously As from poultry litter (or other animal wastes) by amending the wastes with the stabilized nanoparticles. The specific objectives were to: 1) prepare and characterize the desired stabilized Fe-Mn nanoparticles using a water-soluble starch or CMC as a stabilizer, 2) investigate the effects of the stabilizers and pH on the phosphate adsorption capacity of the nanoparticles, and 3) test the effectiveness of the stabilized nanoparticles for reducing leachability of phosphate in PL through batch and column experiments.

3.2 Materials and Methods

3.2.1. Materials

Chemicals of analytical or higher grade were used in this research. $FeCl_2 \cdot 4H_2O$, $KMnO_4$, CMC (sodium salt, MW = 90,000), and a hydrolyzed potato starch were purchased from Acros Organics (Morris Plains, NJ, USA). $Na_2HPO_4 \cdot 7H_2O$ and NaOH were purchased from Fisher Scientific (Pittsburgh, PA, USA). Hydrochloric acid, sulfuric acid and nitric acid were purchased from Mallinckrodt Chemical (St. Louis, MO, USA). $K(SbO)C_4H_4O_6$ and $(NH_4)_6Mo_7O_{24}$ solutions were purchased from Ricca Chemical (TX, USA). Ascorbic acid was purchased from Alfa Aesar (MA, USA).

A commercial PL with the trade mark Black Hen was purchased from a local store Lowes (Opelika, AL, USA). The processed granular PL was first air-dried (at room temperature of 21 ± 1 °C and humidity of $45 \pm 2\%$), sieved through a 2-mm screen and then used in the experiments. **Table 3-1** gives the elemental compositions of the poultry litter sample.

Table 3-1. Elemental compositions of a commercial poultry litter sample.

As	24.52 ± 1.98 (mg/kg)
Pb	1.44 ± 0.04 (mg/kg)
P	14359 ± 778 (mg/kg)
C	3.65 ± 0.01 (wt.%)
N	0.45 ± 0.01 (wt.%)
S	0.14 ± 0.01 (wt.%)

* Based on air-dried PL weight Trace element data given as mean of duplicates; errors refer to deviation from the mean.

A sandy soil was taken from the E.V. Smith Research Field (Tallassee, AL, USA). The soil was first sieved through a 2-mm screen, then washed with tap water to remove soluble compounds and suspended solids, and then air-dried (An and Zhao, 2012). The salient soil properties include: OM (organic matter) = 0.1 wt.%, CEC = 0.5 meq/100g, Fe = 4 mg/kg, P < 1 mg/kg, and no As was detected. The hydraulic conductivity was measured to be 6.3 ± 0.5 cm/day following the constant head method. All solutions were prepared with ultrapure DI water (18.2 Ωcm^{-1}).

3.2.2 Preparation and characterization of Fe-Mn nanoparticles

Stabilized Fe-Mn oxide nanoparticles were prepared following the redox-precipitation method as described in a prior work (Xie et al., 2015). In brief, a desired volume (0-30 mL) of a starch or CMC stock solution (1 wt.%) was added into a 250 mL glass flask containing 150 mL of an $FeCl_2$ solution (2.39 mM) and mixed for 20 min under N_2 purging. Then, 10 mL of a $KMnO_4$ solution (11.9 mM) was added into the mixture under vigorous stirring, and the desired nanoparticles were obtained according to the redox reaction (Eq. 2-2).

The pH of the mixture was adjusted immediately to 7.5 using 1 M NaOH and the total volume of the mixture was maintained at 200 mL by adding DI water (0-10 mL) and/or a phosphate working solution (0-10 mL). The resulting nanoparticle suspension contained 0.1 g/L Fe and 0.03 g/L Mn with a stabilizer concentration of 0-0.15 wt.%. For comparison, bare (non-stabilized) particles were prepared in the absence of a stabilizer via otherwise the same approach. The nanoparticles were allowed to grow for 1 h under shaking at 200 rpm before the subsequent experiments. Fully stabilized nanoparticles were obtained with ≥0.10 wt.% CMC or starch, while partially stabilized or bridged particles were obtained at lower stabilizer dosages. While stabilized nanoparticles remained fully dispersed in water as suspensions, bare or bridged particles settled completely in 10 or 60 min, respectively.

FTIR measurements were performed to investigate the interactions between stabilizers (CMC and starch) and Fe-Mn oxide nanoparticles, and the phosphate adsorption mechanisms. To this end, bare, CMC- or starch-stabilized Fe–Mn nanoparticles before and after adsorption of phosphate were vacuum-dried and ground into fine powders, and then mixed with KBr powder. The mixtures, consisting of 2 wt.% of the nanoparticles, were pressed into thin pellets. FTIR spectra were then obtained using a SHIMADZU IR Prestige-21 spectrometer (Japan) over the

wave number ranging from 4000 to 400 cm^{-1}. For comparison, FTIR spectra for neat CMC and starch were also acquired in the same manner.

3.2.3 Batch tests: adsorption of phosphate from water

A series of batch kinetic tests were carried out to test the phosphate adsorption rate and extent using bare, bridged and stabilized Fe-Mn nanoparticles, respectively. The adsorption tests were initiated by adding a known volume of a phosphate solution into a nanoparticle suspension in accord with the following experimental conditions: total suspension volume = 200 mL, nanoparticle dosage = 0.1 g/L as Fe, initial phosphate = 5 mg/L as P and initial pH = 7.0. The mixtures were continuously mixed on a platform shaker at 200 rpm. At predetermined times, samples were taken, filtered through a 25 nm mixed cellulose esters membrane (MF-Millipore Corp., Billerica, MA, USA), which was able to completely remove the nanoparticles, but did not remove the soluble phosphate. The filtrates were then acidified to pH < 2.0 with 1M HNO_3 and analyzed for P. All the tests were conducted in duplicates and control tests were carried out without the nanoparticles.

Adsorption equilibrium tests were carried out by equilibrating the phosphate adsorption batch systems for 48 h. To obtain the adsorption isotherms, the initial phosphate concentration spanned from 0 to 100 mg/L as P; to test the stabilizer effects, the concentrations of starch and CMC were varied from 0 to 0.13 wt.%; to test the pH effects, the solution pH was varied from 4 to 11; and to test the effects of competing ions, sulfate (1 mM) or carbonate (1 mM) was introduced in the reactors at pH 7. The pH of the suspensions was kept constant during the course of the experiments using 0.1 M HCl and 0.1 M NaOH. $NaNO_3$ was maintained at 0.01 M in all the reactors to simulate the background ionic strength.

3.2.4 Batch tests: leachability of phosphate in poultry litter

Batch desorption tests were carried out to test the P leaching rate from PL with or without the nanoparticle amendment. The leaching tests were initiated by mixing 1 g of an air-dried PL sample with 200 mL of DI water or a suspension of starch- or CMC- stabilized Fe-Mn particles (Fe = 0.1 g/L, starch or CMC = 0.1 wt.%). The pH of the mixture was kept at 6.8 ± 0.4. The mixtures were continuously mixed on a platform shaker operated at 200 rpm at room temperature. Samples were then taken, filtered and analyzed for total P and inorganic P.

3.2.5 Column tests: Leachability of P from nanoparticle-amended poultry litter upon simulated land application

To test the hypothesis that the nanoparticle amendment can not only retain P that would be lost from PL, but also reduce the P leaching ability from PL when the PL is land-applied as a fertilizer. Column elution tests were carried out to investigate the transport behavior of nanoparticle adsorbed P under simulated land application. The column experimental setup consists of an HPLC pump (Series II), a Plexiglas column (inner diameter = 10 mm and length = 150 mm; Omnifit, Cambridge, England), and a fraction collector (Eldex Laboratories, Napa, CA, USA). Before the column tests, 5 g of a PL sample was treated with 50 mL of a CMC-stabilized Fe-Mn nanoparticle suspension (0.2 g/L Fe with 0.2 wt.% CMC) for 96 hours following the procedure in the batch tests. The mixture of the PL and nanoparticles was then air-dried on a glass plate, and then mixed with the sandy soil at a PL-to-soil ratio of 1:4 by weight to simulate the land application of PL. The total P mass in each column bed was kept the same (i.e., 23 mg). Then, 6.2 mL of the PL-soil mixture was then dry-packed into the column that was pre-loaded with 3.1 mL of the sandy

soil. Column elution tests were then initiated by pumping a simulated groundwater (7 mM NaCl and 0.86 mM $CaSO_4$ at pH 6.5) through the PL-soil bed in the down-flow mode (flow rate = 0.05 mL/min). The effluent samples were collected by the fraction collector. The samples were acidified to pH 3.0 to dissolve all the particles using 5 M HNO_3, then filtered through the 25 nm membrane, and then the filtrates were analyzed to give the total P and As (i.e., soluble + nanoparticles-bound). To qualify the soluble P and As in the effluent, aliquots of the samples were also directly filtered to remove the nanoparticles and nanoparticles-bound P and As, and the filtrates analyzed without acidification. For comparison, P and As elution curves were also acquired with untreated PL under the identical operating conditions. To facilitate a fair comparison, the total masses of P and As were kept equal for the two cases.

3.2.6 Analytical methods

The total P, As, Fe and Mn concentrations were analyzed by a Varian 710-ES ICP OES, which offered a detection limit of 3, 2, 0.2, 0.05 μg/L, respectively. The inorganic phosphate was determined per EPA method 4500-P E (Ascorbic Acid Method) using a HP UV-Vis absorption spectroscopy. The solution pH was measured using an Oakton pH meter (pH 510 Benchtop Meter, Oakton, CA, USA).

The elemental analysis of the PL and sandy soil was performed following the EPA method 3050B. Microwave heating was employed to digest the PL samples, which is superior to the conventional hot plate heating for enhanced reaction control and thus improved precision (Lorentzen and Kingston, 1996). Briefly, air-dried PL samples (0.5 g each) were digested in sealed Teflon containers in a microwave with 1 mL H_2O_2 for 15 min and followed by 5 mL of nitric acid for 30 min and diluted to 50 mL water after digestion. Elemental analysis was then carried out

with an inductively coupled plasma-mass spectrometry (Perkin-Elmer Elan 6000 ICP-MS) for As, Pb, P, C, N and S.

3.3 Results and Discussion

3.3.1 Characterization of Fe-Mn nanoparticles

Based on our previous study (Xie et al., 2015), the TEM-based mean diameter of the CMC-stabilized nanoparticles was estimated to be 38 ± 9 nm, whereas the starch-stabilized nanoparticles appeared as bridged aggregates with a mean primary particle size of 47 ± 11 nm. The bare particles were present larger aggregates ranging from tens to hundreds of nm. The DLS-based hydrodynamic diameter was 286 ± 27 nm and 198 ± 13 nm for CMC- and starch-stabilized nanoparticles, respectively. The zeta potential for starched nanoparticles was nearly neutral over the pH range of 3.5-7.1, and turned to slightly negative thereafter to around -8 mV at pH 10; in contrast, the zeta potential turned much more negative to -19 mV to -42 mV for CMC-stabilized nanoparticles.

(a)

Fe-Mn

CMC Fe-Mn

CMC

Starch Fe-Mn

Starch

3400

3450

3500

3430

3500

2900

540

1412

1620

1050

1640

1440

1630

1412

1650

1450

1050

Transmittance

Wavenumber, cm^{-1}

4000   3500   3000   2500   2000   1500   1000   500
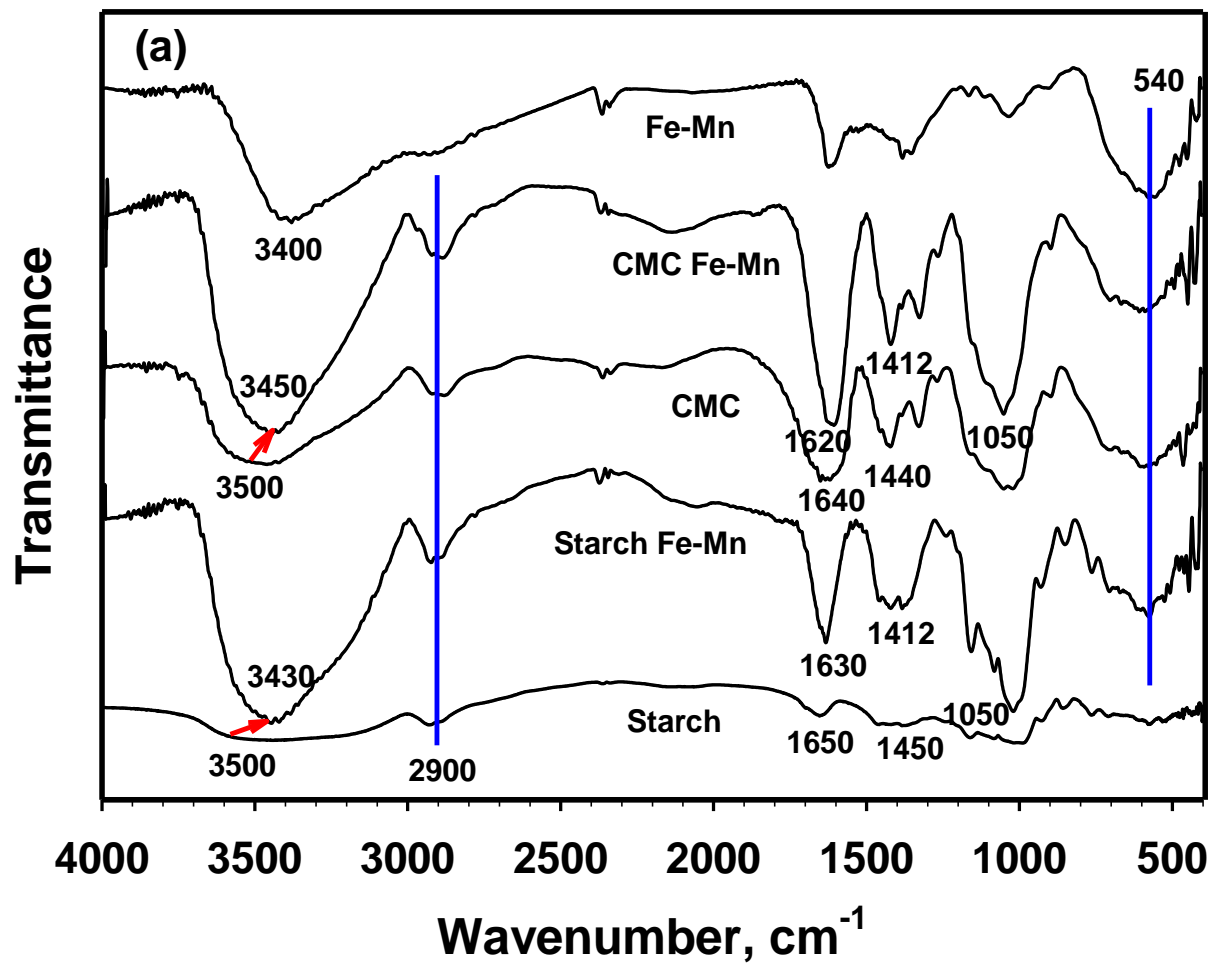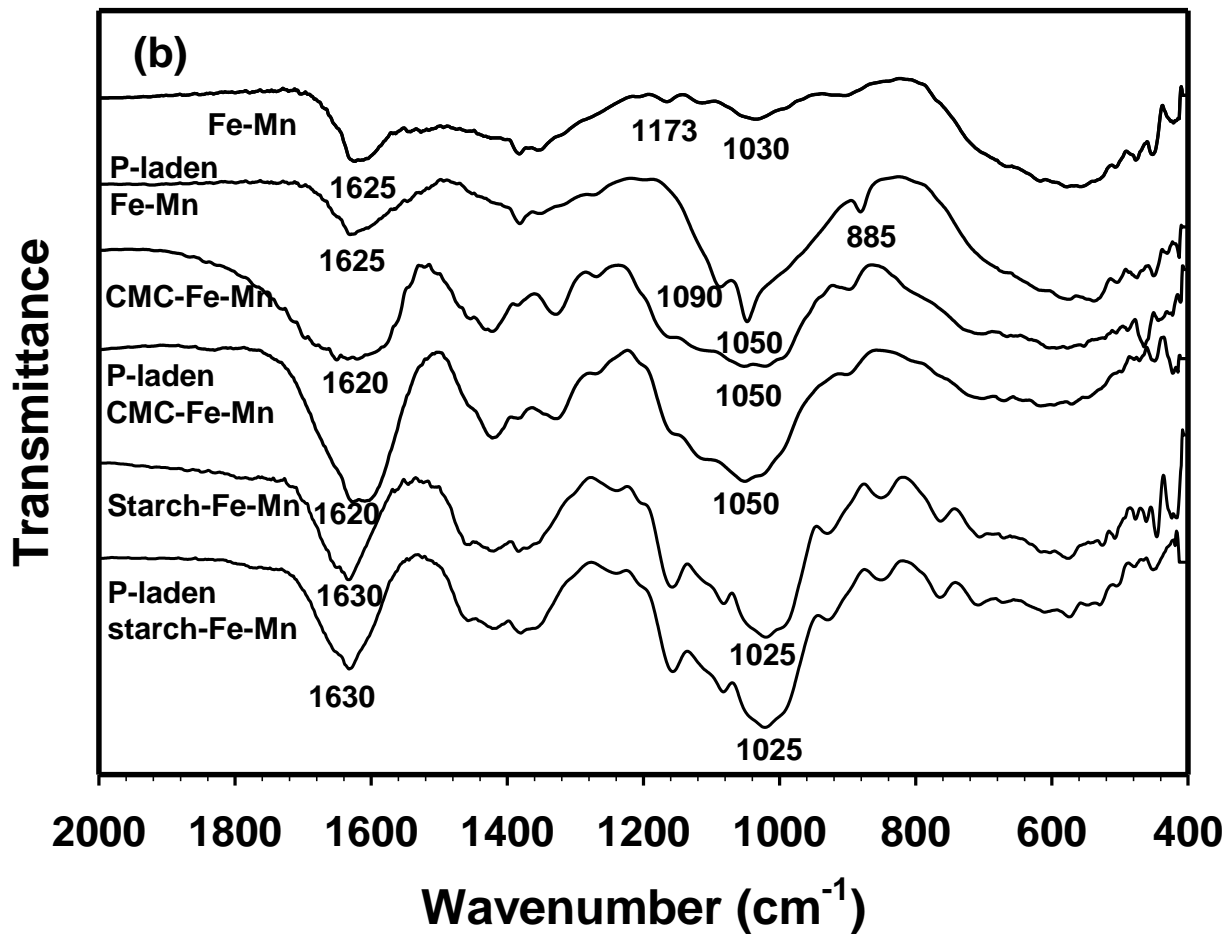
Figure 3-1. FTIR spectra of (a) neat CMC and starch, and bare, CMC- or starch-stabilized Fe–Mn nanoparticles (arrows indicate shifts of the peaks), (b) Fe–Mn particles before and after phosphate sorbed.

Figure 3-1a presents the FTIR spectra of neat CMC and starch as well as bare and stabilized Fe–Mn nanoparticles. The peaks at ~2900 cm^{-1} (except bare Fe-Mn) indicate the C-H stretching vibrations from the CH$_2$ groups of starch or CMC (An and Zhao, 2012; Maity and Agrawal, 2007). The peaks at 3500 and 1050 cm^{-1} for neat CMC and starch were ascribed to the −OH stretching, and the peaks at 3500 cm^{-1} were shifted to 3450 cm^{-1} for CMC-stabilized Fe-Mn and 3430 cm^{-1} for starch-stabilized Fe-Mn, which is attributed to the enhanced intermolecular hydrogen bonding between the stabilizers and particle surfaces (He et al., 2007). The COO$^-$ group interactions were detected at the peaks of 1640 and 1440 cm^{-1} for neat CMC and 1650 and 1450 cm^{-1} for neat starch, respectively, and these peaks were shifted to 1620 and 1412 cm^{-1} for CMC stabilized Fe-Mn and to 1630 and 1412 cm^{-1} for starch stabilized Fe-Mn. The shift for starch was due to O–H bond from water, indicating more water molecules were bound on the particle surface (An and Zhao, 2012). By comparing the wavenumber separation between the two COO$^-$ peaks, it can be inferred that the bidentate bridging is the primary binding mechanism between the Fe-Mn particles and the stabilizers (Gong et al., 2014). In addition, a peak at 540 cm^{-1} was detected in all cases, indicating the existence of iron (hydr)oxides, which was comparable to the reported characteristic wavenumbers of 560 cm^{-1} for ferrihydrite (Voegelin and Hug, 2003), 580 cm^{-1} for magnetite (Zhang et al., 2005) and 580 cm^{-1} for amorphous iron(III)-hydroxide (Ristić et al., 2007). The FTIR results suggest that the stabilization of the Fe-Mn particles is mainly achieved by the adsorption of stabilizers on the particle surface via carboxylate and hydroxyl groups.

Figure 3-1b shows FTIR spectra for bare and stabilized Fe-Mn particles before and after phosphate adsorption. For the bare Fe–Mn particles, the peak at 1625 cm^{-1} is caused by the deformation of water molecules and indicates the presence of physisorbed water on the oxides (Zhang et al., 2009); the two peaks at 1173 and 1030 cm^{-1} are attributed to the bending vibration

of hydroxyl groups of iron (hydr)oxides (Fe–OH), indicating the band strength of Fe-O groups (540 cm^{-1}) was reduced by the presence of Mn in iron oxide. Similar observations were reported by Zhang et al. (2005) who studied arsenate adsorption by Fe–Ce binary metal oxides, and found the bond strength of Fe–O was weakened and two new peaks at 1126 and 1067 cm^{-1} appeared (Fe–OH groups) in the presence of Ce. Upon the phosphate uptake, the Fe–OH bending bands (peaks at 1173 and 1030 cm^{-1}) disappeared completely, while a new peak appeared at 1050 cm^{-1}. This new band, which is broad and intensive, could be assigned to the asymmetry P-O vibration (Zhang et al., 2009), which indicates that the surface hydroxyl groups were replaced by the adsorbed $H_2PO_4^-$ or HPO_4^{2-}, i.e., phosphate is bound to the nanoparticles through Fe-O-P complexation, which is a ligand exchange process. Arai and Sparks (2001) compared FTIR bands for phosphate species dissolved in water and sorbed on the surface of ferrihydrite and observed two peaks for monoprotonated phosphate (HPO_4^{2-}) at 1077 cm^{-1} (symmetric bending) and 989 cm^{-1} (symmetric stretching). After adsorption, the peaks were shifted to 1070 and 1020 cm^{-1}, indicating the formation of inner sphere surface complexes (in the form $\equiv Fe_2PO_4$), which is similar to phosphate binding on goethite surfaces (Luengo et al., 2006). For stabilized Fe-Mn particles, the peaks for P-O upon P adsorption was overlapped with those of the COO^- and $-OH$ groups, resulting in a stronger peak intensity compared to those without phosphate. The FTIR results suggest that the phosphate adsorption occurred via ligand exchange with hydroxyl groups on the particle surface and through inner sphere complexation.

3.3.2 Effect of stabilizers on phosphate sorption

Figure 3-2 shows the equilibrium phosphate uptake by Fe-Mn particles prepared with various concentrations of starch or CMC. Based on particle stability analysis, the critical

stabilization concentration, i.e., to the minimum stabilizer needed to completely stabilize the nanoparticles (0.1 g/L as Fe), was 0.10 wt.% for starch or 0.08 wt.% for CMC. Compared to the bare Fe-Mn particles, the particles prepared with the sub-CSC stabilizer concentrations offered lower phosphate adsorption capacity. Yet, increasing the stabilizer concentration progressively increased the phosphate uptake, and a maximum uptake was observed at 0.1 wt.% for both CMC and starch, where the uptake was ~10% higher than that for the bare particles. Further increasing the stabilizer concentration resulted in inhibited phosphate uptake.
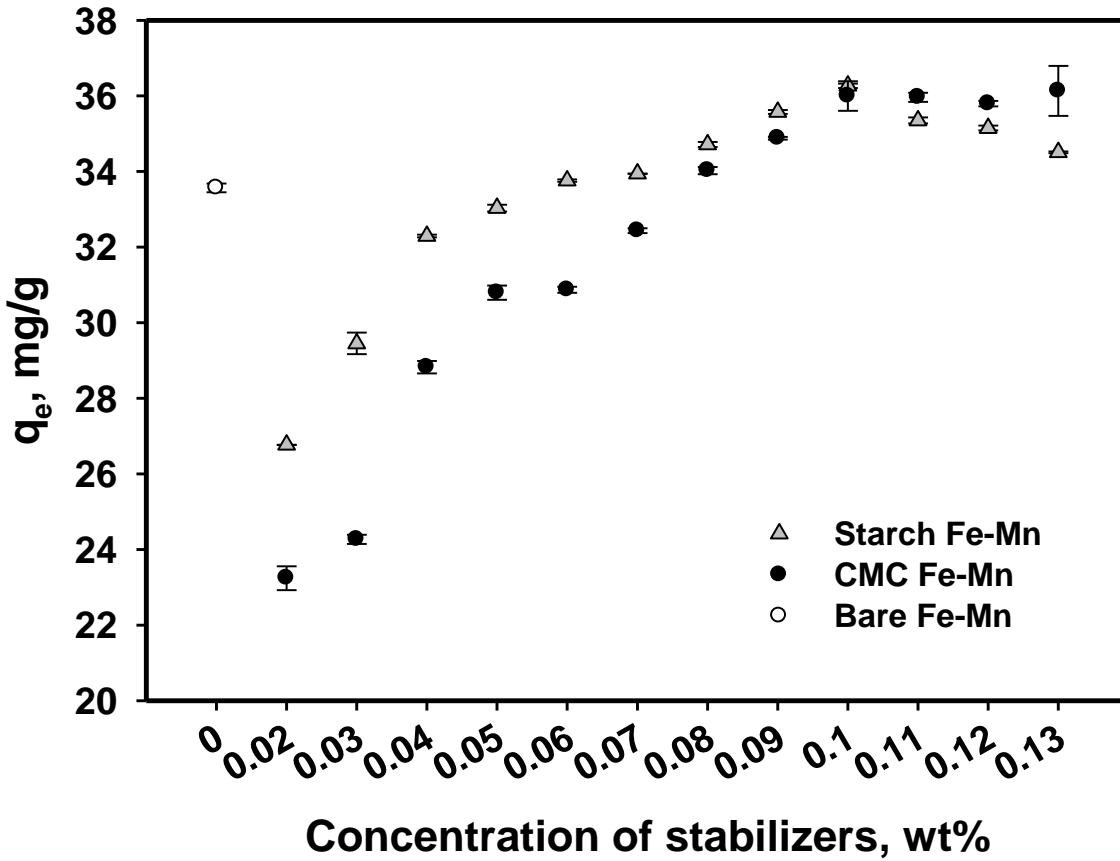
Figure 3-2. Equilibrium phosphate uptake (q$_e$) as a function of stabilizer type and concentration. Experimental conditions: Fe-Mn = 0.1 g/L as Fe; pH = 6.8-7.2; Initial P = 5 mg/L. Data are plotted as mean of duplicate, error bars are calculated as standard deviations.

The use of the stabilizers can pose some contrasting effects on the phosphate uptake. First, increasing the concentration of the stabilizers results in smaller particles, which offer greater specific surface area and higher adsorption capacity. Second, elevating the surface excess of the stabilizer molecules on the particles can inhibit the phosphate uptake both thermodynamically and kinetically by occupying and/or blocking the adsorption sites. Third, the stabilizer coating on the particle surface can alter the surface potential, which in turn can greatly impact the interactions between the particles and phosphate oxyanions. The lower uptake at the sub-CSC stabilizer concentration is attributed to surface blocking effects of the stabilizers. However, with elevated stabilizer concentrations, the gain in specific surface area outweighs the surface blockage until a maximum uptake point is reached (at ~0.1 wt.%). Further increasing the stabilizer concentration results in greater surface blocking with little further gain in specific surface area. Between starch and CMC, the coating of the neutral starch molecules on the particle surface renders a rather neutral zeta potential at the experimental pH 7.0, while the sorption of the highly negative CMC molecules (pK_a = 4.3) gives a very negative surface potential (-40 mV). As phosphate are present predominantly as $H_2PO_4^-$ and HPO_4^{2-}, adsorption of phosphate will have to overcome a greater energy barrier due to the electrostatic repulsive effect. . On the other hand, CMC stabilizes the particles through both electrostatic and steric interactions, whereas starch stabilizes through only steric repulsion. Consequently, CMC is a much more effective stabilizer that gives smaller nanoparticles (38±9 nm for CMC-stabilize Fe-Mn and 47±11 nm for starched Fe-Mn).

From the practical application standpoint, the fully stabilized nanoparticles not only offers 10% greater phosphate capacity, but also the convenience that these well-dispersed particles can be more easily delivered in and mixed with PL. Furthermore, the applied nanoparticles, which are richly loaded with phosphate, can be easily distributed in the top soil, acting as a slow-releasing P

source for crops. In the subsequent tests, 0.1 wt.% was chosen as the optimal stabilizer concentration for both starch and CMC.

3.3.3 Phosphate sorption kinetics
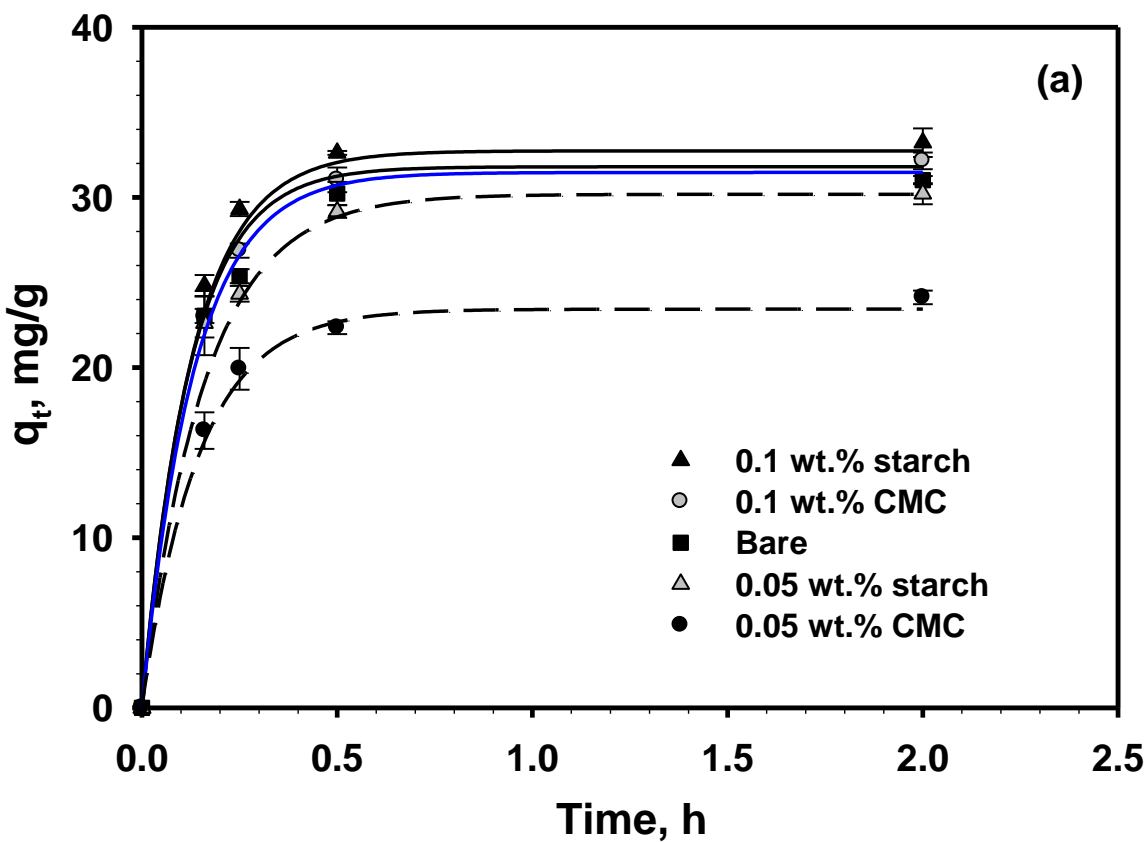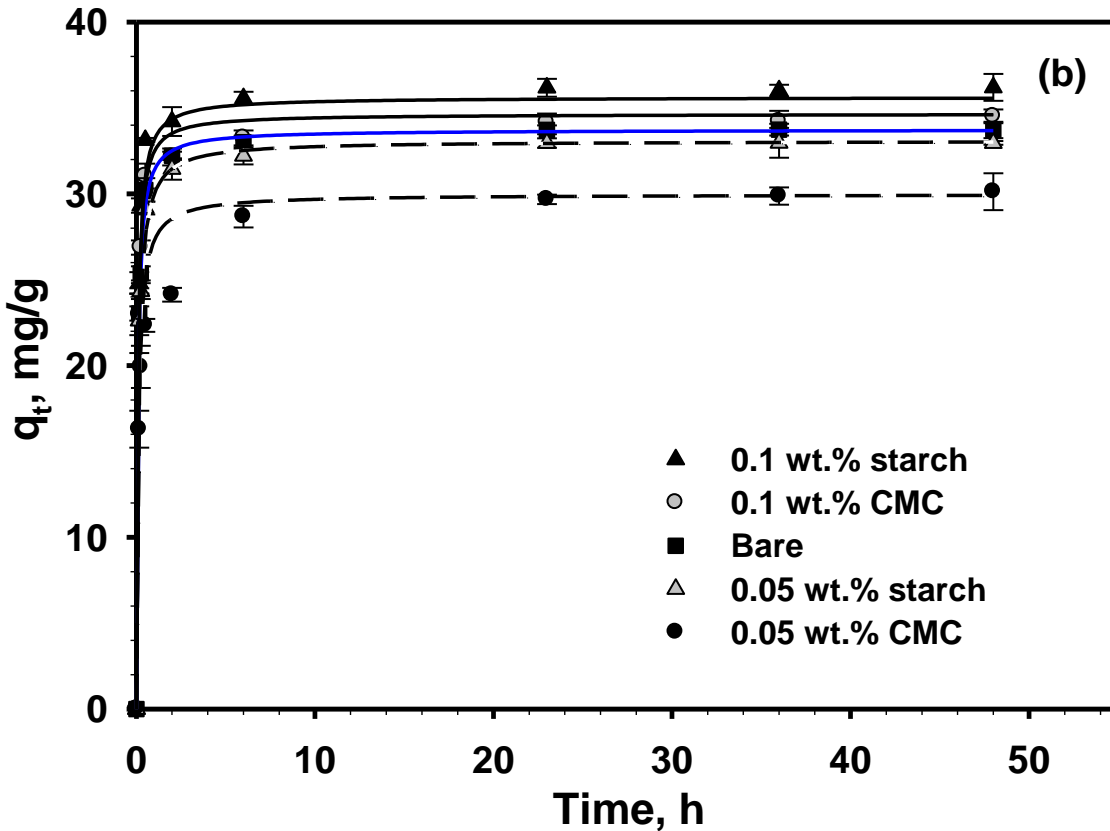
Figure 3-3. Phosphate uptake as a function of time using bare, partially stabilized and fully stabilized Fe-Mn nanoparticles under otherwise identical conditions: (a) 0-2 h; (b) 0-48 h. Experimental conditions: CMC or starch = 0.1 wt.% for fully stabilized particles, CMC or starch = 0.05 wt.% for partially stabilized particles, Fe-Mn = 0.1 g/L as Fe, Initial P = 5 mg/L. Solution pH was kept at 7.0 ± 0.2 in all cases. Symbols: Experimental data; Lines: (a) Pseudo first-order kinetic model simulations, (b) Pseudo second-order kinetic model simulations.

Figure 3-3 shows phosphate adsorption rates for bare, partially stabilized, and fully stabilized Fe-Mn nanoparticles at a nanoparticle dosage of 0.1 g/L as Fe under otherwise identical conditions. The control tests with DI water, 0.1 wt.% starch or CMC solution indicated no mass lose due to reactor adsorption, filtration and sample processing. Overall, the phosphate adsorption

reached equilibrium within 24 h. The process consisted of two distinct stages: a rapid initial uptake, where more than 80% of phosphate was removed in 2 h, followed by a much slower gradual adsorption phase until the equilibrium reached. The initial rapid uptake is characteristic of fine particles and is attributed to the small particle size and easier accessibility to the adsorption sites than for conventional granular materials; while the slower second stage is due to: 1) steric and electrostatic resistance, 2) elevated mass transfer resistance in the micropores of the aggregates, and 3) additional mass transfer barrier due to the sorbed stabilizer molecules. Overall, the nanoparticles offered much faster adsorption rates than conventional adsorbents such as ion exchangers and iron hydro(oxides).

The equilibrium uptake follows the order of: Starch-stabilized Fe-Mn (94%) > CMC-stabilized Fe-Mn (93%) > Bare Fe-Mn (87%) > Starch-bridged Fe-Mn (85%) > CMC-bridged Fe-Mn (80%). Overall, the starch-stabilized nanoparticles offered the highest capacity and fastest adsorption rate. For example, at 0.5 h, starch-stabilized Fe-Mn removed 90% of the initial P, while CMC-stabilized and bare nanoparticles removed 84% and 80%, respectively. The greater uptake and faster rate of both starch- and CMC-stabilized nanoparticles are attributed to the larger specific surface area and smaller size of the nanoparticles. Between CMC and starch, although CMC resulted in smaller particles, the highly negative surface of CMC-stabilized particles provided an unfavorable condition due to electrostatic exclusion to the target phosphate oxyanions.

Figure 3-3a shows that the pseudo-first-order kinetic model was able to adequately simulate the experimental kinetic data during the initial rapid uptake (0-2 h) for all cases, while the pseudo-second-order kinetic model was more suitable for the whole adsorption process (0-48 h) (**Figure 3-3b**). **Table 3-2** gives the models, the best-fitted rate constants and the correlation coefficient (R^2). Good data fitting ($R^2 > 0.92$) was observed for both kinetic model for all types of

nanoparticles, suggesting that at the initial rapid adsorption stage the phosphate concentration is the rate-limiting step, while at the following gradual adsorption stage the chemisorption process is the rate-limiting step, involving valency forces through sharing or exchanging of electrons between phosphate and Fe-Mn particles as covalent forces and ion exchange (Ho, 2006). This result is comparable with the findings by Zhang et al. (2009) and Yan et al. (2010), who studied phosphate adsorption kinetics on non-stabilized Fe-Mn oxides and various bentonites, respectively.

Table 3-2. Best fitted kinetic model parameters for phosphate adsorption by various particles.

Kinetic models	Parameters	Bare	CMC-stabilized	Starch-stabilized	CMC-bridged	Starch-bridged
Pseudo First order	R^2	0.925	0.995	0.982	0.997	0.925
$q_t = q_e(1-e^{-k_1 t})$	q_e mg/g	30±2	31.5±0.8	31.8±0.9	23.4±0.5	28±2
	k_1 1/h	6.2±0.9	7.5±0.7	8.1±0.9	6.9±0.5	7±2
Pseudo Second order	R^2	0.998	0.996	0.992	0.923	0.970
$q_t = q_e^2 k_2 t/(1+k_2 q_e t)$	q_e mg/g	33.7±0.7	35.7±0.2	36.4±0.8	30±2	32±1
	k_2 g/(mg h)	0.40±0.02	0.44±0.03	0.46±0.01	0.29±0.04	0.49±0.02

Note: t is the reaction time, q_t (mg/g) is the sorbed phosphate at time t, q_e (mg/g) is the sorbed phosphate at equilibrium, k_1 (1/h) and k_2 (g/(mg h)) are the rate constants of the pseudo-first-order and pseudo-second-order kinetics model, respectively.

3.3.4 Effects of pH and competing co-ions on phosphate adsorption
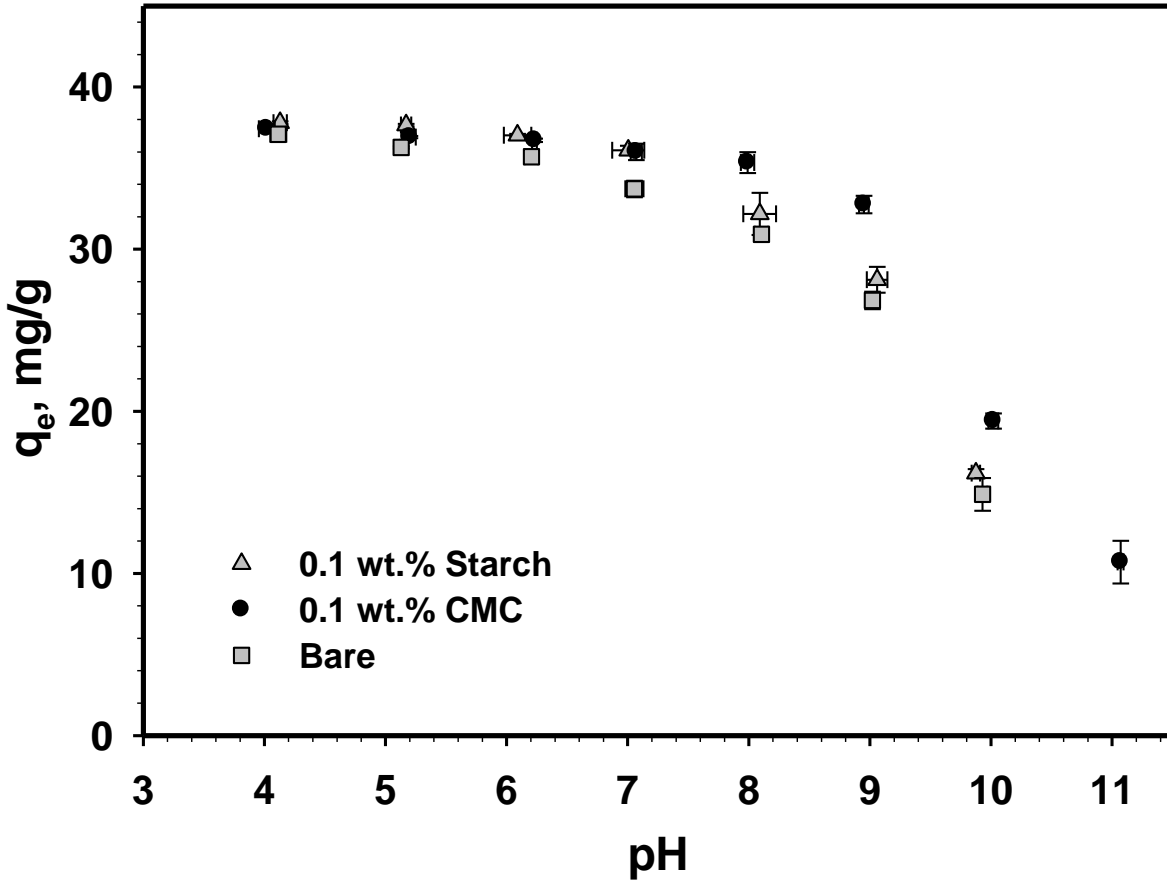
Figure 3-4. Equilibrium phosphate uptake as a function of solution pH for bare, stabilized Fe-Mn nanoparticles. Experimental conditions: Initial P = 5 mg/L, Fe-Mn = 0.1 g/L as Fe, CMC or starch = 0.1 wt.%, Equilibrium time = 48 h.

Figure 3-4 shows effects of pH on the equilibrium phosphate uptake for bare and starch- or CMC- stabilized Fe-Mn particles. While the adsorption edge profile is consistent with other types of iron based materials (e.g., Antelo et al., 2005; Long et al., 2011; Lǚ et al., 2013), the high phosphate capacity spanned over a broader pH range of 4-8 for the both starch- and CMC-stabilized Fe-Mn. . Evidently, the use of the stabilizers, especially CMC, buffered the pH effect. A sharp capacity drop was observed at pH ≥9, though the CMC-stabilized nanoparticles appeared to be more resistant to the competitive effects of OH$^-$ ions. Throughout the pH range, stabilized particles outperformed bare particles.

Solution pH can affect both phosphate speciation and the surface potential of the particles. In addition, pH can also affect the uptake of starch and CMC on the core Fe-Mn oxides, thereby affecting particle stabilization and particle sizes. In the experimental pH range, the predominant phosphate species are $H_2PO_4^-$ and HPO_4^{2-}. The pH of point of zero charge (PZC) for the bare particles is 6.2 (Xie et al., 2015). At lower pH, the particle surface tends to be positively charged for bare particles, nearly neutral for starch-stabilized particles and less negative for CMC-stabilized particles. As such, the surface is favorable for interacting with phosphate anions at lower pH. At elevated pH, the more negatively charged particle surface becomes increasingly repulsive toward phosphate anions. At pH ≥ 9, the OH$^-$ ions become more competitive, resulting in the observed sharp drop in phosphate uptake (Zhao and Sengupta, 1998; 2000). It is noteworthy that the highest capacity was observed at pH 4-5 although >10% of the nanoparticles were dissolved.
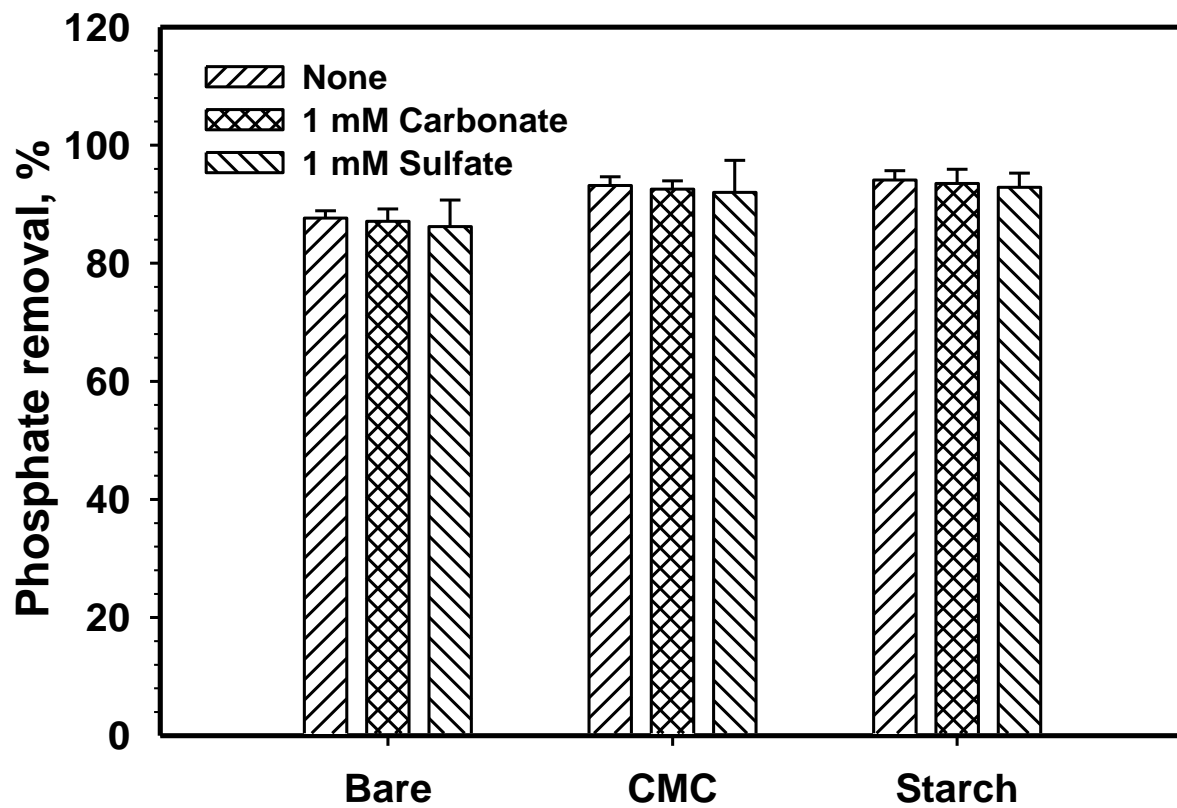
Figure 3-5. Effects of competing anions on phosphate removal by bare and stabilized Fe-Mn particles. Experiment conditions: Initial P = 5 mg/L, Fe-Mn = 0.1 g/L as Fe, CMC or starch = 0.1 wt.%, pH = 7.0 ± 0.2, carbonate or sulfate = 1 mM, Equilibrium time = 48 hrs.

Figure 3-5 shows the effects of competing anions (e.g., sulfate and carbonate) on the phosphate removal by Fe-Mn nanoparticles. The results indicate that the presence of 1 mM sulfate or 1 mM carbonate had negligible effect on the equilibrium phosphate uptake, which is attributed to the stronger ligand characteristics of phosphate and the stronger Lewis acid-base interactions between Fe and phosphate anions (i.e., formation of Fe-O-P complexes) (An et al., 2005; Zhang et al., 2009). This observation suggests that the nanoparticles are more selective toward stronger ligands, and thus, may be used for selective removal of strong ligands in contaminated wastewater, soil or solid/hazardous wastes.

3.3.5 Phosphate sorption isotherms

Figure 3-6 shows phosphate sorption isotherms for bare and stabilized Fe-Mn nanoparticles. The Freundlich (**Eq. 3-1**) and Langmuir (**Eq. 3-2**) isotherm models were used to interpret the experimental data:

$$q = K_F c_e^{1/n} \tag{3-1}$$

$$q = \frac{bQ_{max}C_e}{1+bC_e} \tag{3-2}$$

where q is the equilibrium solid phase phosphate concentration (mg/g), C_e is the aqueous phase phosphate concentration (mg/L), K_F is the Freundlich equilibrium adsorption capacity constant, n is the Freundlich adsorption intensity constant, b is the Langmuir affinity coefficient (L/mg) and Q_{max} is the Langmuir maximum adsorption capacity (mg/g).
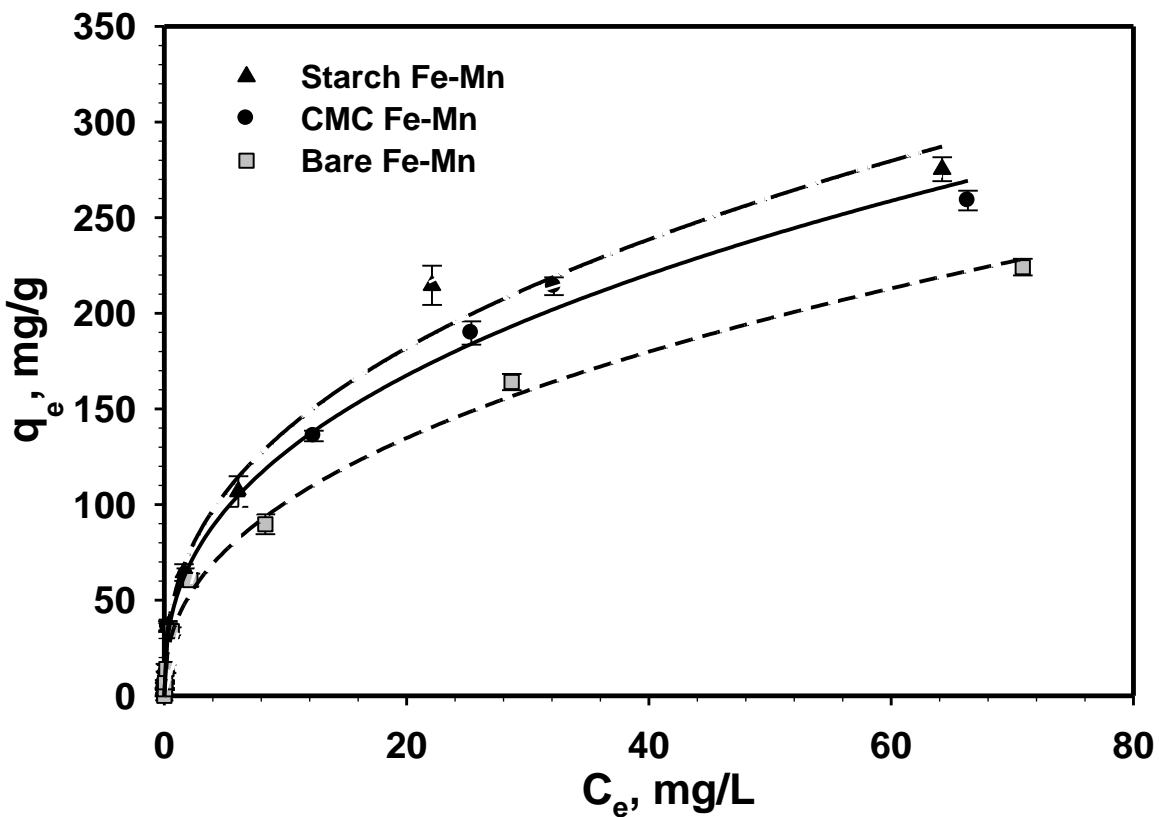
Figure 3-6. Phosphate sorption isotherms for bare and stabilized Fe-Mn nanoparticles at pH 7.0 ± 0.2. Initial phosphate = 0 − 100 mg/L, Fe-Mn = 0.1 g/L as Fe, stabilizer concentration = 0.1 wt%. Symbols: Observed data; Lines: Freundlich model simulations.

Table 3-3. Best-fitted Freundlich and Langmuir isotherm model parameters for phosphate adsorption by bare and stabilized Fe-Mn nanoparticles.

Isotherm models	Parameters	Bare	CMC-stabilized	Starch-stabilized
Freundlich	R^2	0.987	0.993	0.994
	K_F	39±3	51±4	56±6
	n	2.4±0.8	2.5±0.5	2.6±0.4
Langmuir	R^2	0.969	0.978	0.981
	Q_{max} (mg/g)	250±24	300±28	310±22
	b (L/mg)	0.08±0.02	0.08±0.01	0.10±0.02

Table 3-3 summarizes the best-fitted model parameters and correlation coefficients. Both models offered good fittings with $R^2 \geq 0.967$ in all cases, though the Freundlich model displayed better fittings ($R^2 \geq 0.987$). The best-fitted Q_{max} values are 250 ± 24, 300 ± 28, and 310 ± 22 mg-P/g for bare, CMC- and starch-stabilized Fe-Mn nanoparticles, respectively. The capacity values are much greater than those reported for other adsorbents, such as 12.7 mg-P/g for Al-bentonites (Yan et al., 2010), 55.73 mg-P/g for Fe-Al-Mn adsorbents at 25 ^{o}C (Lǚ et al., 2013), and 14.9 mg-P/g for Fe-Zr oxides (Long et al., 2011). The Freundlich K_F values are 39 ± 3, 51 ± 4 and 56 ± 6 for bare, CMC- and starch-stabilized Fe-Mn nanoparticles. These capacity values are remarkably higher than those of a synthetic Fe-Mn oxides material by Zhang et al (2009), which gave a K_F value of 27.0 ($R^2 = 0.98$) and a Q_{max} value of 33.2 mg-P/g ($R^2 = 0.76$). The difference is primarily due to the difference in the particle size, i.e., and the aggregated particle size in their work was 10-30 μm, which is >200 times larger than those of the starch- or CMC-stabilized counterparts.

3.3.6 Batch tests: immobilization of P and As in the PL

A large fraction of phosphorus in PL is water leachable and can be easily flushed out without being effectively utilized by crops (Codling et al., 2002; Hunger et al., 2004; Moore and Miller, 1994). Controlling P release not only increases crop utilization, but also reduces the runoff loss of water-leachable P. As shown in **Table 3-1**, the mean value of total P in the PL was determined at 14.4 g/kg. **Figure 3-7a** shows the P desorption rates and extent during batch desorption tests by DI water or in the presence of bare, starch- and CMC-stabilized Fe-Mn nanoparticles. In the DI water system, the equilibrium water soluble P concentration was ~26.3 mg/L, which translates into 5.2 g/kg, i.e., 36.4% of the total P in PL. Of the water extracted P, 80%

± 5% was determined to be inorganic P with the rest being organic P, which is comparable with

the data reported by others (He et al., 2006).
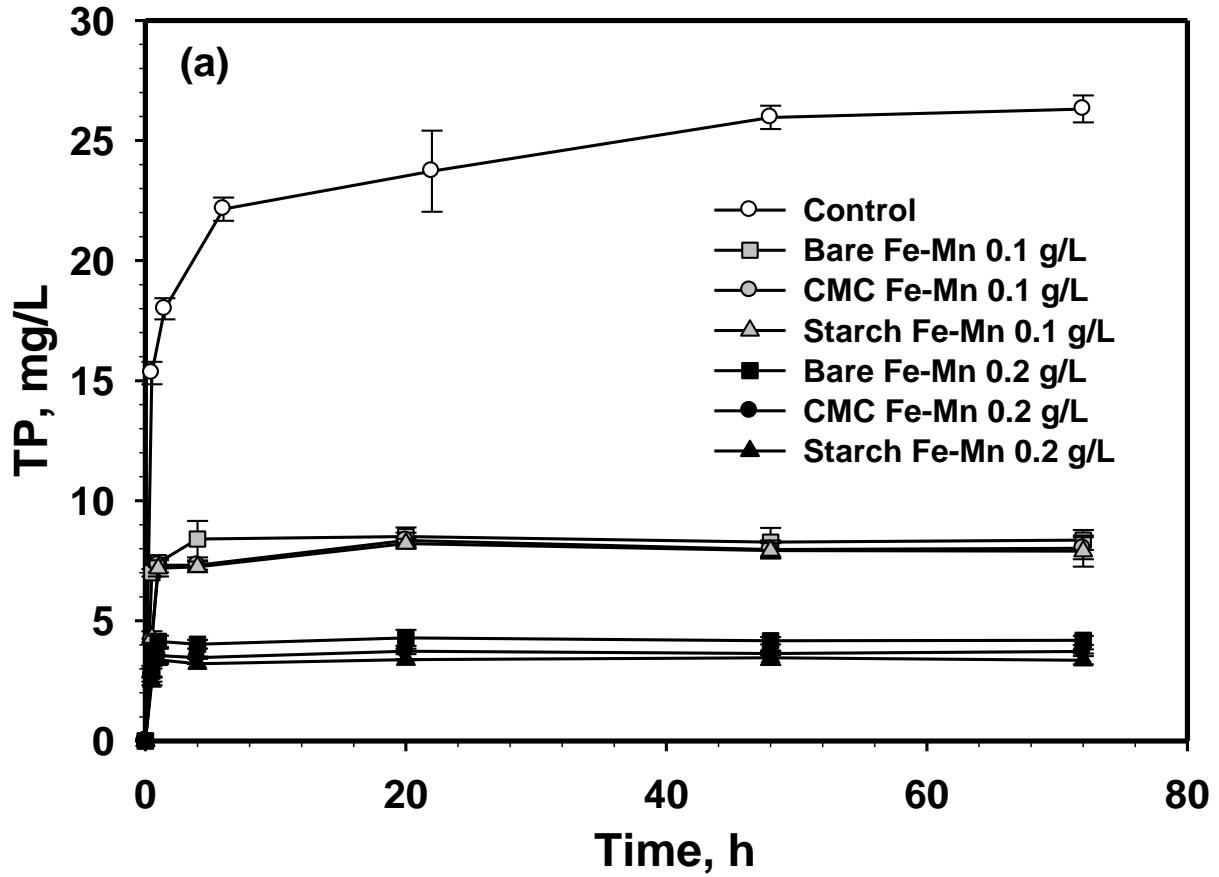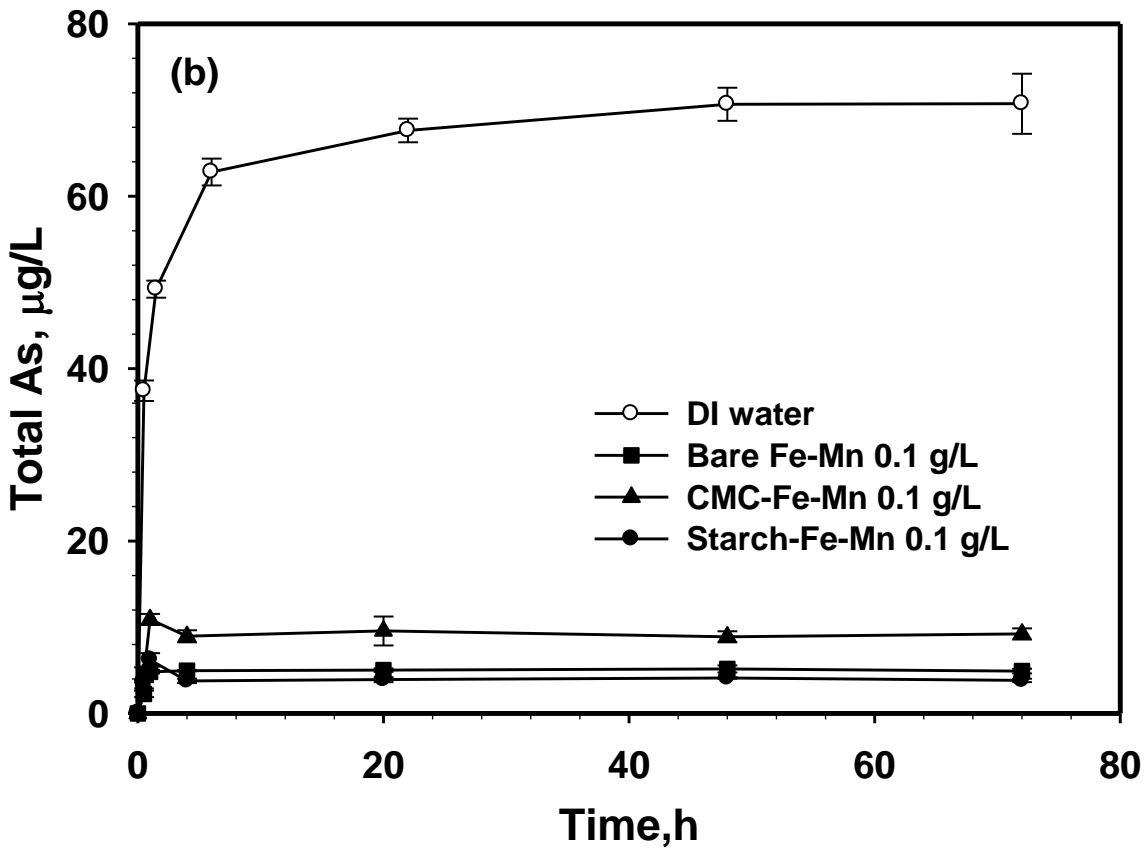
Figure 3-7. Desorption of total phosphorus (a) and arsenic (b) from poultry litter in the absence and presence of various Fe-Mn nanoparticles as a function of time. Experimental conditions: Fe-Mn = 0.1 or 0.2 g/L as Fe, starch or CMC = 0.1 or 0.2 wt.%, poultry litter = 1 g, solution volume = 200 mL, pH = 7.0 ± 0.2.

The addition of 0.2 g/L of bare, CMC- or starch-stabilized Fe-Mn lowered the water-leachable P by 84%, 86% and 87%, respectively, i.e., from 26.3 mg/L to 3.4-4.2 mg/L. The inorganic P in the remaining P was less than 15% in all cases. When the nanoparticle dosage was lowered to 0.1 g/L as Fe, the removal of soluble P was lowered to ~69% for all three types of nanoparticles. Despite the high organic content of the PL, equilibrium was reached within 24 h in all cases. The tests were followed for more than 15 days, and the leachable P concentration remained constant.

Arsenic has been another major environmental contamination concern related to disposal or land application of PL as arsenic based chemicals have been widely used in the U.S. poultry practices. A fortuitous effect of the nanoparticle amendment is the simultaneous immobilization of arsenic in PL. **Figure 3-7b** shows the arsenic desorption kinetics during the same batch desorption tests with or without the Fe-Mn nanoparticles. The result shows that 58% of the total As (24.52 mg/kg, **Table 3-1**) in the PL leached out by water extraction, resulting in an equilibrium As concentration of ~70 μg/L in the water phase. At a dose of 0.1 g/L as Fe, the leachable As was reduced by 93%, 95% and 87% for bare, starch- and CMC-stabilized nanoparticles. The high sorption capacity of inorganic arsenic by CMC-stabilized Fe-Mn nanoparticles was reported by An and Zhao (2012), with a Langmuir Q_{max} of 272 mg/g for As(V) and 338 mg/g for As(III) at pH = 5.1. The major As species in most PL samples is roxarsone (36% to 88%) (Jackson et al., 1999), which could be directly adsorbed by metal oxide, similar to those of inorganic arsenate and monomethylated arsenate (Chen and Huang, 2012). Roxarsone and inorganic arsenate share many chemical properties including the same oxidation state (+V) for As, the arsenate group, and three acid dissociation constants associated with the arsenate acid group. It is thus plausible that the sorption mechanism of roxarsone is similar to that of arsenate. In addition, as roxarsone or other

organic arsenic species are transformed to As(V) (Thirunavukkarasua et al., 2002), in fact, all the arsenic originally present in PL is expected to be transformed to inorganic As(V) upon sufficient weathering (Garbarino et al., 2003), the Fe-Mn particles can directly take up both As(III) and As(V). Given that arsenate is an even stronger ligand than phosphate, it is postulated that arsenate is more strongly bound to the nanoparticles, which greatly mitigating the toxic effects of the soluble As from PL.

The cost of Fe-Mn particles for industrial application is estimated at \$1.8/kg-Fe (bare), \$2.2/kg-Fe (starch stabilized) and \$2.8/kg-Fe (CMC stabilized) based on the industrial grade chemical prices (e.g., \$250/ton for $FeCl_2 \cdot 4H_2O$, \$1,200/ton for $KMnO_4$, \$400/ton for starch, \$1,000/ton for CMC). 0.02 kg of particles (as Fe) are needed to immobilize of 1 kg of PL, i.e., the estimated cost to treat 1 kg of PL is about \$0.036-0.056.

3.3.7 Column tests: curbing the leachability of P and As in poultry litter

CMC-stabilized Fe-Mn nanoparticles were further tested for controlling P and As leachability under simulated land application of PL, as the nanoparticles offer better soil deliverability (Xie et al., 2015) and comparably high phosphate capacity compared to starch-stabilized Fe-Mn. The column elution tests simulate a scenario where PL is applied to the top of soil as a fertilizer, which is subjected to either surface water runoff or groundwater leaching. **Figure 3-8a** shows the P elution profiles from untreated and nanoparticle treated PL when applied to the 8-cm top soil. For the untreated PL bed, 66% of P initially in the bed was eluted in 16 bed volumes (BVs), with a peak concentration of 300 mg/L. This fraction of water-leachable P can be easily lost into the environment without being utilized by the crops. In contrast, for the nanoparticle treated PL, only 23% of the total P was eluted, of which 81% was associated with the nanoparticles

and 19% was soluble P. The soluble peak P concentration was reduced to <20 mg/L, and the total eluted soluble P was lowered from 66% to 4.4%. Evidently, storing the most-leachable P on the nanoparticles not only prevents the runoff loss of P, but also provides a slow-releasing nutrient source that sustains the long-term plant need as the P-laden nanoparticles are spread in the soil pores After the 16-BV leaching, the total P was 16.4 mg/L, of which 1.5 mg/L was soluble P. When the leaching tests were extended to >30 BVs, the steady-state soluble P stayed at 1.0 mg/L. **Figure 3-8b** displays As elution profiles during the column runs. Over 79% of total As in the untreated PL bed was eluted during the 16-BV leaching, while only 25% was eluted for the nanoparticle-amended PL, of which 80% was associated with the nanoparticles and 20% was soluble As. The final As concentration was <2 μg/L, which is much lower than the maximum contaminant level of 10 set by US EPA. Because of the stronger binding of As, the particle-sorbed arsenic is expected to be much less leachable than P.
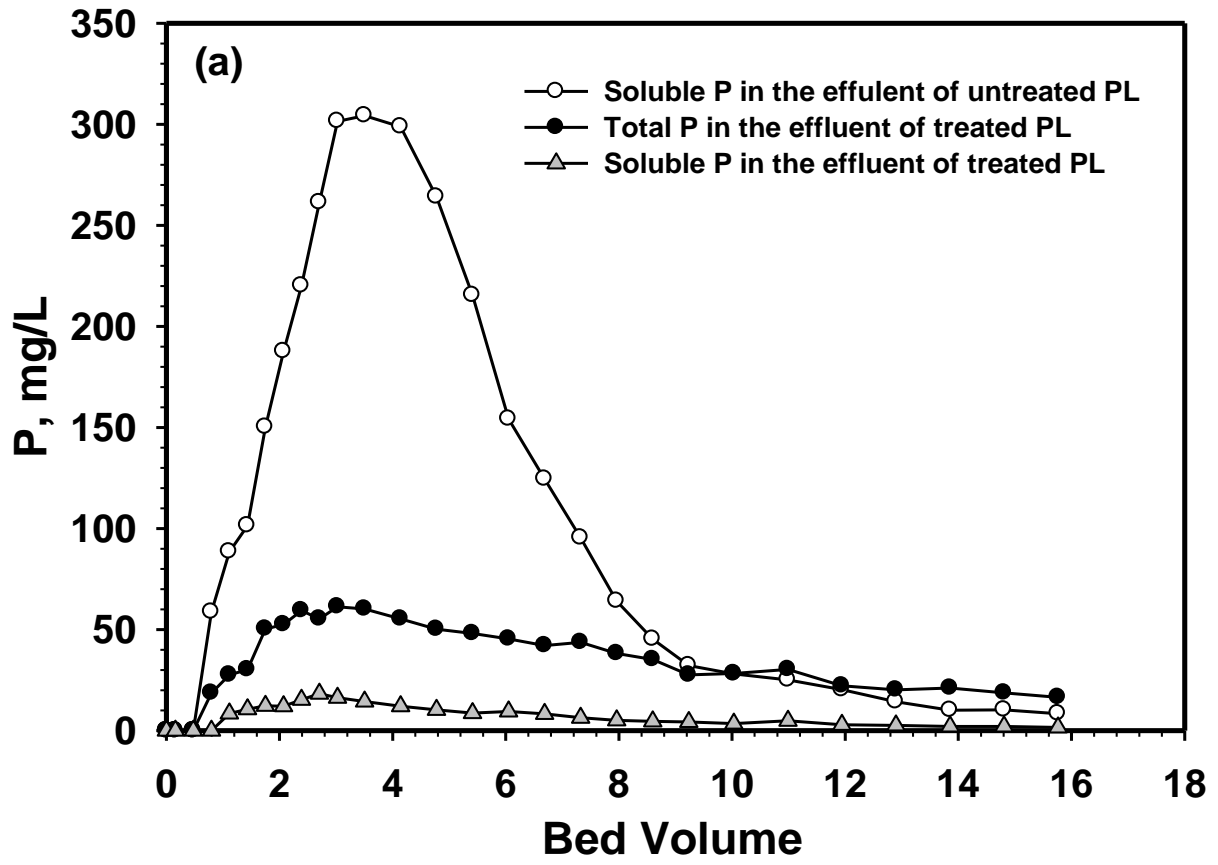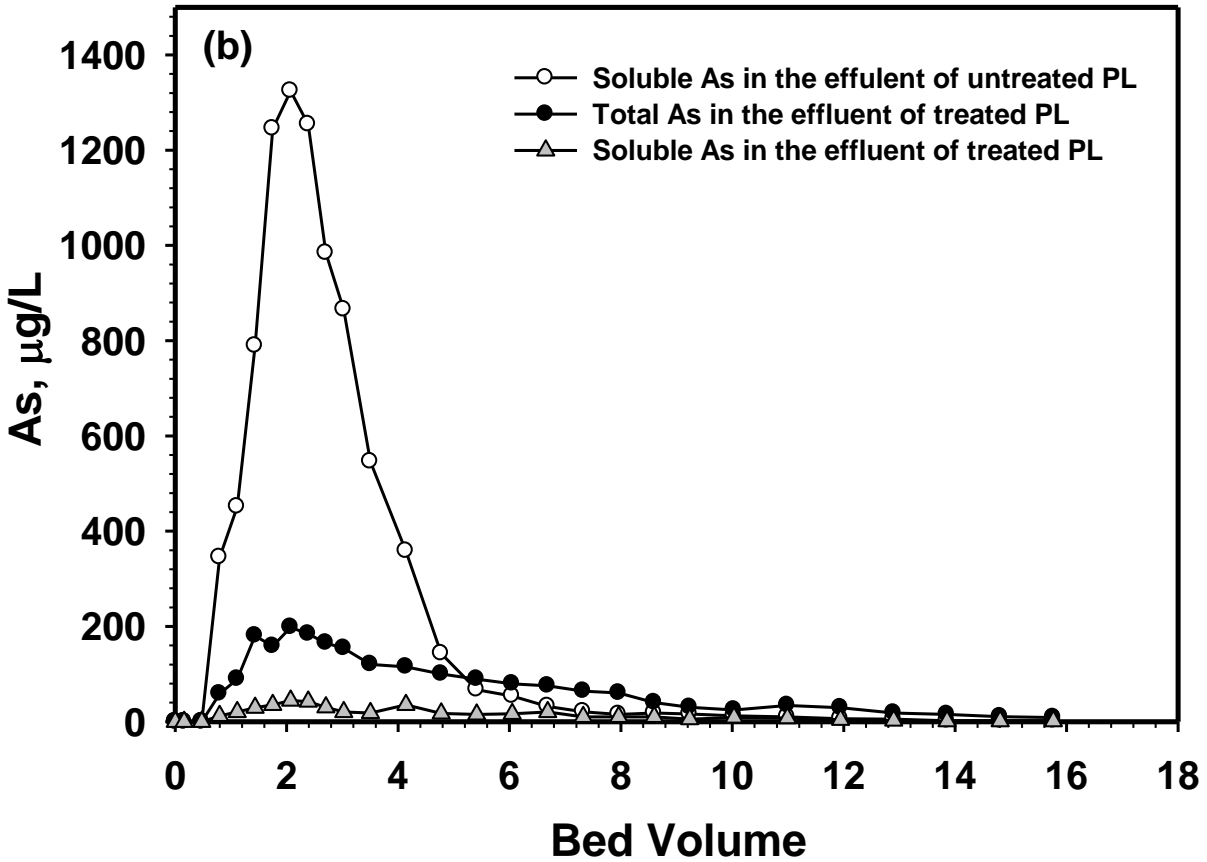
Figure 3-8. Elution profiles of P (a) and As (b) from untreated PL and nanoparticle-treated PL when mixed with a sandy soil and subjected to a simulated groundwater flow. Experimental conditions: total P in each column bed = 23 mg, total As in each column bed = 39 µg, PL-to-Soil ratio = 1:4, flow rate = 0.05 mL/min, bulk volume of PL-soil mixture = 9.4 mL.

3.4 Conclusions

    To our knowledge, this has been the first work on tailoring nutrient release from poultry litter using nanoparticles. The key findings are summarized as following:

- Starch- and CMC-stabilized Fe-Mn nanoparticles offer much greater phosphate removal capacity than bare Fe-Mn nanoparticles. The Langmuir maximum capacity was determined at 250, 300 and 310 mg-P/g for bare, CMC- and starch-stabilized nanoparticles, respectively. The stabilized particles also displayed much faster adsorption kinetics than conventional adsorbents. In addition, the stabilized nanoparticles are more easily deliverable and applicable to treating PL and the subsequent land application.

- FTIR analyses revealed that the formation of the inner sphere Fe-O-P complexes is a underlying mechanism for the high capacity and affinity of the nanoparticles toward phosphate.

- The Fe-Mn nanoparticles are able to function optimally over a broad pH range of 4-9, and significant capacity drop occurs at pH >9.

- The stabilized nanoparticles can effectively adsorb P well under rather harsh environmental conditions, such as high concentrations of dissolved organic matter and competing co-ions (e.g., sulfate and bicarbonate), which are exemplified by PL. Batch tests indicated that the stabilized Fe-Mn nanoparticles can reduce the water leachable P in PL by >86% at a dosage of 0.2 g/L as Fe, and fortuitously, the nanoparticles can diminish the water leachable arsenic from PL by 87-95% at a dose of 0.1 g/L as Fe.

- Under conditions of simulated land application of PL, the nanoparticle amendment of PL reduced the water soluble P from 66% (for untreated PL) to 4.4%. The treatment also lowered to peak soluble P concentration by a factor of >20 (from 300 mg/L to <20 mg/L).

By transferring the peak soluble P to the nanoparticle-bound P, the nanoparticles not only greatly reduce the potential runoff loss of P from PL, but also provide a long-term slow-releasing nutrient source. Moreover, the nanoparticle treatment was able to immobilize arsenic from PL, thereby greatly mitigate the toxic impacts of arsenic on plants and groundwater.

The PL-treatment technology proposed in this work appears promising for facilitating more efficient utilization of nutrients from animal wastes and for more sustainable agricultural practices.

Chapter 4. *In situ* Reductive Immobilization of Uranium in Soil Using Stabilized

Iron Nanoparticles

Presented in this chapter is a kind of stabilized ZVI nanoparticles designed for reductive immobilization of U(VI) in soil. Batch and column tests were conducted to investigate the U(VI) immobilization effectiveness by stabilized nanoparticles. The remobilization potential, leachability and bioaccessibility of immobilized U-laden soil were tested. The travel distance of stabilized ZVI nanoparticles was estimated by model through column breakthrough tests and transport modeling.

4.1 Introduction

Uranium (U^{238}) is a common radioactive element in nature widely existing in soil and rock worldwide, and more than 7 U.S. states have an average U concentration above 3 mg/L equivalent uranium (Duval et al., 2005). Various anthropogenic activities can cause uranium contamination of soil and groundwater, including mining and refining of nuclear materials, nuclear fuel manufacturing, nuclear weapon tests or nuclear power plant accidents, and radioactive waste disposal (Choy et al., 2006; Gavrilescu et al., 2009). In 2013, the world's total uranium production of U_3O_8 was 70,015 tonnes, 64% of which was contributed by Kazakhstan, Canada and Australia (WNA, 2014). In the U.S., the total uranium concentrate production from mines was 1792 tonnes in 2013 and 1888 tonnes in 2014, mainly produced in Utah, Wyoming, Texas and Nebraska (USEIA, 2014). The average concentration of uranium in the U.S. groundwater is ~3 μg/L (i.e., 2

pCi/L), and the maximum contaminant level of uranium in drinking water was regulated at 30 µg/L (i.e., 20 pCi/L) by the U.S. EPA (USEPA, 2011). However, the concentration of uranium in soil varies in a wide range from 0.3 to 11.7 mg/kg (UNSC, 1993). The general daily maximum intake of soluble uranium salts for an individual is 0.5 µg per kg of body weight established by the World Health Organization. Over intake of uranium may lead to renal dysfunction and even kidney failure (Choy et al., 2006).

Uranium in soil and groundwater can exist in a variety of species and oxidation states depending on the geochemical properties (e.g., pH, DO, NOM, carbonate), microbial activity, and physical effects (e.g., soil texture and hydraulic regimes) (Gavrilescu et al., 2009; Wang et al., 2013). Accordingly, the solubility, mobility and bioavailability of U are affected by these factors (Chang et al., 2014). Generally, the oxidized form, U(VI), is soluble in natural waters as the uranyl (UO_2^{2+}) and is commonly complexed with inorganic and organic ligands (especially with those of oxygen donor atoms), while the reduced form, U(IV) exists as uraninite (UO_2), which is sparingly soluble (i.e., log K for the hydrolysis reaction is -52.0 ± 0.8 (Rai et al., 1990)) and much less mobile in groundwater (Chang et al., 2014; Jackson et al., 2005; Wersin et al., 1994). Thus, U(VI) and its complexes are considered as the predominant contaminant species that pose high risks to human and ecological health (Igwe et al., 2005).

To mitigate uranium exposure and mobility, most of soil remediation technologies for U contaminated sites have been based on the reductive precipitation by converting soluble U(VI) to insoluble U(IV) through chemical and/or biochemical mechanisms (Fiedor et al., 1998; Lovely et al., 1991; Scott et al., 2005; Wu et al., 2006). In addition, adsorption has also been used to remove or immobilize U in soil and groundwater using various inorganic and organic adsorbents (e.g., Fe-

and Mn-(hydr)oxides, organic matter, and ion exchangers) (Bednar et al., 2007; Clifford and Zhang, 1994; Li et al., 2013; Xie et al., 2009).

The conventional reductive remediation technologies are largely *ex-situ*, which involve two general steps: 1) extracting U from contaminated soil using a strong ligand (e.g., citrate acid and bicarbonate) (Choy et al., 2006; Gavrilescu et al., 2009); and 2) subsequent biodegradation, chemical reduction and/or photodegradation (Francis and Dodge, 1998; Gu et al., 2005). Another common practice has been the permeable reactive barrier, i.e., intercepting the contaminant by permeable walls filled with reactive material (Boyd and Hirsch, 2002). A number of studies have demonstrated that U(VI) can be effectively removed from water by iron minerals, such as mixed ferrous/ferric hydroxides (O'Loughlin et al., 2003), hematite (Xie et al., 2009), goethite, lepidocrocite, mackinawite (Moyes et al., 2000), pyrite or magnetite (Scott et al., 2005), and granular or powder ZVI (Yan et al., 2010). Laboratory studies have indicated that ZVI particles can effectively remove U(VI) from a surrogate groundwater stream when applied in batch tests (Fiedor et al., 1998; Gu et al., 1998) and PRBs tests (Cantrell et al., 1995). The mechanisms of U(VI) removal from solution include: (a) reduction of U(VI) by ZVI to the less soluble U(IV) form; (b) chemisorption of U(VI) onto the iron corrosion products; and (c) coprecipitation, i.e., a combination of reduction, sorption and precipitation. The redox reaction is thermodynamically favorable in acidic media according to the following stoichiometry (Fiedor et al., 1998):

$$Fe^0 + 1.5UO_2^{2+} + 6H^+ = Fe^{3+} + 1.5U^{4+} + 3H_2O \qquad E^0 = +0.17V \qquad \textbf{(4-1)}$$
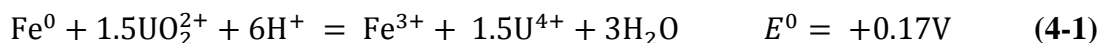
Riba et al. (2008) studied reduction of uranyl by synthetic nZVI and observed that 1000 mg/L uranyl was reduced by 2.9 mM nZVI in 10 min at pH of 5-6, and the U concentration can be lower to < 10 μg/L under carbonate rich water by nZVI (Crane et al., 2011). Yan et al. (2010) found the U(VI) reduction rates by synthesized nZVI decreased with increasing pH, bicarbonate

and calcium in the solution. However, the major bottlenecks of *in situ* U soil remediation are the soil deliverability and the reoxidation/remobilization of reduced U(IV). Dickinson and Scott (2010) observed that ZVI-immobilized U remained stable in 48 h under both oxic and anoxic conditions, but significant re-oxidation and dissolution of precipitated U occurred after 48 h. In addition, the reoxidation and solubilization of bioreduced U(IV) were observed even under sustained reducing conditions due to the microbial respiration (Wan et al., 2005). Stabilized ZVI nanoparticles hold great promise for *in situ* remediation of contaminated soil and groundwater due to their high reactivity and soil deliverability (He and Zhao, 2007, 2005; He et al., 2007; Xu and Zhao, 2007). To facilitate soil delivery and *in situ* remediation of soil and groundwater, He and Zhao (2007) and He et al. (2007) synthesized a class of polysaccharide stabilized nZVI. A green polysaccharide, CMC or starch, was employed to prevent particle aggregation and to facilitate soil delivery of the nanoparticles. The high reactivity and soil deliverability of the stabilized nanoparticles have been tested in various bench- and field scale tests (Bennett et al., 2010; He et al., 2010; Kocur et al., 2014).

The objectives of current work were to determine the effectiveness of stabilized nZVI for reductive immobilization of U(VI) sorbed in soil through both batch and column experiments, and to investigate the influences of pH, bicarbonate, oxygen and microbial activities on the immobilization and remobilization processes of uranium.

4.2 Materials and Methods

4.2.1 Materials

All chemicals used in this study were of analytical grade. $FeSO_4 \cdot 7H_2O$, $NaHCO_3$, CMC (sodium salt, MW = 90,000), Uranium standard solution, and Tris(hydroxymethyl)aminomethane

(Tris) were purchased from Acros Organics (Morris Plains, NJ, USA). Uranyl nitrate hexahydrate crystal was purchased from International Bio-Analytical Industrial Inc. (FL, USA). All solutions were prepared with ultrapure deionized (DI) water (18.2 Ωcm^{-1}).

A sandy soil was taken from the Smith Research Field (Tallassee, AL, USA). The soil was pre-washed with tap water to remove soluble compounds and suspended solids, and then air-dried and sieved through a 2-mm screen. The soil properties were described in **Table 2-1** and the key properties include: organic matter = 0.1%, cation exchange capacity = 0.5 meq/100g, Fe = 4 mg/kg, uranium = 0, and hydraulic conductivity = 6.3 ± 0.5 cm/day.

U(VI)-spiked soil samples were prepared by mixing 100 g of the air-dried soil with 500 mL of a U(VI) solution containing 100 mg/L of U(VI) in a batch reactor at pH 6. After 2 weeks of equilibration, the supernatant was decanted and the U(VI)-laden soil was rinsed twice with DI water. The final U(VI) loading on the soil was determined to be 395 mg-U/kg-dry-soil by measuring aqueous-phase U concentrations, which was confirmed by measuring the solid-phase U via EPA Method 3050B (USEPA, 1996).

4.2.2 Preparation of ZVI nanoparticles

The stabilized ZVI nanoparticles were prepared following the method described by He and Zhao (2007) per the following stoichiometry,

$$Fe^{2+} + 2BH_4^- + 6H_2O = Fe^0 + 2B(OH)_3 + 7H_2 \tag{4-2}$$

First, 10 mL of an FeSO$_4$·7H$_2$O stock solution (21.4 mM) was added into 100 mL of stabilizer solution (CMC or starch) at a desired ratio of Fe^{2+}:stabilizer ratio in a 250 mL filter flask, and mixed for 20 min under N$_2$ purge. Then, the flask was attached to a vacuum line, and the redox reaction was set on by dropwise adding 10 mL of a borohydride solution (42.8 mM) at 5 mL/ min

into the CMC-Fe^{2+} or starch-Fe^{2+} solution under vacuum and shaking at 230 rpm for 5 min, and then left still for 10 min. The resulting ZVI suspension contained 0.1 g/L as Fe and 0.2 wt.% of CMC or starch. The pH of the suspension was buffered at 6~8 using the Tris buffer and 1M HCl right after preparation. To test ZVI dosage effects, the nanoparticle suspension was also prepared at 0.2 g/L with 0.3 wt.% of a stabilizer.

4.2.3 Batch tests

A series of batch kinetic tests were conducted to investigate the effectiveness of the stabilized nZVI for reducing water-leachable U from the U(VI)-spiked soil under various conditions. Briefly, 2 g of the U(VI)-laden soil was mixed with 80 mL of a nanoparticle suspension (0.1 g/L Fe with 0.2 wt.% CMC or starch) or a background stabilizer solution (0.2 wt.% CMC or starch) in a polycarbonate vial at pH 6.0±0.2. The vials were sealed and rotated on an end-to-end rotator (Glas-Col, Terre Haute, IN, USA) at 60 rpm, and then sacrificially sampled at pre-determined times. The samples were filtered through a 50 nm mixed cellulose esters membrane (MF-Millipore Corp., Billerica, MA, USA) on a polyphenylsulfone filter (Pall Corporation, USA) under N_2 atmosphere. The filtrates were then acidified by 5 M HNO_3 and the aqueous U concentration was analyzed by a Varian 710 ES ICP optical emission spectrometer (Palo Alto, CA, USA) (detection limit ~ 80 μg/L) or by a kinetic phosphorescence analyzer (KPA-11, Chemchek Instruments, Richland, WA) (detection limit ~ 1 μg/L). Control tests were carried out in the absence of the nanoparticles. All experiments were conducted in duplicate at room temperature (22 ± 1°C) in an anoxic glove box under N_2 atmosphere.

To study the influence of nanoparticle dosage and pH, the batch tests were conducted at various ratios of soil-to-nanoparticle (i.e., 1 g/25 mL, 1 g/40 mL, 1 g/50 mL), at the nanoparticle concentration of 0.1 g/L and 0.2 g/L, and at pH 6 to 8).

To exam the remobilization potential of immobilized U, the nanoparticle treated soil samples were first freeze-dried under vacuum at -50°C using a VirTis Freezemobile freeze dryer (Gardiner, NY, USA) for 48 h, and then subjected to U-desorption kinetic tests in DI water at a solid-solution ratio of 1 g/50 mL under the following conditions: 1) oxic, 2) anoxic, and 3) anoxic in the presence of $NaHCO_3$ (1 mM). The remobilization tests were followed for 1 year.

To exam the effects of the nanoparticle treatment on the biological activity and effects of microbial activity on the stability of immobilized U, a series of batch kinetic tests were conducted in the presence of active microbial growth. A natural mixed culture of anaerobic microbes were obtained from a lake sediment (Auburn, AL, USA) and were fed intermittently to maintain a steady state using a nutrition solution by He et al. (2005). Then the microbial culture was inoculated into 400 mL of the CMC-nZVI suspension in 500 mL polycarbonate bottles, each containing 8 g of contaminated soil which have been mixed for 24 h, and 100 mL of nutrition solution was added into the anaerobic reactor to initialize the culture. The feed solution was added daily at 7 mL/day starting from Day 13 of the inoculation. The suspension was sampled at 7 mL each over the course of one month, and the total bacteria number (TBN) (cell/mL) was estimated following the fluorochrome staining method (Kepner and Pratt, 1994). In brief, a glutaraldehyde (GTA) fixative solution (50%, wt/wt) was added to preserve samples (final concentration, 1%). The bottles were processed with an ultrasonic treatment (40 kHz) for 10 minutes to release and disperse the bacteria from particle aggregates. The solids were then separated by centrifugation at 3000 rpm for 5 minutes, and the supernatant was sampled for bacterial numeration. Approximately a final

concentration of 100 mg/L acridine orange (AO) were added in the filter tower apparatus with a black membrane filter (pore size, 0.2 μm) for staining in a dark room. Allow AO to react with sample for 3 minutes, while occasionally swirling the filter funnel contents. After that, draw funnel contents through the filter tower under low vacuum. Rinse the membrane filter with a volume of sterile water approximately equal to that of the sample to remove excess stain, enhancing the image contrast. Place a small drop of immersion oil on a labeled, acetone-cleaned glass microslide. Place another drop of immersion oil on top of the black membrane filter, and top with a clean coverglass. The prepared microslides were counted within one week using a Nikon Labophot epifluorescence microscope (Tokyo, Japan) with 460-485 mm interference excitation and a 515-545 barrier filter. As a comparison, the batch kinetic tests were also carried out without the nanoparticle suspension or contaminated soil in parallel under otherwise identical conditions.

4.2.4 XPS Analysis

The freeze-dried nanoparticle treated soils for remobilization tests were used to prepare the specimen for XPS analysis. The specimen was pressed into double-sided carbon tape to a thickness which insured that the emitted photoelectrons would originate only from the specimen. Photoemission measurements were performed in a load-locked Kratos XSAM 800 surface analysis system equipped with a hemispherical energy analyzer. The base pressure of this ion- and turbo-pumped system was 8×10^{-9} torr as read on a nude ion gauge.

The XPS analyzer was a 127 mm radius double-focusing concentric hemispherical energy analyzer (CHA) equipped with an aberration compensated input lens (ACIL). XPS spectra were recorded in the fixed analyzer transmission (FAT) mode with a pass energy of 80 eV, appropriate for acquisition of medium resolution, high signal-to-noise spectra. The magnification of the

analyzer in the FAT mode was selected to collect electrons from the smallest allowable (5 mm^2) area on the specimen. The resolution of the instrument at the operating parameters was measured from FWHM of the Ag3d$_{5/2}$ peak to be 1.0 eV. The XPS energy scale was calibrated by setting the Ag3d$_{5/2}$ line on clean silver to exactly 368.3 eV referenced to the Fermi level. Due to specimen charging during X-ray irradiation, the energy axis of each XPS spectra has been shifted to make the C1s binding energy line equal to 284.5 eV, which is the C1s peak (C-H and C-C bonds) assigned by Fiedor et al. (2003) to reference charge affected uranium materials. The potential measured on a typical sample was 0.5 V. The photoelectrons were excited by a water-cooled, conventional (i.e., non-monochromatic) dual anode X-ray gun. The angle of the incidence of the X-ray beam with the specimen normal was 51.5°. MgKα (1253.6 eV) radiation was used exclusively. Due to the low surface concentration of uranium, after data acquisition, the U4f region was mathematically smoothed by the Savitzky and Golay (1964) routine in order to help determine the peak binding energies. The XPS surface composition was calculated based on the Scofield (1973) cross-sectional values accounting for the instrumental transmission function in the FAT mode of operation. After compound synthesis, the powdered specimens were carried to the surface laboratory under normal atmospheric conditions (i.e., not under a nitrogen or inert atmosphere).

4.2.5 Column tests

Column breakthrough tests were carried out in sandy soil to investigate the deliverability of the stabilized nZVI in soil. The column setup included a Harvard Apparatus PHD 2000 syringe pump (Plymouth Meeting, PA, USA), a Plexiglas column (inner diameter = 10 mm, length = 120 mm, Omnifit, Cambridge, UK), and a fraction collector (Eldex Laboratories, Napa, CA, USA). First, 12 g of the sandy soil was added from the top into the column containing nitrogen-sparged

background solution (0.84 mM NaCl and 0.16 mM NaHCO$_3$, pH 7.5) under constantly patting with a plastic rod, resulting in a soil porosity of 0.34 and a bulk bed volume of 8.8 mL. Length = 11.2 cm, unit pore volume = 2.99 mL, bed volume = 8.79 mL, EBCT = 29.9 min.

Then, a stabilized nZVI suspension (Fe = 0.1 g/L with 0.2 wt.% CMC or starch) or a KBr solution (50 mg/L as Br$^-$) was pumped through the column in the down-flow mode at a flow rate of 0.1 mL/min, which can be converted to a pore velocity of 6.2×10^{-3} cm/s. To investigate the effects of hydrodynamic conditions, the breakthrough tests of CMC-nZVI were also carried out at a pore velocity of 0.0124, 3.1×10^{-3}, 6.2×10^{-4} cm/s. The effluent was collected by the fraction collector, and the samples were then acidified by 5 M HNO$_3$ to dissolve the nanoparticles. The concentration of the nanoparticles in the effluent was then determined by measuring the total iron content in the samples.

In situ U immobilization tests were carried out in the same column configuration by treating the U-laden soil using the stabilized nZVI. To simulate the treatment for fresh contaminated soil, the U-laden sandy soil was packed in the column containing nanoparticle suspension. To simulate the treatment for the groundwater saturated contaminated soil, the U-laden sandy soil was packed in the column containing nitrogen-sparged background solution and the nanoparticle suspension was injected after 16 pore volumes of oxygen-free 0.2 wt.% CMC. The column parameters were the same as the transport test. U in the effluent was determined as soluble U and total U. To determine soluble U, the effluent samples were first filtered through the 50 nm membrane to remove all the particles; the filtrate was then analyzed for soluble U. To determine the total U, which includes soluble and nanoparticle-sorbed U(VI) and insoluble U(IV), the samples were first treated with 5 M HNO$_3$ to completely dissolve the nanoparticles, and then

analyzed for U. For comparison, parallel elution tests of the U-laden soil were carried out using 0.2 wt.% CMC solution under otherwise identical conditions.

4.2.6 Bicarbonate extraction

To quantify U(VI) removal by each of the mechanisms, a bicarbonate extraction method was adopted to determine the extractable U(VI) (Gu et al. 1998). The solid-to-bicarbonate extractant ratio was kept constant at 1 g/20 mL throughout the experiment, i.e., 2 g of soil per 40 mL of degassed $NaHCO_3$ solution (0.5 M), and N_2-purged for 10 min first, then mixed for 2 hours under anoxic condition. The mixture was filtered, and filtrate was analyzed for U(VI). The method will not extract any UO_2.

4.2.7 Batch tests: U(VI) reduction by H_2 gas

To investigate the effect of H_2 on the U(VI) reduction in solution under room temperature ($22\pm1°C$), batch tests were conducted to reduce U-laden soil by purging H_2 gas into the soil-water system. The solid-to-solution ration was kept at 1 g/40 mL, i.e., 3 g of fresh U-laden soil was added into 120 mL DI water under continuous H_2-purge at pH of 5.5 ± 0.2. At pre-determined times, the mixture solution was sampled and filtered, and analyzed for U(VI). Control tests were carried out in the absence of the H_2 gas under identical conditions.

4.2.8 Leaching tests of immobilized U from soil

To investigate the leaching of immobilized U from soil under different conditions, the untreated and column-treated soil samples were subjected to TCLP (EPA Method 1311), WET (California HML Method 910) and PBET (Physiologically Based Extraction Test) procedures,

which are related to hazardous waste leachability in landfill or bioaccessibility (Jovanovic et al., 2012; Kelley et al., 2002; Liu and Zhao, 2007b). For TCLP leachability tests, the nanoparticle treated soil samples were freeze-dried and then subjected to the TCLP fluid No. 1 (0.57% glacial acetic acid + 0.64 N NaOH, pH 4.93±0.05) at a solid-to-solution ratio of 1 g to 20 mL. The mixtures were rotated at 30 rpm for 19 h. For WET leachability tests, the freeze-dried soil samples were mixed with the extraction fluid (0.2 M citric acid solution, pH 5.0) at a solid-to-solution ratio of 1 g to 10 mL for 48 h. The PBET followed the procedures by Kelley et al. (2002). In brief, 0.1 g of a freeze-dried soil sample (untreated or nanoparticle treated) was mixed with 10 mL of the extracting liquid (i.e., 0.4 M glycine with a pH adjusted to ~2.3 with HCl to mimic the conditions in the gastric system and small intestines) in 15 mL high-density polyethylene vials. The mixtures were then mixed on an end-to-end rotator placed in an incubator at 37°C for 1 h. Following the equilibration, the samples were centrifuged at 6000 rpm for 20 min. Then, the supernatants were filtered with the 50 nm membrane, and the filtrates were analyzed for U. The U leachability were was quantified by,

$$\text{Leachability of U} = \frac{C_U \times V}{M_U} \tag{4-3}$$

where C_U is the U concentration in the extraction solution (mg/L), V is the volume of the solution, and M_U is the initial mass of U in the soil before the extraction.

4.3 Results and Discussions

4.3.1 Immobilization of U(VI) in soil: Batch tests

4.3.1.1 U desorption from U-laden soil in the absence or presence of nZVI

To facilitate the application of *in situ* immobilization of uranium, the nanoparticles are required to: 1) be deliverable in soil under moderate external pressure; 2) offer decent

immobilization effectiveness on target contaminants; 3) remain in a confined area without spreading when the external pressure is removed. Both CMC and starch were employed in our prior works to facilitate the stabilization of the nZVI (He and Zhao, 2007, 2005), which can form a cover layer on the surface of nZVI and thereby prevent the agglomeration of nanoparticles. It was shown by the FTIR results (He et al., 2007) that both carboxymethyl and hydroxyl group bondings exist in the interaction between CMC and nZVI. The size of stabilized nZVI can be manipulated via controlling the concentration of stabilizer during preparation by affecting the growth and aggregation of nanoparticles, e.g., the optimal CMC/Fe molar ratio for both stabilization and deliverability of nZVI is 0.0124 (i.e., 0.1 g/L Fe with 0.2 wt.% CMC, with a mean hydrodynamic diameter of 18.6 nm).
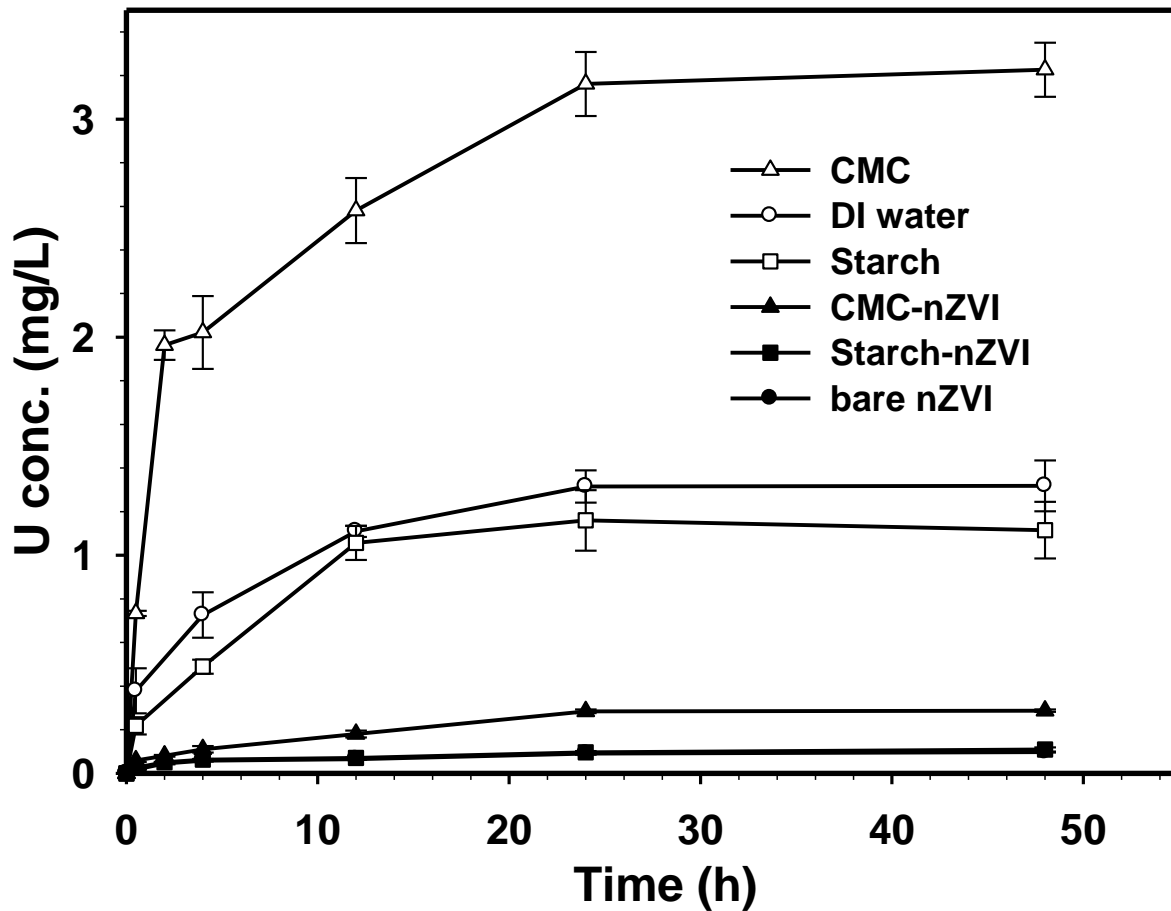
Figure 4-1. Desorption rates of U from a U-laden sandy soil in the absence or presence of bare or stabilized ZVI nanoparticles. Experimental conditions: Initial U in soil = 395 mg/kg; Soil/solution = 1 g/40 mL; Fe = 0.1 g/L, CMC = starch = 0.2 wt.%, pH = 6.0-6.5. Data are plotted as mean of duplicate, error bars are calculated as standard deviations.

Figure 4-1 shows the leaching rates of soluble U(VI) from the U-laden soil in the absence or presence of bare, CMC- or starch-stabilized nZVI. In all cases, the desorption equilibrium was reached in ~24 h. At equilibrium, DI water leached ~13% of the pre-loaded U(VI) (soluble U = ~1.3 mg/L), while the starch solution leached ~11% (1.1 mg/L) and CMC solution leached ~32% (3.2 mg/L). The soluble U was lowered to 0.11, 0.10 and 0.28 mg/L, respectively, when 0.1 g/L of bare, starch- or CMC-stabilized nZVI was present, i.e., reducing the U leaching by 90%, 91% and 75% compared to the DI water leaching.

Much more U was leached out from the soil with the CMC solution than starch and DI water, which is due to the formation of soluble U-CMC complexes based on the FTIR results (Popescu et al., 2013). Earlier, Popescu et al. (2013) reported formation of new U-O and O-U-O FTIR peaks in the region of 900-400 cm^{-1}. Starch-nZVI and bare ZVI offered relatively higher immobilization effectiveness than CMC-nZVI, which can be attributed to the stronger complexation effects of CMC in the solution phase. Between the two stabilizers, CMC provided better particle stabilization and smaller particle size (He and Zhao, 2007, 2005), whereas starch-nZVI offered relatively higher U removal. CMC-nZVI was employed for further tests for its superior soil deliverability and good U removal effectiveness.

4.3.1.2 U immobilization mechanism

In the soil, water and nZVI system, U(VI) can be immobilized mainly through direct adsorption of U(VI) and reductive precipitation in the form of UO_2. Based on bicarbonate extraction tests, ~85% of the sorbed U was due to reduction of U(VI) to U(IV) and ~15% was due to direct adsorption of U(VI) onto the solid phase. As a comparison, ~96% of the total U was

detected in the aqueous phase when the fresh U-laden soil samples upon bicarbonate extraction tests.

The nature of U binding was further explored by XPS analysis. **Figure 4-2a** shows the XPS spectra for U-laden soil following the treatment by CMC-nZVI. The powdered surface is largely composed of C, O, and Fe with a very small amount of U (~ 0.2 wt.%) and other elements which are low-level surface contaminants (Sn, Na, and Ca). A large fraction of the C and O XPS signals are due to the presence of CMC. Ca is a common surface active contaminant found on many metal surfaces.
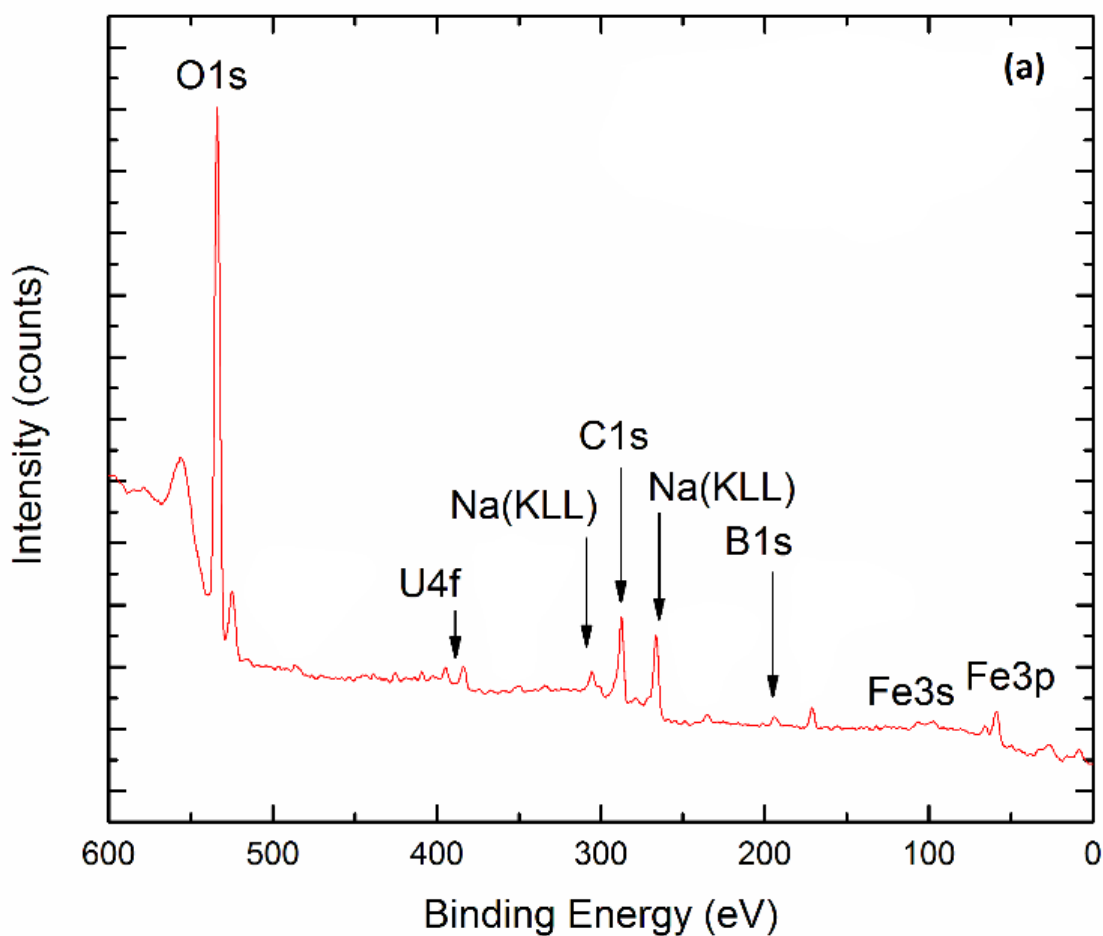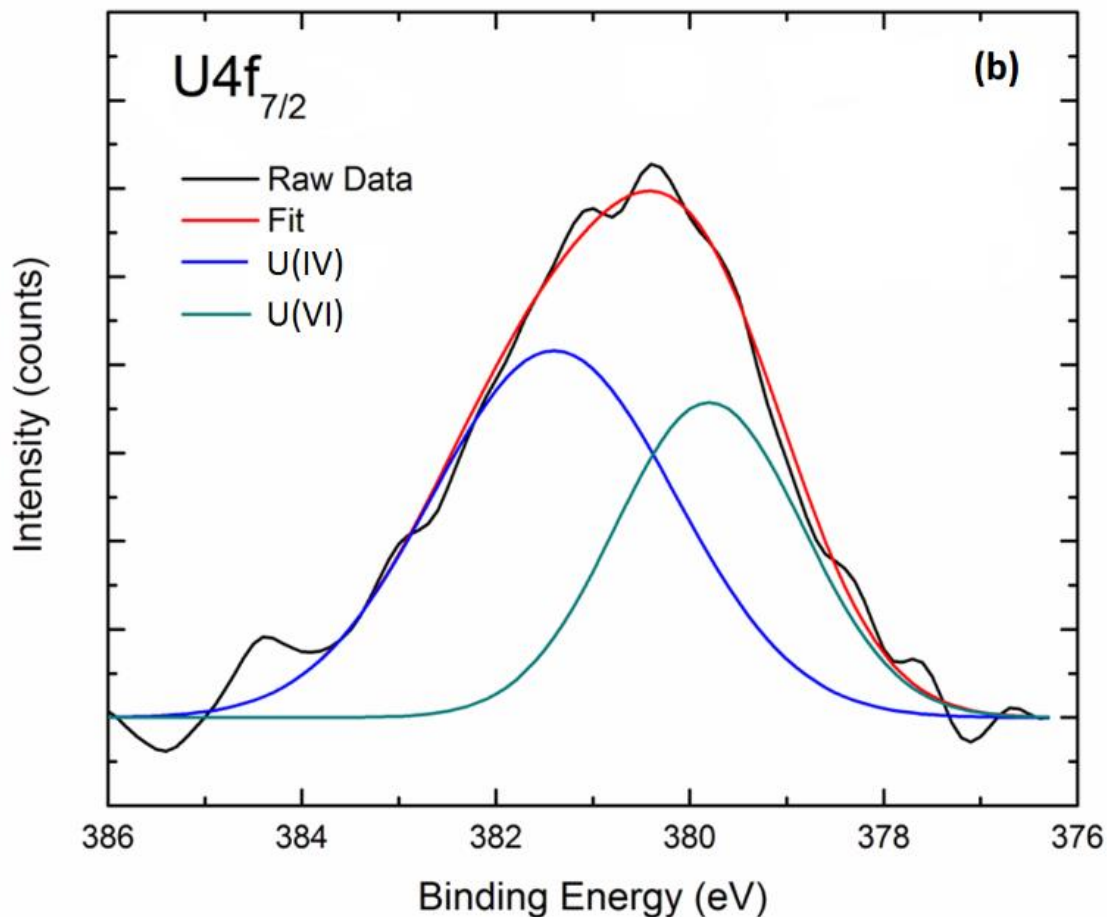
Figure 4-2. (a) XPS survey spectrum for CMC-nZVI treated uranium contaminated soil. The amount of U corresponds to ~ 0.2 wt. % as calculated by XPS. (b) High resolution spectrum over the U4f7/2 peak. The peak energy is at 380.8 eV referenced to C1s = 284.5 eV. Deconvolution of the peak into U(IV) (381.4 eV, 60%) and U(VI) (379.8 eV, 40%) chemical species. The reduced chi-square fitting parameter is 3.4.

Figure 4-2b shows the high resolution photoemission scans over the $U4f_{7/2}$ peak for the specimen. The broad $U4f_{7/2}$ feature is successfully de-convoluted by two subpeaks. Work by Fiedor et al. (1998) allows for comparison to standard uranium oxide compounds which are labeled in the figure. It is clear that U exists on the surface as both U(IV) and U(VI). The peak energy of the $U4f_{7/2}$ (380.8 eV) is close to the value measured for native uranium oxide (380.8 eV) (S. Yan et al., 2010). The ratio of U(IV) (381.4 eV) to U(VI) (379.8 eV) is ~ 60/40 as measured by the relative peak areas of U(IV)/ U(VI) in the deconvolution, which demonstrated that both U(IV) and U(VI) existed on the surface of treated contaminated soil. This observation shows when the U-laden soil is treated by CMC-nZVI, U(VI) is reduced to UO_2. Comparably, the ratio of U(IV) to U(VI) in the sample was measured at ~ 85/15 by the bicarbonate extraction in anoxic condition. The U(VI) fraction on the soil surface is higher than that measured by the bicarbonate extraction method, which can be attributed to partial reoxidation of U(IV) to U(VI) as the specimen was exposed to atmospheric air during preparation and transfer to the surface analytical system. Nonetheless, the XPS spectra provide compelling evidence that the nZVI particles indeed reduce U(VI) to UO_2.

4.3.1.3 ZVI dosage effects
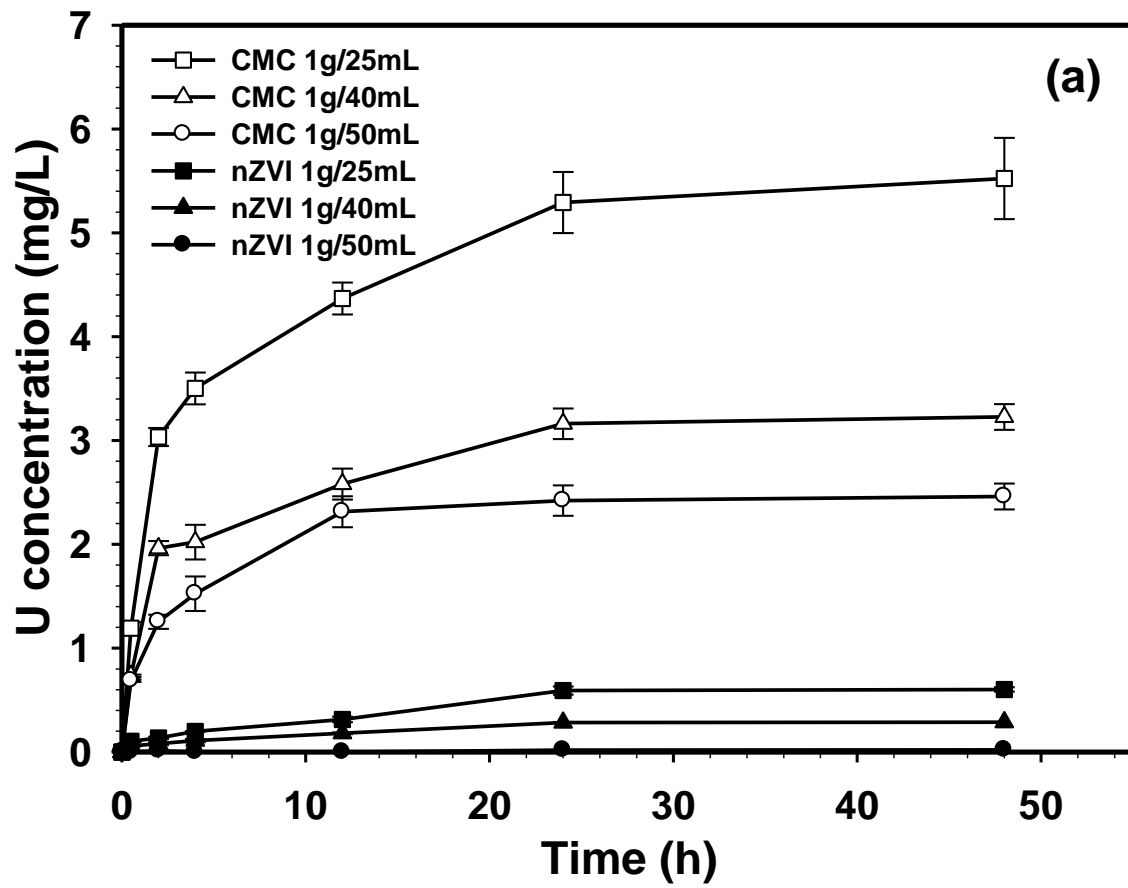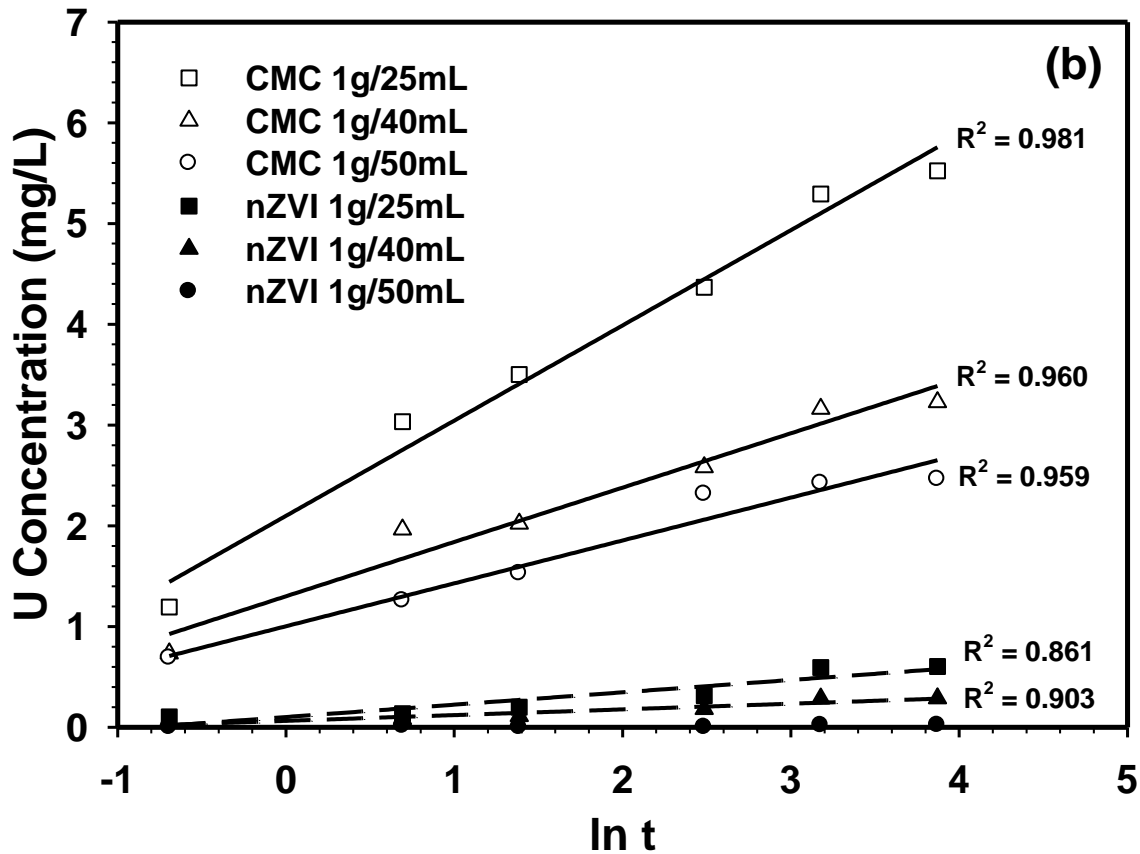
Figure 4-3. (a) Effects of solid-to-solution ratio on desorption rate of U from a U-laden sandy soil in the absence or presence of CMC-nZVI. Experimental conditions: Initial U in soil = 395 mg/kg; Soil/solution ratios = 1 g/25 mL, 1 g/40 mL, and 1 g/50 mL; nZVI = 0.1 g/L as Fe, CMC = 0.2 wt.%, pH = 6.0-6.5. **(b) Linearized model fittings to the experimental data.** Symbols: Experimental data; Lines: Simple Elovich model simulations.

Figure 4-3a shows the desorption kinetics of uranium from U-spiked soil at the solid:liquid ratios of 1:25, 1:40, and 1:50 (g:mL) in the presence of the background CMC solution or CMC-stabilized nZVI at pH 6. At equilibrium, the soluble U concentrations in the CMC control solutions were 5.5, 3.2 and 2.5 mg/L, respectively, when at the solid-to-solution ratios of 1:25, 1:40, and 1:50; in the presence of 0.1 g/L of CMC-nZVI, the corresponding soluble U was reduced to 0.61, 0.28 and 0.02 mg/L, i.e., when one gram of the U-laden soil is treated with 25, 40, and 50 mL of the nZVI suspension, the solution-leachable U can be by 89%, 91% and 99%, respectively.

The desorption kinetic data were fitted by three empirical kinetic models, including the first-order model (Machida et al., 2004), the parabolic diffusion model (Raven et al., 1998), and the simplified Elovich model (assume $\alpha\beta t \gg 1$ and check it later) (Chien and Clayton, 1980; Polyzopoulos et al., 1986). The equations and the fitting coefficients of determination (R^2) were listed in **Table 4-1**. The simple Elovich model provided the best data fitting with the highest coefficient of determination ($R^2 \geq 0.959$). **Figure 4-3b** shows the linearized model fittings to the experimental data (U concentration vs. ln t). Evidently, the simple Elovich equation is able to adequately interpret the kinetics of uranium desorption with and without the nanoparticles, in which the assumption was checked that $\alpha\beta t \gg 1$ for all cases (e.g. $\alpha\beta t \geq 4.6$ for the case of CMC 1g/25mL starting from the first data point). The α value is equivalent to the initial gradient which varied different q_e and different extractant volumes (Ho and McKay, 2009). It has proved that the simple Elovich model is suitable to investigate any changes of surface reactivity in the sorbents during the desorption and good for highly heterogeneous systems such as the uranium desorption from soils (Chien and Clayton, 1980). The failed fittings with the first order and the diffusion models further indicate the uranium desorption kinetics is a chemisorption process, not limited either by uranium concentration or intraparticle radial diffusion (Raven et al., 1998).

Table 4-1. **Various empirical models used for fitting U desorption kinetic data and the resultant fitting coefficients of determination (R^2)**

Kinetic models	Governing Equation	Transformed Linear Equation	R^2		
			1:25	1:40	1:50
First order	$\ln q_t = \ln q_0 - k_1 t$	$\ln q_t$ vs t	0.648	0.600	0.572
Parabolic diffusion	$q_t = q_0 + k_p t^{0.5}$	q_t vs $\ln t^{0.5}$	0.834	0.811	0.810
Simple Elovich	$q_t = \dfrac{1}{\beta}\ln\alpha\beta + \dfrac{1}{\beta}\ln t$	q_t vs $\ln t$	0.981	0.960	0.959

Note: q_t and q_0 are the amounts of U in the soil (mg kg^{-1}) at time t (h) and 0, respectively; k_1 is the first-order rate constant (h^{-1}); k_p is the diffusion rate constant (mg kg^{-1} h$^{-0.5}$); α and β are constants during any one experiment, α regards the initial U desorption rate, β is U desorption constant.
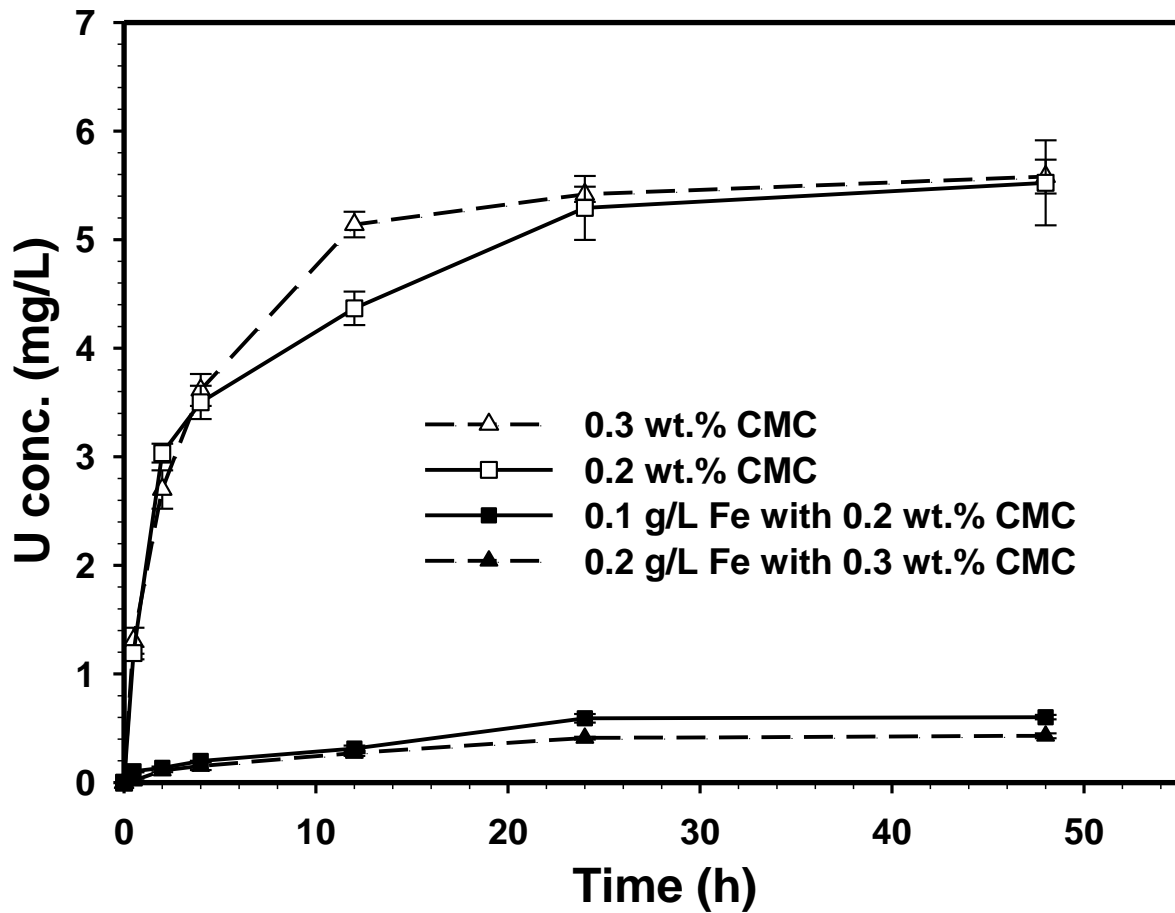
Figure 4-4. Effects of Fe concentration on desorption rate of U from a U-laden sandy soil in the absence or presence of CMC-nZVI. Experimental conditions: Initial U in soil = 395 mg/kg; Soil/solution = 1 g/25 mL; Fe = 0.1 or 0.2 g/L, CMC = 0.2 or 0.3 wt.%, pH = 6.0-6.5.

When the nZVI concentration was increased from 0.1 g/L (0.2 wt.% CMC) to 0.2 g/L (0.3 wt.% CMC), the equilibrium soluble U concentration (at 48 h) was only modestly suppressed from 0.60 to 0.42 mg/L (**Figure 4-4**). The desorption rate of U from the soil was slightly increased when the CMC concentration in the control was increased from 0.2 to 0.3 wt.%. Based on the bicarbonate extraction tests, ~85% of the removed U(VI) was due to the reductive precipitation in the presence of 0.1 g/L nZVI, while ~90% of U(VI) was reduced to U(IV) when treated 0.2 g/L nZVI. It is evident that the increasing of iron concentration didn't contribute much to the entire U immobilization, but enhanced the U(VI) reduction, which could be due to the limited specific mass transfer area (solid-to-solution ratio) and increased reductive potential (iron concentration).

4.3.1.4 pH effects on U immobilization
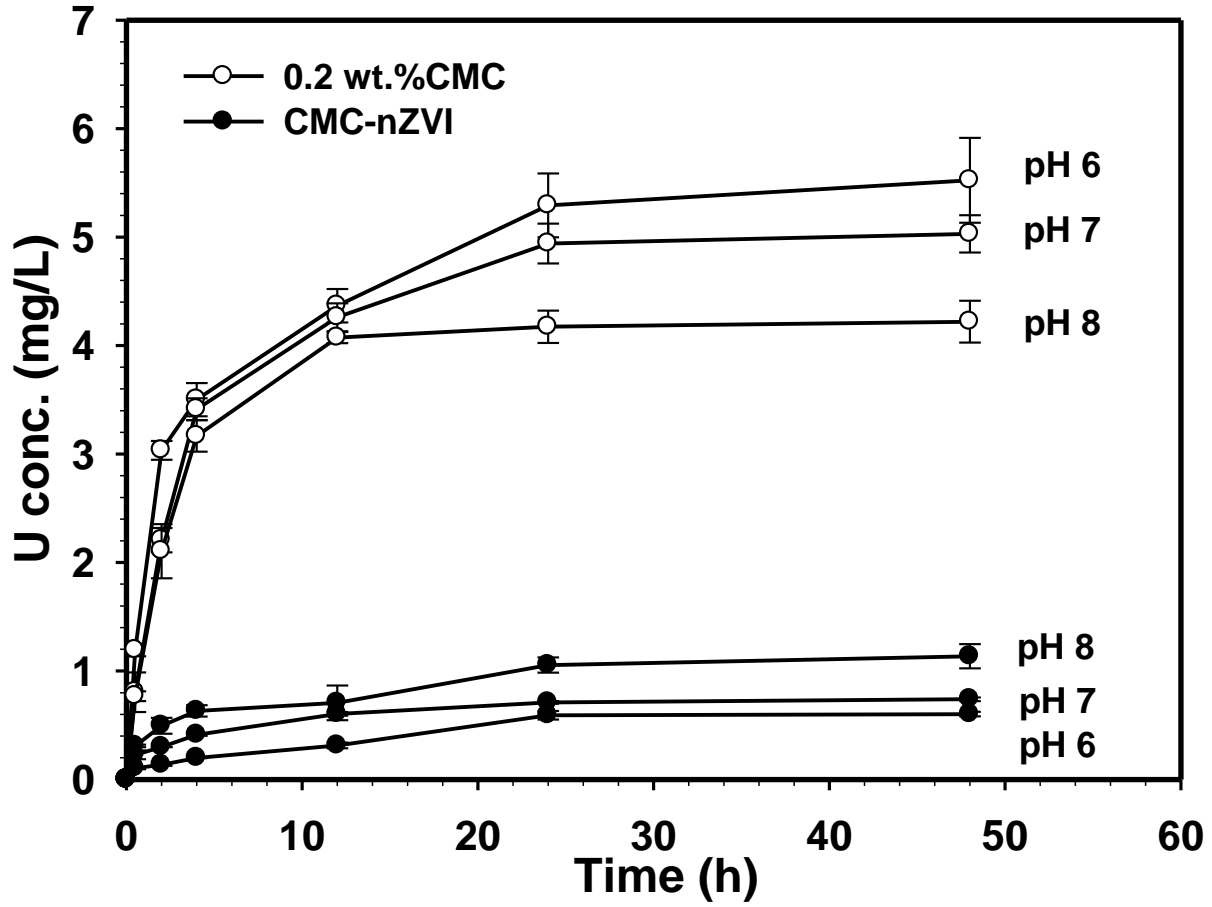
Figure 4-5. Effects of pH on desorption rate of U from a U-laden sandy soil in the absence or presence of CMC-nZVI. Experimental conditions: Initial U in soil = 395 mg/kg; Soil/solution = 1 g/25 mL; Fe = 0.1 g/L, CMC = 0.2 wt.%, pH varies from 6 to 8.

Figure 4-5 shows the U desorption rates from the U-laden soil at three treatment pH levels. At 48 h, the background CMC solution leached out 35%, 32% and 27% U from the soil at pH 6, 7 and 8, respectively, indicating U is more leachable at lower pH. Noubactep et al. (2003) reported a U(VI) solubility of 0.95 mg/L at pH 7.2. In this study, it is evident that the presence of CMC enhanced the U solubility due to the formation of CMC-U complexes (both U(VI) and U(IV) species may complex with CMC). The effects of ligands on U solubility effects (e.g., $NaHCO_3$ and humic acid) have been well known studied (Zhou and Gu, 2005). High concentrations of uranium (up to 50 mg/L) was detected in groundwater at the Field Research Center in Oak Ridge, TN, by Wu et al. (2006). Thus, the uranium solubility in water is strongly affected by pH, ionic strength and organic compounds. In the aqueous solution, the speciation of U(VI) depends on the hydrolysis products of (UO_2^{2+}), including $UO_2(OH)^+$, $(UO_2)_2(OH)_2^{2+}$, $(UO_2)_3(OH)_5^+$, $(UO_2)_4(OH)_7^+$, $(UO_2)_2(OH)_2$, $(UO_2)_3(OH)_7^-$, $(UO_2)_2(OH)_3^-$. At lower pH, the concentrations of the positively charged U species are higher (Hyun et al., 2012), resulting in more U-CMC complex, i.e., more U is dispersed in the aqueous phase by the dissolved CMC molecules, which agrees with the results by Popescu et al. (2013).

Contrarily, the immobilization by CMC-nZVI was more favored at lower pH (**Figure 4-5**), i.e., the final soluble U concentration was 0.6, 0.7 and 1.1 mg/L at pH 6, 7 and 8, respectively. The pH-dependence of U(VI) reduction can be described by the proposed reaction equation (Fiedor et al. 1998):

$$Fe^0 + 1.5UO_3^{2+} + 6H^+ = Fe^{3+} + 1.5U^{4+} + 3H_2O \qquad E_0 = +0.17V \quad \textbf{(4-4)}$$

Eq. 4-4 reveals that the reduction of U(VI) is thermodynamically favored at acidic pH. In addition, the surface of CMC-nZVI is more negative at elevated pH, which progressively repels the negatively charged U(VI) hydroxide species what are more favorably formed at alkaline pH.

However, the corrosive dissolution of the stabilized nZVI becomes prohibitively fast at pH <5. Therefore, this technology is best suitable for the pH range of 6 to 8. Commercially available ZVI is generally much larger aggregates that are coated with a thicker layer of iron oxide layer, and thus is more resistant acidic pH. Klimkova et al. (2011) studied the uranium removal from acid mine water and found commercial nZVI was effective at pH 3.

$$Fe^0 + 2H_2O \ = \ Fe^{2+} + 2OH^- + H_2 \qquad \textbf{(4-5)}$$
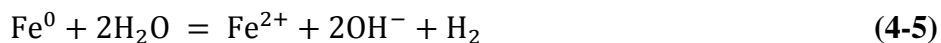
One common concern of synthesized nZVI is that Fe^0 may react with water (**Eq. 4-5**) with the resultant Fe^{2+} and H_2 released into the solution. H_2 is a potential reductant for U(VI) although the reactive lifetime for the CMC-nZVI is very short and most of the nanoparticles trend to react with U(VI) (He and Zhao, 2008). As reported (Perrin et al., 2001; PIJOLAT, 1997), H_2 has been able to reduce U_3O_8 to UO_2 under high temperature (e.g., 510-550 °C) by thermogravimetry. To investigate the effect of H_2 on the U(VI) reduction in solution under room temperature, batch tests were conducted to reduce U-laden soil using H_2 gas. The presence of saturated H_2 (i.e., solubility = 1.5 mg-H_2/L at 22°C) slightly affected the U desorption rate and less than 5% of leachable U was reduced after 12 hours at pH of 5.5 ± 0.2 (**Figure 4-6**). Therefore, the U(VI) reduction by H_2 produced by the reaction between Fe^0 and water is not considered as a factor in this study.
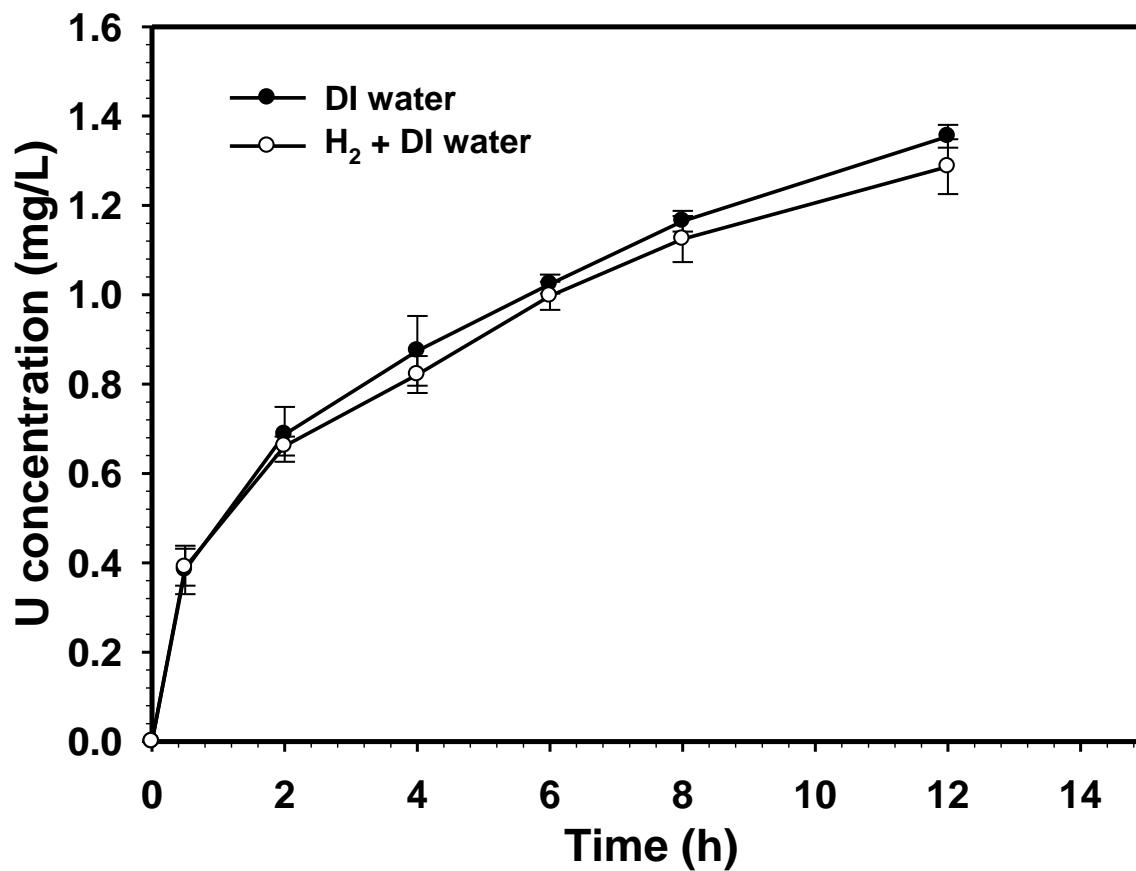
Figure 4-6. Effects of the H₂ gas on desorption rate of U from a U-laden sandy soil.
Experimental conditions: Initial U in soil = 395 mg/kg; Soil/solution = 1 g/40 mL; pH = 5.5 ±
0.2.

4.3.2 Remobilization of uranium and bioactivity effects
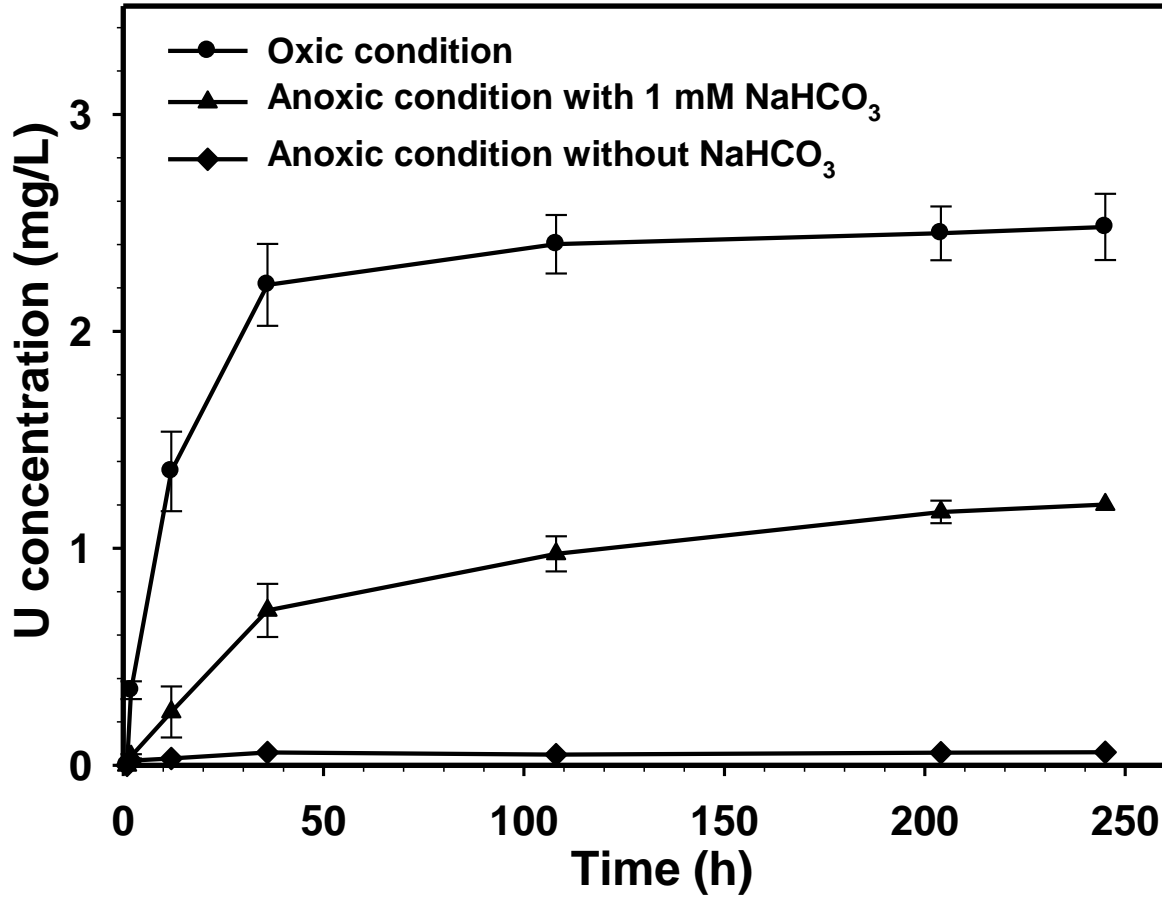
Figure 4-7. Remobilization of CMC-nZVI immobilized U in a sandy soil under anoxic and oxic conditions with or without bicarbonate. Treatment conditions: Initial U in soil = 395 mg/kg, Soil/solution = 3 g/150 mL, Fe = 0.1 g/L, CMC = 0.2 wt.%, pH = 6.0-6.5; Desorption experiments: Soil/solution = 3 g-freeze-dried soil sample/150 mL-DO free DI water, oxic = open to air (DO = ~10 mg/L), anoxic = sealed in the reactor.

Figure 4-7 profiles the remobilization of U from the soil that was treated by 0.1 g/L of CMC-nZVI at 1 g/50 mL (**Figure 4-3**). The treated soil samples were subjected to three different conditions, namely, anoxic (i.e., desorption with DO-free DI water), anoxic with 1 mM bicarbonate, and oxic. Under the anoxic condition without bicarbonate, no soluble U was detected until at Day 10 when 0.06 mg/L (0.7% of total U) was detected in the solution. Long term monitoring showed the soluble U reached and remained at 0.24 mg/L (i.e., 3% of total U) after 1 year of aging. In the presence of 1 mM $NaHCO_3$, 15% of the total U (1.2 mg/L) was leached out after 10 days, and increased to 24% of total U (1.9 mg/L) after 1 year. Bicarbonate has been known to strongly complex with U(VI) and has been commonly used for extracting uranium from contaminated soil (Phillips et al., 1995; Zhou and Gu, 2005). Therefore, the excess of leached uranium in the presence of 1 mM of $NaHCO_3$ under anoxic condition would account for the U(VI) sorbed on the surfaces of particles or soil which was not reduced to U(IV) during the CMC-nZVI treatment.

When the nZVI treated soil was exposed to the air, 27% of the immobilized U (2.2 mg/L) was leached into the aqueous phase in 2 days, 31% (2.5 mg/L) in 10 days, and 52% after 1 year, indicating the immobilized U tends to be reoxidized under oxic condition. The desorption steady state was reached at ~ 6 months. Wan et al. (2005) also found the bioreduced insoluble U(IV) was reoxided and solubilized after 100-500 days under sustained reducing conditions, i.e., the U(IV) content in the total U decreased from 87% on Day 107 to 58% on Day 346, which was due to the enhanced formation of highly stable carbonato-U(VI) complexes by microbial respiration and carbonate accumulation under neutral to slightly alkaline conditions.
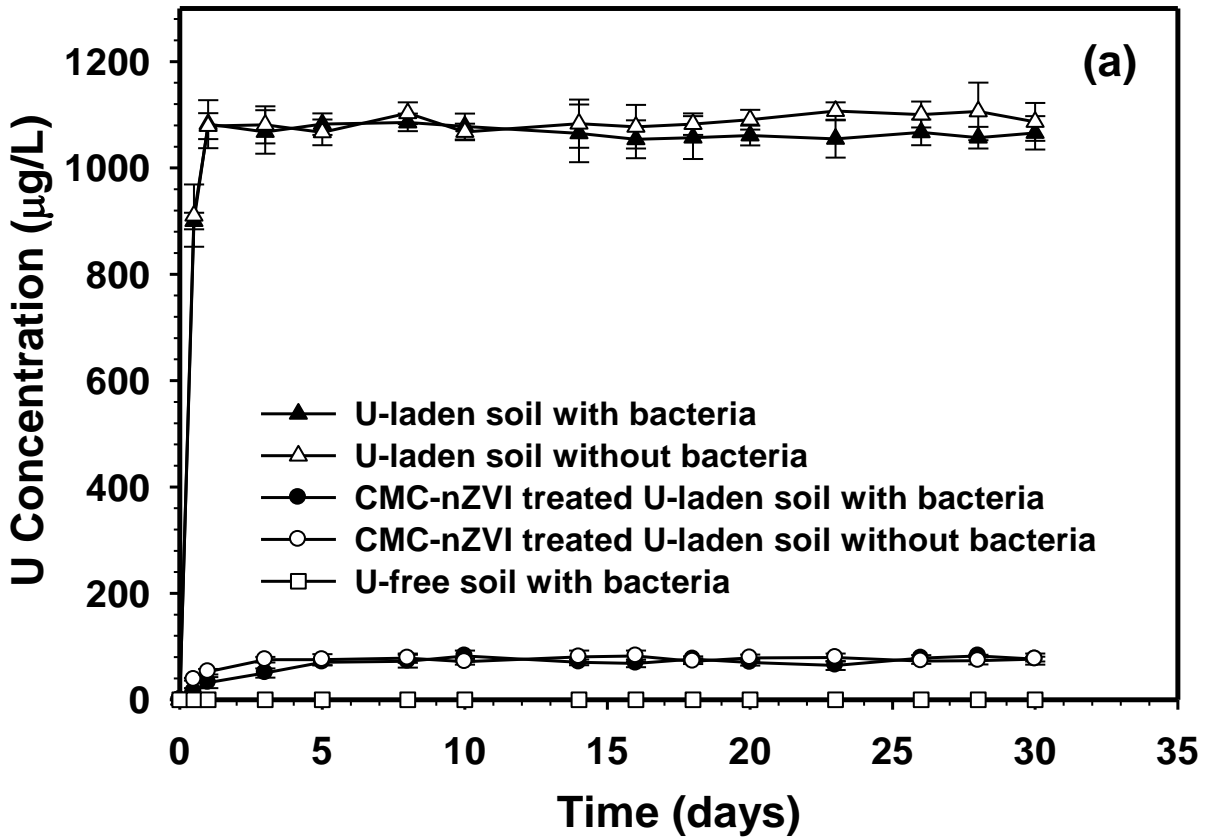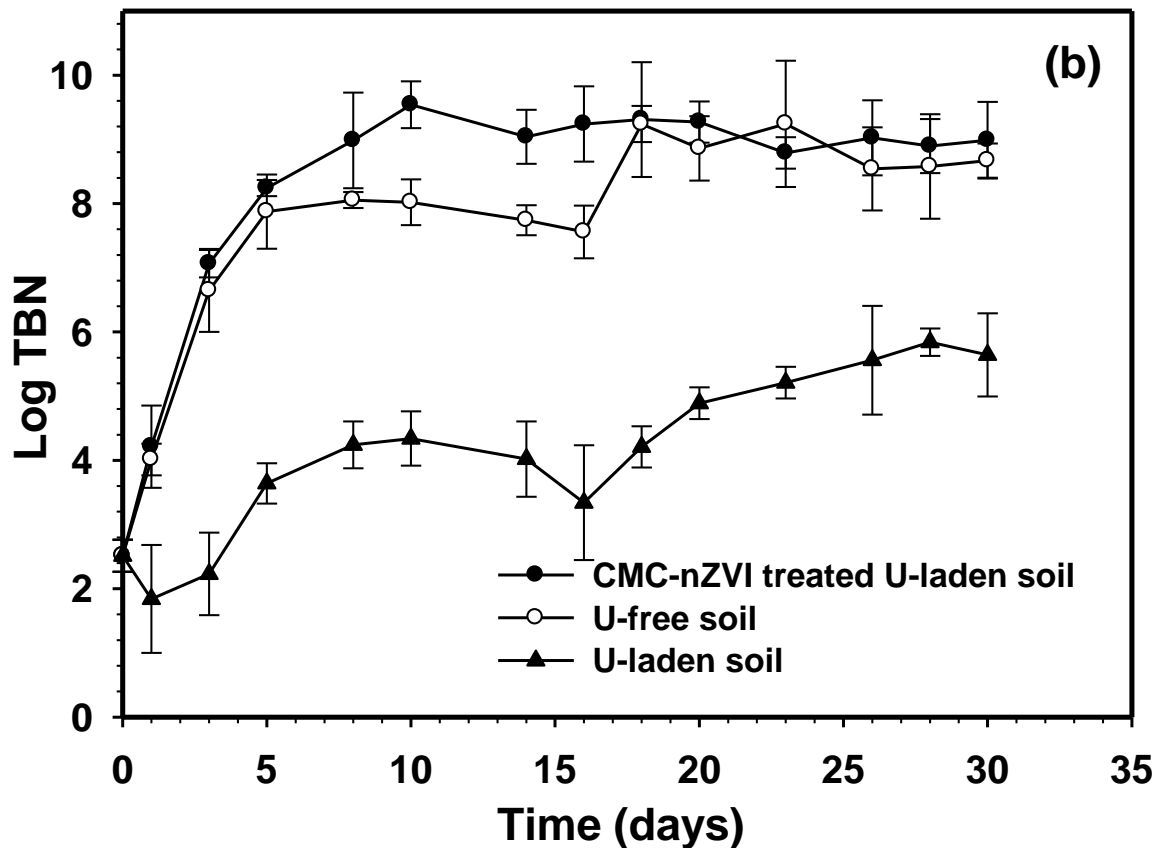
Figure 4-8. (a) U leaching from soil samples (U-laden soil, CMC-nZVI treated U-laden soil, U-free soil) in the presence and absence of active microbial activity; (b) Total bacteria number during continuously fed batch culture in the presence of untreated U-laden soil, CMC-nZVI treated U-laden soil, and U-free soil. Experiential conditions: total U in both treated and untreated U-laden soil = 395 mg/kg, pH=6.5 ± 0.6, temperature=21 ± 1 °C.

Figure 4-8a shows the transient U leaching in the presence of active microbial activity (log TBN at steady state varies from 6~9 in different cases). The equilibrium soluble U concentration leached from the untreated U-laden soil was ~1100 μg/L in both presence and absence of bacteria. No U was detected in the system of U-free soil, culture solution and microbial community, which means no U was produced by microbial activity. For the CMC-nZVI treated soil, the soluble U remained below 80 μg/L (i.e., less than 1 % of total U) in 30 days, indicating that microbial activities and related by-products (e.g., extracellular polymeric substances, bio-decomposed CMC) will not remobilize the immobilized U.

Figure 4-8b shows a fortuitous effect of the U-immobilization treatment. Comparing the TBN value in the batch tests of U-laden soil and U-free soil under identical conditions, i.e. log TBN at steady state was ~6 for the former and ~9 for the latter, evidently, it is clear that the U-laden soil has a negative effects on the bacteria growth even though there was no effect of microbial activity on the U desorption. Whereas, the bacteria growth in the batch tests of U-free soil and CMC-nZVI treated soil are comparable (log TBN ~ 9), indicating that the bio-toxicity of U(VI) in soil will inhibit the bioactivity and the CMC-nZVI treatment can effectively reduce the U(VI) bio-toxicity with no further harmful effects on bacterial growth.

4.3.3 Transport of nZVI in soil
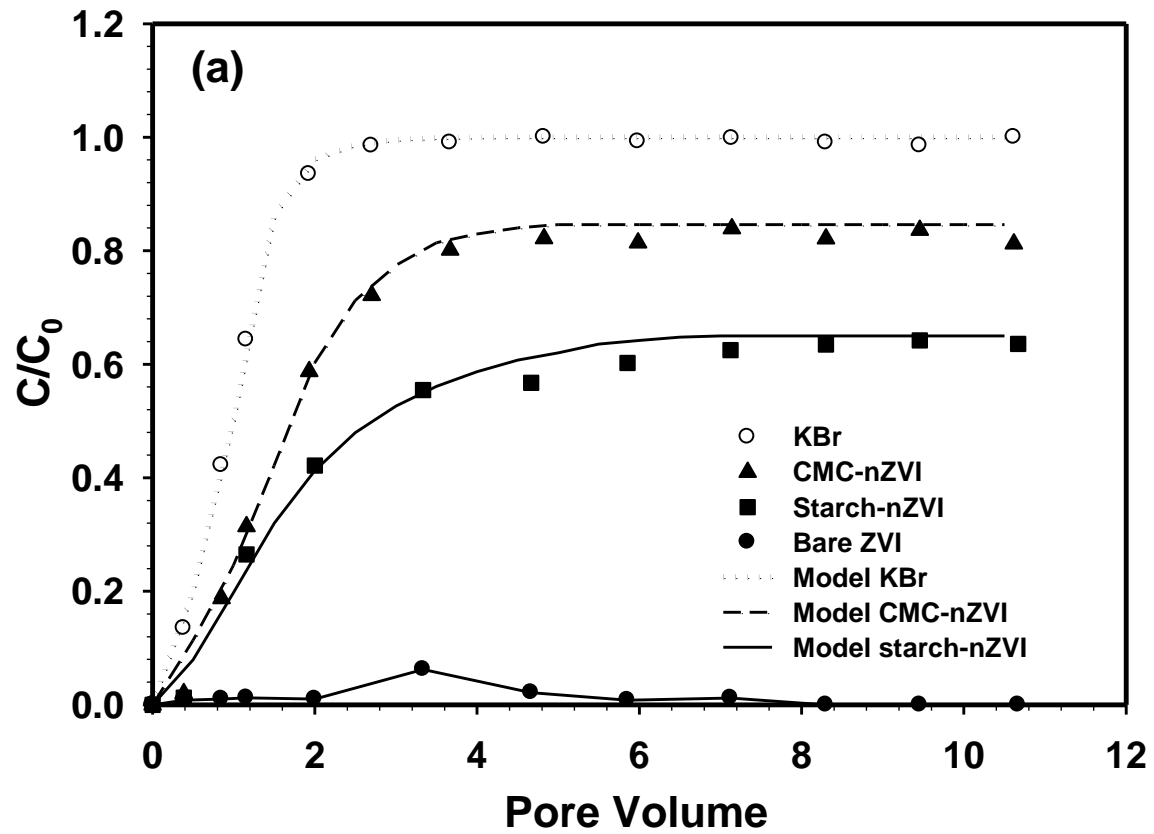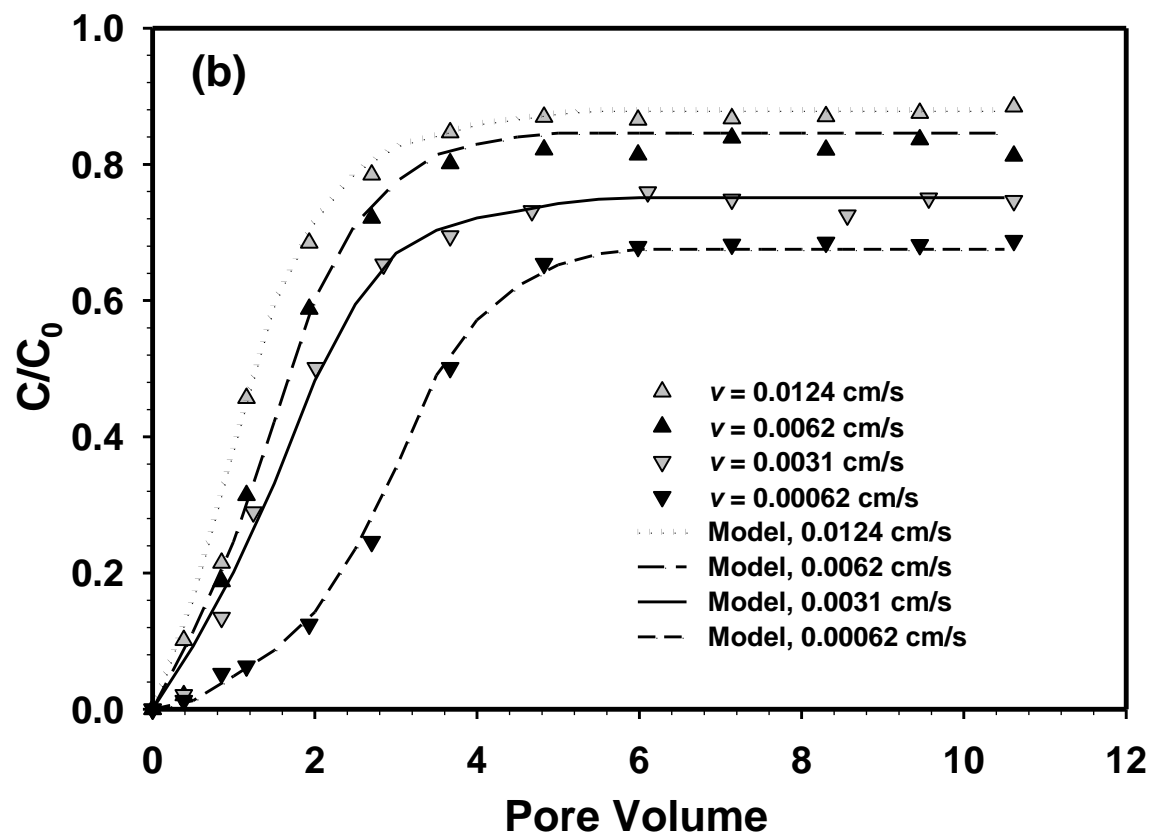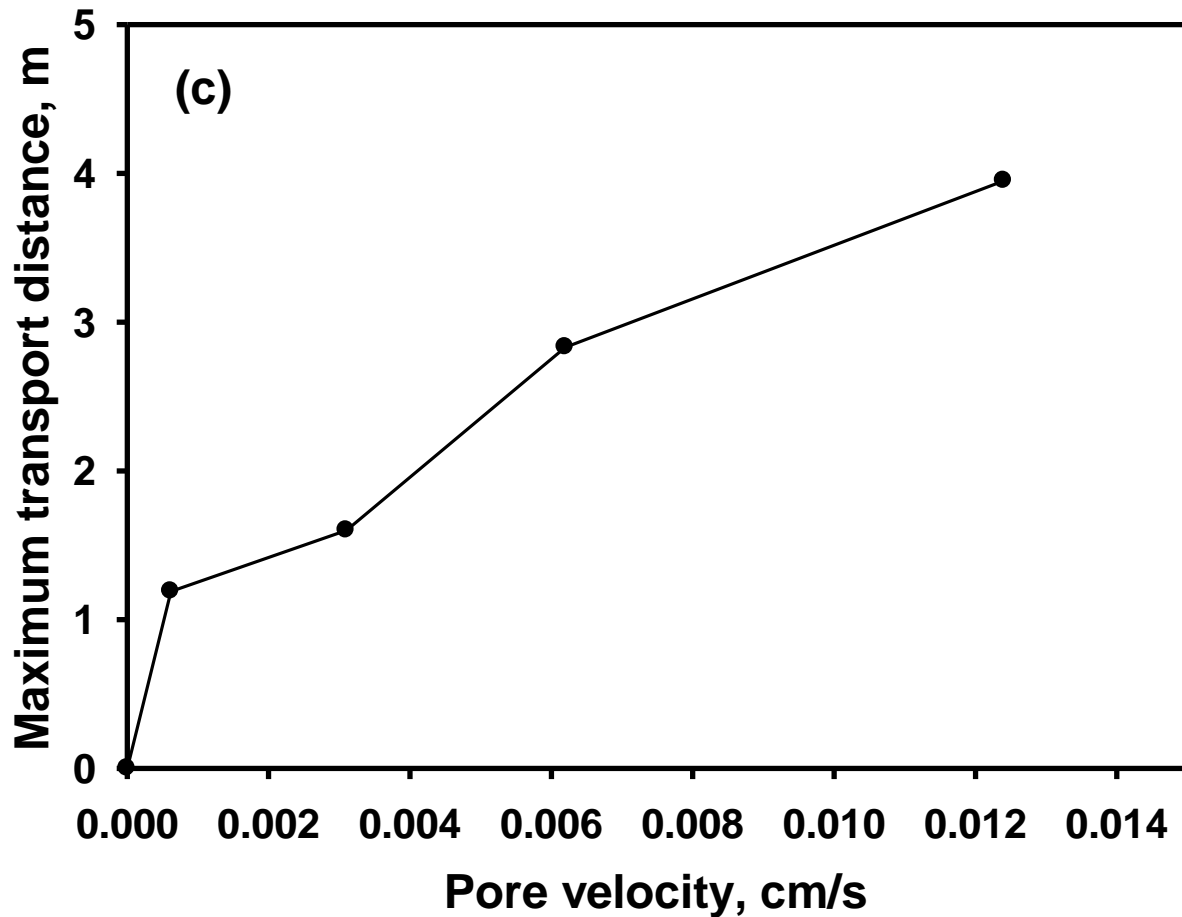
Figure 4-9. (a) Breakthrough curves of bromide, bare and stabilized ZVI nanoparticles through a sandy soil bed at a pore velocity (v) of $6.2 \times 10\text{-}3$ cm/s. (b) Breakthrough curves of CMC-nZVI through a sandy soil bed at a pore velocities. (c) Maximum transport distance of CMC-nZVI in the soil as a function of pore velocity. Br- = 50 mg/L, Nanoparticle = 0.1 g/L as Fe, CMC = starch = 0.20 wt.%, pH = 7.0. Symbols: Experimental data; Lines: Model simulations.

Column breakthrough tests were conducted to investigate the soil deliverability of the stabilized nanoparticles. **Figure 4-9a** compares the breakthrough curves of bare, CMC- or starch-stabilized nZVI and a non-reactive tracer solution (KBr) in a sandy soil at a pore velocity of 6.2×10^{-3} cm/s, and **Figure 4-9b** profiles the breakthrough behaviors of CMC-nZVI at various pore velocities. The breakthrough data were interpreted using the CXTFIT code. The hydrodynamic dispersion coefficient (D) was obtained by fitting the equation of continuity to the tracer breakthrough curve, the information was then used to facilitate simulation of the breakthrough curves of the nanoparticles (Feinstein and Guo, 2004).

At the pore velocity of 6.2×10^{-3} cm/s, the full breakthrough of CMC-nZVI occurred after ~3 PVs with a steady C/C_0 (effluent to influent Fe concentration) of ~0.85 (i.e., ~15% of the particles was consistently retained in the soil) (**Figure 4-9a**). For starch-nZVI, the full breakthrough took place after 6 PVs with a much lowered C/C_0 of ~0.65, indicating much greater retention by the soil matrix. In comparison, the full breakthrough of the tracer occurred at ~2 PVs ($C/C_0 = $ ~1), and the bare nZVI was all trapped on top of the soil bed. The more gradual breakthrough of the nanoparticles reflects the greater mass transfer resistance, dispersion, and soil filtration effects of the nanoparticles than the tracer (Chen et al., 2006). Considering that the challenge for *in situ* remediation has been the poor deliverability, CMC-nZVI is likely more suitable for application although starch-nZVI showed modestly higher immobilization effectiveness in the batch tests (**Figure 4-1**). Consequently, CMC-nZVI was further studied for in the subsequent column tests.

Figure 4-9b shows that when the pore velocity was increased to 0.012 cm/s, the full breakthrough plateau increased to ~0.88, whereas the C/C_0 value decreased to 75% and 68% when the pore velocity was lowered to 3.1×10^{-3} and 6.2×10^{-4} cm/s, respectively, . The amount of

nanoparticle retained in the soil bed during the 10 PVs of breakthrough tests was 19%, 26%, 33% and 47%, respectively, at the pore velocities of 1.2×10^{-2}, 6.2×10^{-3}, 3.1×10^{-3} and 6.2×10^{-4} cm/s. This observation indicates that the nanoparticle transport and retention can be manipulated by controlling the injection pressure. The delivered nanoparticles serve as a strong electron source and a sink that facilitates uranium immobilization thorough concurrent reduction, adsorption and precipitation. The subsequent elution tests showed that the deposited nanoparticles were irreversible, i.e., not leachable through water elution (data not shown).

The maximum travel distance L_{max} for the particles was estimated based on the classical filtration theory (He et al., 2009; Tufenkji and Elimelech, 2004):

$$L_{max} = -\frac{2}{3}\frac{d_c}{(1-f)\alpha\eta_o}\ln(0.01) \qquad (4\text{-}6)$$

where L_{max} is the travel distance over which 99% removal of the nanoparticles occurs, d_c is the collector grain diameter, f is the bed porosity, α is the attachment efficiency representing the fraction of collisions between particles and collectors that result in an attachment, η_o is the overall single collector removal efficiency. The calculations follows the procedures in section 2.3.5 and the model parameters were given in **Table 4-2**.

Table 4-2. Experimental conditions and model parameters for simulating the breakthrough curves of the CMC-nZVI

Porous media	Flow rate (mL/min)	Pore velocity (cm/s)	C/C_0	$\eta_{o \times 10^{-5}}$	α	L_{max} (m)
	0.20	1.2 x 10^{-2}	0.88	9.8	3.491	3.95
	0.10	6.2 x 10^{-3}	0.85	20.8	2.295	2.83
Sandy soil	0.05	3.1 x 10^{-3}	0.75	44.5	1.899	1.60
	0.01	6.2 x 10^{-4}	0.68	263	0.429	1.19

Figure 4-9c plots L_{max} as a function of pore velocity. The results indicate that once delivered, the nanoparticles will remain in a confined domain under typical natural flow conditions. For example, at a groundwater velocity of 0.1 m/d, L_{max} of the nanoparticles is 1.1 m.

4.3.4 Immobilization of Uranium in soil by nZVI: column test
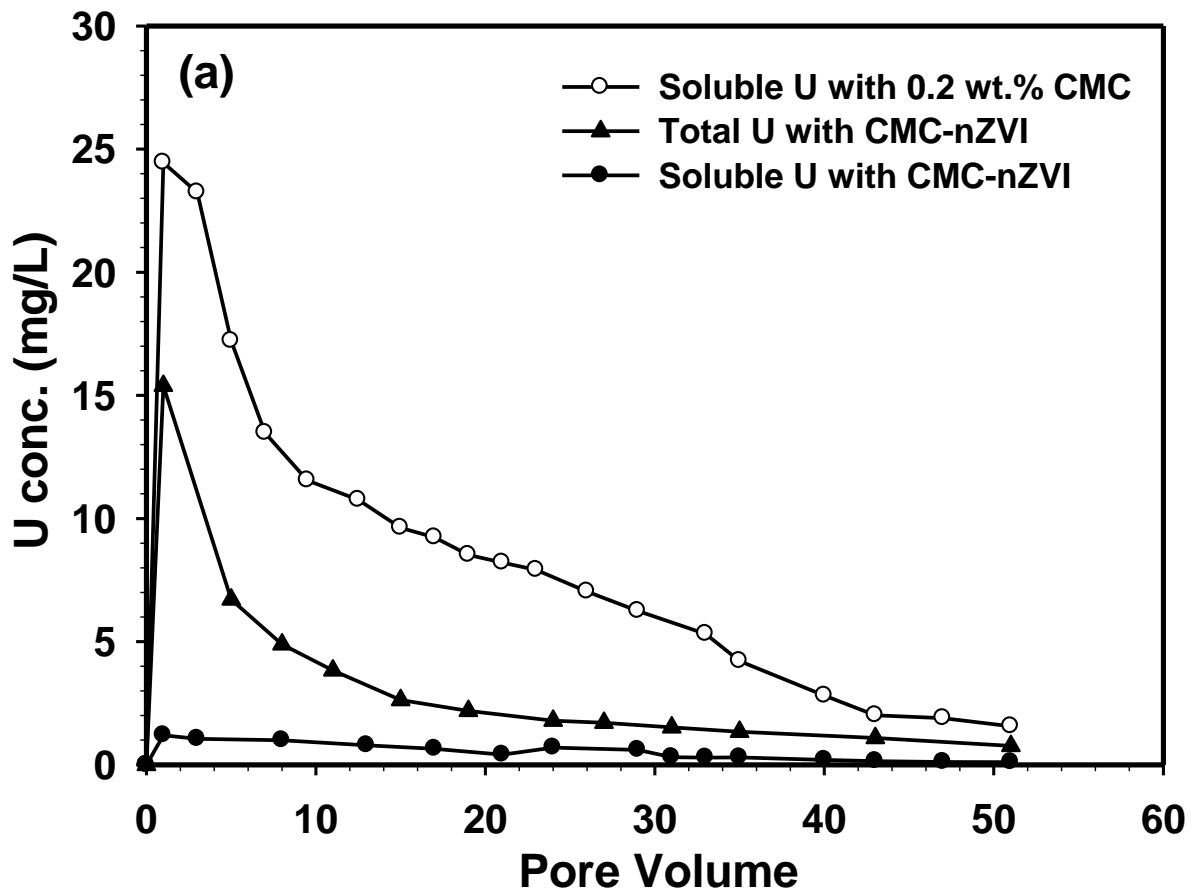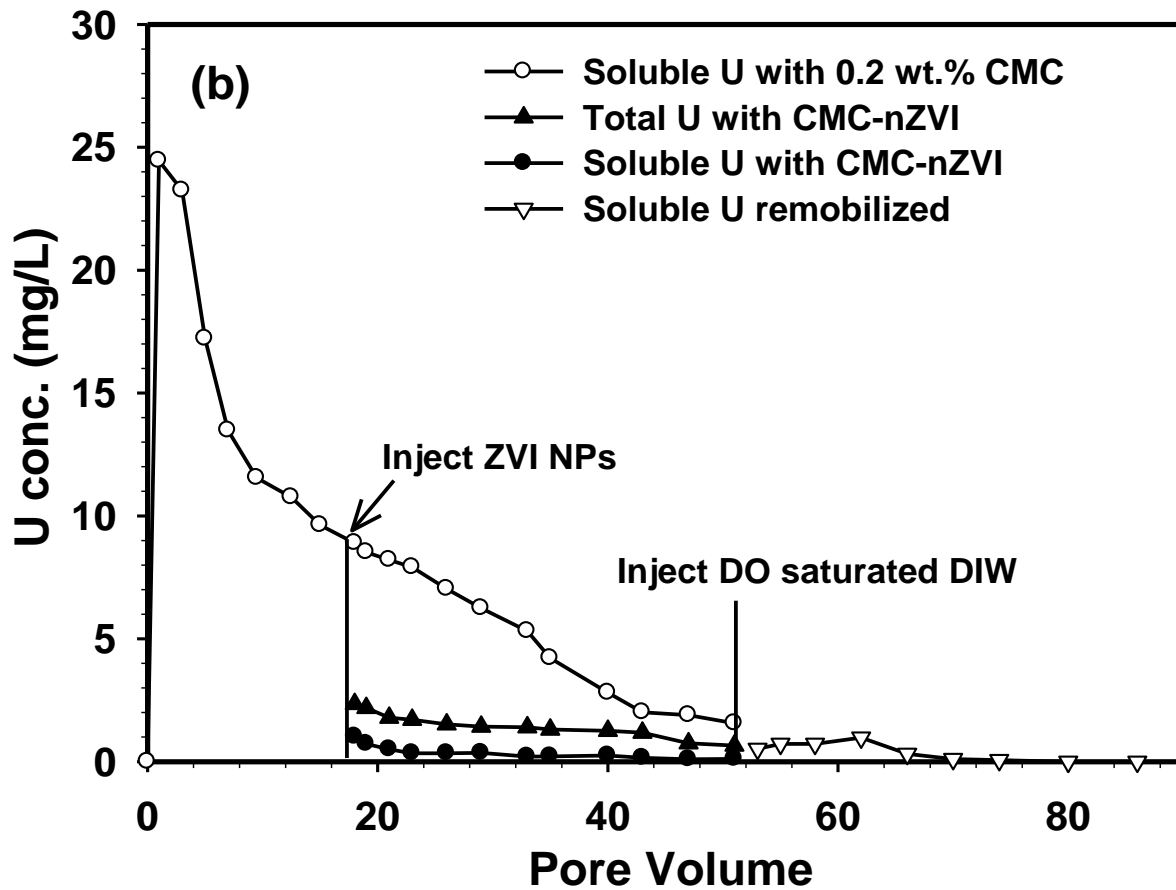
Figure 4-10. (a) U concentration histories during column elution tests by passing a 0.2 wt.% CMC solution or a suspension of CMC-nZVI through a U-laden sandy soil. (b) U concentration histories during three stages of column elution tests: elution by the CMC solution (0-16 PVs), treatment by CMC-nZVI suspension (16-50 PVs), and elution by DO-saturated DI water (50-88 PVs). Initial U(VI) in soil = 395 mg/kg, nZVI = 0.1 g/L as Fe, CMC = 0.2 wt.%, pH = 6.0-6.5, EBCT = 30 min, pore velocity = 6.2×10^{-3} cm/s.

The same fixed-bed column configuration was employed to simulate the application of the CMC-nZVI for *in situ* immobilization of U(VI) in the soil. **Figure 4-10** compares the U elution profiles when the U-laden soil was eluted with 0.2 wt.% CMC or treated with the CMC-nZVI suspension. The elution curves by the background CMC solution displayed a sharp chromatographic peaking of U followed by a gradual tailing profile. Mass balance calculations indicated that the CMC solution eluted ~28% (1.21 mg/4.34 mg) of the soil-sorbed U with a peak U of 24.5 mg/L during the 50 PVs of elution. The nanoparticle amendment in **Figure 4-10a** simulates treating a freshly contaminated soil, where the nanoparticle suspension as introduced without any elution by water. Following the 50 PVs of nanoparticle treatment, ~10% of total U was eluted with a peak U of 15.4 mg/L, of which ~82% was associated with the nanoparticles and ~18% soluble U. Compared to the control, the CMC-nZVI reduced the water-leachable and soluble U by 93% (from 28% to 1.8% of the total U). Based on the transport study, the nanoparticle-associated U in the effluent will be eventually immobilized as the nanoparticles are caught by the downstream soil matrix upon release of the external injection pressure.

Figure 4-10b simulates the scenario that the U contaminated soil had subjected to water leaching before it was treated by CMC-nZVI, i.e., the U-laden soil in the column was first eluted by the CMC solution for 16 PVs and then treated with the CMC-nZVI suspension. The 16 PVs of the solution washing eluted ~18% of the soil-sorbed U. Following the injection of 3 PVs of the nanoparticles, the total U concentration in the effluent sharply dropped to less than 1.5 mg/L and the soluble U concentration less than 0.3 mg/L, compared to ~8 mg/L in the control test. At 50 PVs, the soluble U concentration was less than 50 μg/L and the total soluble U eluted during the nanoparticle treatment was less than 1% of the pre-loaded U.

To investigate the remobilization potential of the nanoparticle-immobilized U in the soil column, DO containing DI water (8 mg/L, pH 7) was subsequently injected at 50 PVs. Considering DO is one of the strongest and most abundant oxidants of U(IV), the hypothesis is that the reoxidation of U(IV) will occur within several hours based on the reported results in batch or sediment column experiments (Hee et al., 2007; Wan et al., 2005). However, the soluble U in effluent remained at ~0.6-0.9 mg/L until ~ 70 PVs, where U became undetectable (**Figure 4-10b**). The remobilized U was less than 1% of the U in the soil right before the nanoparticle injection. This result indicates that the reductively immobilized U in soil bed is more resistant to reoxidation and remobilization than in the batch tests, which could be due to the remaining ZVI particles in the soil. The retained ZVI in soil after the injection may serve as electron sources or oxygen scavengers and inhibit the reoxidation of U(IV), and the beginning U dissolution is limited by surface-oxidation as reported by Bi and Hayes (2013). In addition, the formation of iron oxides and reduced U(IV) occurred in the soil bed, the soil matrix effects may also lead the resistant to the reoxidation and remobilization (Baldock and Skjemstad, 2000).
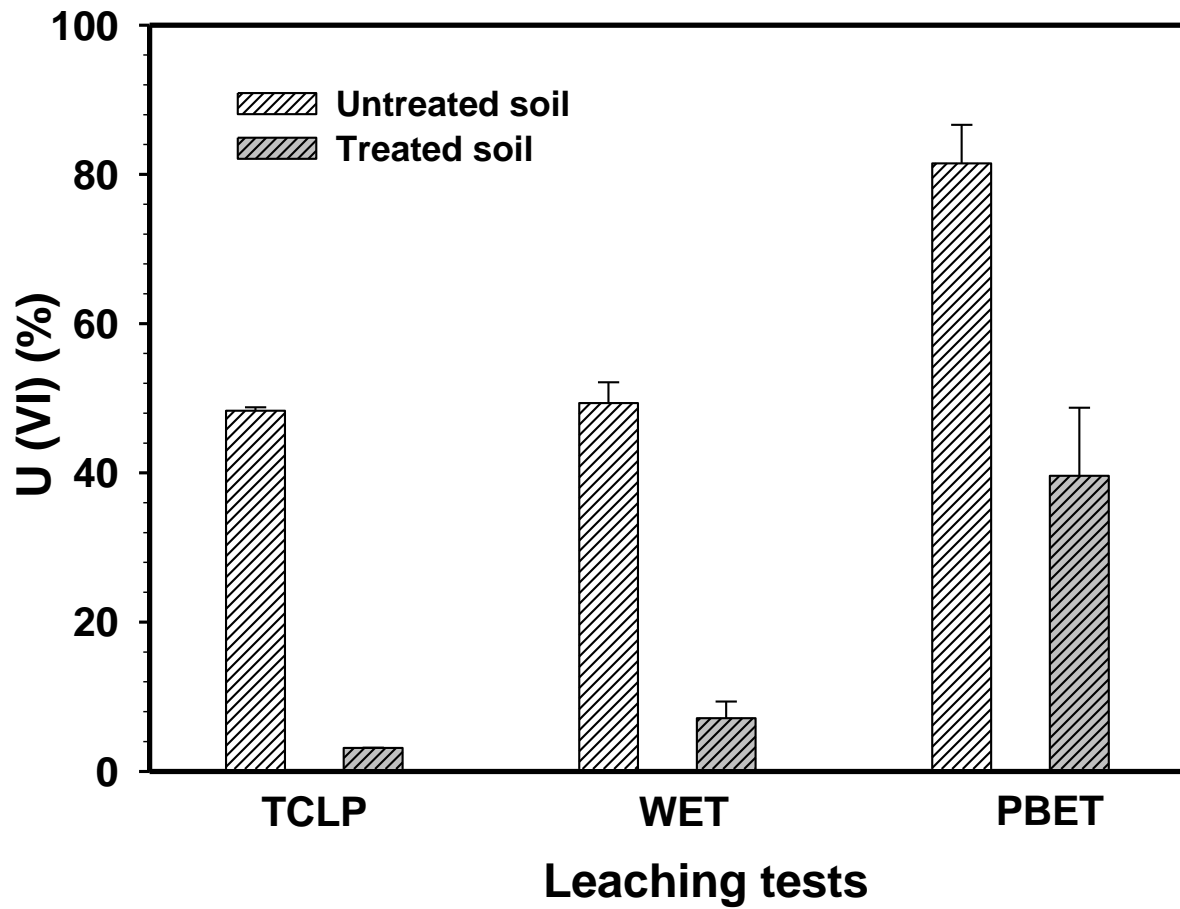
Figure 4-11. TCLP, WET and PBET leachability for U-laden soil that was untreated or treated in Figure 4-10b at 50 PV.

To test leachability of U in the soil after the nanoparticle treatment, the soil following treatment of **Figure 4-10b** and untreated soil samples were subjected to the TCLP, WET and PBET procedures. **Figure 4-11** shows that the TCLP-based leachability (**Eq. 4-3**) was 48% and 3% for the untreated and nanoparticle-amended soil samples, respectively, the WET-based leachability was 49% and 7%, and PBET-based leachability was 81% and 39%. Based on the bicarbonate extraction, the soil samples from **Figure 4-10b** contained ~11% of U(VI) and ~89% of U(IV). After the TCLP and WET procedures, the amount of U(IV) remained the same in the soil samples, only U(VI) leaching out during the leachability tests. In contrast, ~31% of the insoluble U(IV) in the soil sample solubilized into aqueous phase after PBET procedure (i.e., pH ~ 2.3). The much reduced leachability is attributed to the strong sink effect of the soil-retained ZVI nanoparticles. Practically, the nanoparticle amendment may facilitate converting hazardous wastes into non-hazardous wastes by lowering the contaminant leachability, thereby greatly reducing the waste disposal cost.

4.4 Conclusion

The key findings are summarized as following:

- Both starch- and CMC-and stabilized ZVI nanoparticles are able to effectively convert soluble U(VI) to its immobile form U(IV) and reduce the mobility and bio-toxicity of uranium. Reductive precipitation of U(VI) to U(IV) is the primary immobilization mechanism in ZVI treatment based on XPS analysis.

- The immobilized U remained stable under anoxic condition during one year monitoring, while 52% and 24% of the total U leached out under oxic condition and anoxic bicarbonate condition,

respectively. The presence of active microorganisms showed no effect on the stability of the immobilized.

- Both starch and CMC can act as effective stabilizers to facilitate dispersion and transport of ZVI nanoparticles. Column breakthrough tests indicated that ~15% of the delivered CMC-nZVI nanoparticles were retained in the soil after full breakthrough, compared to 35% for starch-stabilized nZVI. The nanoparticle retention and transport distance can be controlled by manipulating the injection pressure or pore flow velocity.

- Column tests demonstrated that amending the U-laden soil with 50 PVs of CMC-nZVI (0.1 g/L) reduced the effluent soluble U by 93%. The nanoparticle amendment also reduced the TCLP and WET leachability and the PBET bioaccessibility of U in the soil.

Chapter 5. Conclusions and Suggestions for Future Research

5.1 Summary and Conclusions

Stabilized Fe-Mn binary oxide nanoparticles were synthesized and tested for the removal and *in situ* immobilization of Se(IV) in groundwater and soil. A water-soluble starch or food-grade CMC was used as a stabilizer to facilitate the *in situ* delivery of the particles into contaminated soil. TEM images revealed a mean particle size of 47 ± 11 (standard deviation) nm and 38 ± 9 nm, respectively, when 0.1g/L (as Fe) of the nanoparticles were stabilized with 0.1 wt.% starch and 0.1 wt.% CMC. While bare and stabilized nanoparticles showed rapid sorption kinetics, starch-stabilized Fe-Mn offered the greatest capacity for Se(IV). The Langmuir maximum capacity was determined to be 110 and 95 mg-Se/g-Fe for the starch- and CMC-stabilized nanoparticles, respectively, with a high Se(IV) uptake being observed over the typical groundwater pH range of 5-8. Column breakthrough tests indicated that the stabilized nanoparticles were deliverable in a model sandy soil while non-stabilized particles were not. When a Se(IV)-spiked soil was treated *in situ* with the nanoparticles, >92% of the water leachable Se(IV) was transferred to the nanoparticle phase and thereby immobilized as the particles were retained in the downstream soil matrix. The nanoparticle amendment reduced the TCLP leachability and WET leachability of Se(IV) by 76% and 71%, respectively.

Animal wastes generated by the poultry industry in the U.S. have a high content of phosphorus and thus pose a potential risk of serious arsenic contamination as a result of the transformation of roxarsone, most of which will be lost into the environment due to uncontrolled release rates. To address this issue, stabilized Fe-Mn binary oxide nanoparticles were applied for

phosphate adsorption from water and for controlling the leachability of P and As from poultry litter. Starch- and CMC-stabilized Fe-Mn nanoparticles were found to offer considerably greater phosphate removal capacity than bare Fe-Mn nanoparticles, with the Langmuir maximum capacity determined to be 250, 300 and 310 mg-P/g for bare, CMC- and starch-stabilized nanoparticles, respectively. The stabilized particles also displayed much faster adsorption kinetics than conventional adsorbents. The presence of the stabilizers not only enhanced the sorption capacity, but facilitated the delivery and dispersion of the nanoparticles in both the poultry litter and in soil. A high phosphate sorption capacity was observed over a broad pH range of 4-9. FTIR analyses revealed the formation of the inner sphere Fe-O-P complexes to be the underlying mechanism driving the high capacity and affinity of the nanoparticles toward phosphate. When applied to poultry litter, the stabilized nanoparticles were found to reduce the water leachable P in PL by >86% at a dosage of 0.2 g/L as Fe; fortuitously, the nanoparticles also diminished the water leachable As from poultry litter by 87-95% at a dose of 0.1 g/L as Fe. Under conditions of simulated land application of poultry litter, the nanoparticle amendment of poultry litter reduced the water soluble P from 66% (untreated) to 4.4%, and lowered the peak soluble P concentration by a factor of >20 (from 300 mg/L to <20 mg/L). The water soluble As was simultaneously reduced from 79% to 5%. By converting the soluble P to nanoparticle-bound P, the nanoparticles therefore not only greatly reduce the potential runoff loss of P from PL, but also provide a long-term slow-releasing nutrient source. Given their excellent adsorption capacity, easy deliverability, low cost and environmental amity, the stabilized Fe-Mn nanoparticles appear to offer a promising new approach for phosphate recovery from water and for controlling P and As releases from poultry litter or other animal wastes.

With the growth in uranium mining and the increasing need for the disposal of nuclear waste, rising levels of U(VI) in soil and groundwater is now becoming a problem in many areas around the world. Due to its high solubility and mobility, U(VI) is considered a major hazard that threatens both environmental and human health. We therefore prepared and tested a new class of polysaccharide stabilized ZVI nanoparticles for the *in situ* reductive immobilization of U(VI) in soil using a water-soluble starch or food-grade CMC as a stabilizer. The nanoparticles were found to be an effective way to convert soluble U(VI) to its immobile form U(IV), thereby greatly reducing the mobility and bioavailability of the uranium. Reductive precipitation of U(VI) to U(IV) is the primary immobilization mechanism in ZVI treatment based on XPS analysis. Batch experiments indicated that the U(VI) leachability of the contaminated soil was reduced by nearly 99% when a U(VI) spiked sandy soil (395 mg-U/kg-soil) was amended with the CMC-nZVI (0.1 g/L) at a soil-to-liquid ratio of 1 g/50 mL at pH 6.0. When subjected to remobilization tests, <1% of the immobilized U(IV) was released into the aqueous phase under anoxic conditions, rising to 31% in 10 days and 52% after 1 year under oxic conditions. Natural microbial activity did not inhibit the ZVI-facilitated U immobilization, and the reductive immobilization effectively lowered the bio-toxicity of U(VI). Column tests indicated that the CMC-nZVI provides high soil deliverability and both starch and CMC act as effective stabilizers to facilitate the dispersion and transport of ZVI nanoparticles. Column breakthrough tests demonstrated that ~15% of the delivered CMC-nZVI nanoparticles were retained in the soil after full breakthrough, compared to 35% for starch-stabilized nZVI. The nanoparticle retention and transport distance can be controlled by manipulating the injection pressure or pore flow velocity. Column tests indicated that when a U-laden soil bed was treated with 50 pore volumes of the nanoparticle suspension at pH 6.0, water

soluble U was reduced by 93%. This type of *in-situ* immobilization may provide a powerful alternate technology for mitigating the adverse impacts of U in both soil and groundwater.

5.2 Uniqueness and Contribution

1. Fe-Mn binary oxide nanoparticles have high sorption capacity toward a number of anions and can serve as strong absorbents for multiple contaminants such as Se, As, and P. The stabilized Fe-Mn nanoparticles are soil deliverable and the travel distant of the nanoparticles in soil can be manipulated by controlling the injection pressure.

2. Fe-Mn nanoparticles are not oxygen sensitive and can be synthesized either on site or in a manufacturing facility. The cost of the nanoparticles for industry application is acceptable, estimated at \$1.8-2.2/kg-Fe.

3. The nanoparticles were applied by the researcher to the pretreatment sink of the constructed wetland in Shanghai Houtan Park, which won the 2010 ASLA (American Society of Landscape Architects) Award of Excellence. My colleagues and I designed this constructed wetland which is a 1.7 km river that flows through the Houtan Park that serves as a living machine to treat the contaminated water from the Huangpu River and provide safe water throughout the 2010 Shanghai Expo for nonpotable uses. In 2014, I modified the pretreatment of the river water using Fe-Mn nanoparticles based on the concerns expressed regarding the high potential risk posed by anion contaminants such as N, P, and As. Therefore, I have not only synthesized and studied the nanoparticles, but also utilized them in a real world industrial application. As one of the founders of Shanghai Zhonghui Ecological Technologies Co. Ltd, we successfully bid on a 3 year soil remediation project in Chengdu, China, in 2014 based on the application of these stabilized

Fe-Mn nanoparticles and I am eagerly anticipating the opportunity to observe how the nanoparticles work in a large-scale real world project.

5.3 Suggestions for Future Work

The specific recommendations for future work are as follows:

1. X-ray diffraction (XRD), x-ray photoelectron spectroscopy (XPS), extended x-ray absorption fine structure (EXAFS), scanning electron microscopy (SEM), and transmission electron micrograph (TEM) image tests on stabilized Fe-Mn nanoparticles synthesized with CMC and starch before and after treatment would provide more reliable evidence to help elucidate the precise structure of the stabilized nanoparticles.

2. Field implementations and demonstrations of stabilized Fe-Mn nanoparticles in multiple contaminated sites are needed to validate the effectiveness of this novel *in situ* remediation technology. Onsite practical experience would also help reveal any potential limitations in the procedures and methods.

3. There remain a number of unsolved mysteries regarding the environmental fate and impacts of Fe-Mn and ZVI nanoparticles. More extensive experiments need to be conducted to validate the maximum transport distance. The ultimate fate and the dissolution mechanism of the spent nanoparticles pose interesting research questions that also require further investigation.

References

Allard, S., von Gunten, U., Sahli, E., Nicolau, R., Gallard, H., 2009. Oxidation of iodide and iodine on birnessite (delta-MnO$_2$) in the pH range 4-8. Water Res. 43, 3417–26. doi:10.1016/j.watres.2009.05.018

An, B., Liang, Q., Zhao, D., 2011. Removal of arsenic(V) from spent ion exchange brine using a new class of starch-bridged magnetite nanoparticles. Water Res. 45, 1961–72. doi:10.1016/j.watres.2011.01.004

An, B., Steinwinder, T.R., Zhao, D., 2005. Selective removal of arsenate from drinking water using a polymeric ligand exchanger. Water Res. 39, 4993–5004. doi:10.1016/j.watres.2005.10.014

An, B., Zhao, D., 2012. Immobilization of As(III) in soil and groundwater using a new class of polysaccharide stabilized Fe-Mn oxide nanoparticles. J. Hazard. Mater. 211-212, 332–341. doi:10.1016/j.jhazmat.2011.10.062

Antelo, J., Avena, M., Fiol, S., López, R., Arce, F., 2005. Effects of pH and ionic strength on the adsorption of phosphate and arsenate at the goethite-water interface. J. Colloid Interface Sci. 285, 476–86. doi:10.1016/j.jcis.2004.12.032

Arai, Y., Lanzirotti, a, Sutton, S., Davis, J. a, Sparks, D.L., 2003. Arsenic speciation and reactivity in poultry litter. Environ. Sci. Technol. 37, 4083–90.

Arai, Y., Sparks, D.L., 2001. ATR–FTIR spectroscopic investigation on phosphate adsorption mechanisms at the ferrihydrite–water interface. J. Colloid Interface Sci. 241, 317–326. doi:10.1006/jcis.2001.7773

Baldock, J., Skjemstad, J., 2000. Role of the soil matrix and minerals in protecting natural organic materials against biological attack. Org. Geochem. 31, 697–710. doi:10.1016/S0146-6380(00)00049-8

Bednar, a J., Medina, V.F., Ulmer-Scholle, D.S., Frey, B. a, Johnson, B.L., Brostoff, W.N., Larson, S.L., 2007. Effects of organic matter on the distribution of uranium in soil and plant matrices. Chemosphere 70, 237–47. doi:10.1016/j.chemosphere.2007.06.032

Bednar, A.J., Garbarino, J.R., Ferrer, I., Rutherford, D.W., Wershaw, R.L., Ranville, J.F., Wildeman, T.R., 2003. Photodegradation of roxarsone in poultry litter leachates. Sci. Total Environ. 302, 237–45.

Bellows, B.C., 2005. Arsenic in Poultry Litter: Organic Regulations. NCAT.

Bennett, P., He, F., Zhao, D., Aiken, B., Feldman, L., 2010. In situ testing of metallic iron nanoparticle mobility and reactivity in a shallow granular aquifer. J. Contam. Hydrol. 116, 34–46. doi:10.1016/j.jconhyd.2010.05.006

Bi, Y., Hayes, K., 2013. Nano-FeS inhibits UO_2 reoxidation under varied oxic conditions. Environ. Sci. Technol. 48, 632–640. doi:10.1021/es4043353

Borggaard, O.K., Raben-Lange, B., Gimsing, A.L., Strobel, B.W., 2005. Influence of humic substances on phosphate adsorption by aluminium and iron oxides. Geoderma 127, 270–279. doi:10.1016/j.geoderma.2004.12.011

Boyd, G., Hirsch, R.M., 2002. Handbook of groundwater remediation using permeable reactive barries. Academic Press.

Cantrell, K.J., Kaplan, D.I., Wietsma, T.W., 1995. Zero-valent iron for the in situ remediation of selected metals in groundwater. J. Hazard. Mater. 42, 201–212. doi:10.1016/0304-3894(95)00016-N

Chan, Y.T., Kuan, W.H., Chen, T.Y., Wang, M.K., 2009. Adsorption mechanism of selenate and selenite on the binary oxide systems. Water Res. 43, 4412–20. doi:10.1016/j.watres.2009.06.056

Chang, H., Buettner, S.W., Seaman, J.C., Jaffé, P.R., Koster van Groos, P.G., Li, D., Peacock, A.D., Scheckel, K.G., Kaplan, D.I., 2014. Uranium Immobilization in an Iron-Rich Rhizosphere of a Native Wetland Plant from the Savannah River Site under Reducing Conditions. Environ. Sci. Technol. 48, 9270–8. doi:10.1021/es5015136

Chen, J., Kong, H., Wu, D., Chen, X., Zhang, D., Sun, Z., 2007. Phosphate immobilization from aqueous solution by fly ashes in relation to their composition. J. Hazard. Mater. 139, 293–300. doi:10.1016/j.jhazmat.2006.06.034

Chen, K.L., Mylon, S.E., Elimelech, M., 2006. Aggregation kinetics of alginate-coated hematite nanoparticles in monovalent and divalent electrolytes. Environ. Sci. Technol. 40, 1516–1523. doi:10.1021/es0518068

Chen, W., Huang, C., 2012. Surface adsorption of organoarsenic roxarsone and arsanilic acid on iron and aluminum oxides. J. Hazard. Mater. 227-228, 378–85. doi:10.1016/j.jhazmat.2012.05.078

Chien, S.H., Clayton, W.R., 1980. Application of Elovich Equation to the Kinetics of Phosphate Release and Sorption in Soils. Soil Sci. Soc. Am. J. 44, 265–268. doi:10.2136/sssaj1980.03615995004400020013x

Choy, C.C., Korfiatis, G.P., Meng, X., 2006. Removal of depleted uranium from contaminated soils. J. Hazard. Mater. 136, 53–60. doi:10.1016/j.jhazmat.2005.11.011

Clifford, D.A., Zhang, Z., 1994. Modifying ion exchange for combined removal of uranium and radium. J. Am. Water Work. Assoc. 86, 214–227.

Codling, E.E., Chaney, R.L., Sherwell, J., 2002. Poultry litter ash as a potential phosphorus source for agricultural crops. J. Environ. Qual. 31, 954–61.

Cortinas, I., Field, J.A., Kopplin, M., Garbarino, J.R., Gandolfi, A.J., Sierra-Alvarez, R., 2006. Anaerobic biotransformation of roxarsone and related N-substituted phenylarsonic acids. Environ. Sci. Technol. 40, 2951–7.

Crane, R. a., Dickinson, M., Popescu, I.C., Scott, T.B., 2011. Magnetite and zero-valent iron nanoparticles for the remediation of uranium contaminated environmental water. Water Res. 45, 2931–2942. doi:10.1016/j.watres.2011.03.012

Das, J., Das, D., Dash, G.P., Parida, K.M., 2002. Studies on Mg/Fe hydrotalcite-like-compound (HTlc) I. Removal of inorganic selenite (SeO3(2-)) from aqueous medium. J. Colloid Interface Sci. 251, 26–32. doi:10.1006/jcis.2002.8319

Dickinson, M., Scott, T.B., 2010. The application of zero-valent iron nanoparticles for the remediation of a uranium-contaminated waste effluent. J. Hazard. Mater. 178, 171–9. doi:10.1016/j.jhazmat.2010.01.060

Duc, M., Lefevre, G., Fedoroff, M., Jeanjean, J., Rouchaud, J.C., Monteil-Rivera, F., Dumonceau, J., Milonjic, S., 2003. Sorption of selenium anionic species on apatites and iron oxides from aqueous solutions. J. Environ. Radioact. 70, 61–72. doi:10.1016/S0265-931X(03)00125-5

Duval, J.S., Carson, J.M., Holman, P.B., Darnley, A.G., 2005. Terrestrial radioactivity and gamma-ray exposure in the United States and Canada: U.S. Geological Survey Open-File Report 2005-1413. Available online only.

EC, 2014. Report on critical raw materials for the EU: Report of the Ad hoc Working Group on defining critical raw materials. Eauropean Commision.

El-Shafey, E.I., 2007. Removal of Se(IV) from aqueous solution using sulphuric acid-treated peanut shell. J. Environ. Manage. 84, 620–7. doi:10.1016/j.jenvman.2007.03.021

Elzinga, E.J., Tang, Y., McDonald, J., DeSisto, S., Reeder, R.J., 2009. Macroscopic and spectroscopic characterization of selenate, selenite, and chromate adsorption at the solid-water interface of gamma-Al2O3. J. Colloid Interface Sci. 340, 153–9. doi:10.1016/j.jcis.2009.08.033

FDA, 2015. Arsenic-based Animal Drugs and Poultry. [WWW Document]. URL http://www.fda.gov/AnimalVeterinary/SafetyHealth/ProductSafetyInformation/ucm257540.htm

Feinstein, D.T., Guo, W.X., 2004. STANMOD: A suite of windows-based programs for evaluating solute transport. Ground Water 42, 482–487. doi:10.1111/j.1745-6584.2004.tb02615.x

Felton, G.K., Carr, L.E., Habersack, M.J., 2007. Nutrient fate and transport in surface runoff from poultry litter stock piles. Trans. ASABE 50, 183–192.

Fiedor, J.N., Bostick, W.D., Jarabek, R.J., Farrell, J., 1998. Understanding the Mechanism of Uranium Removal from Groundwater by Zero-Valent Iron Using X-ray Photoelectron Spectroscopy. Environ. Sci. Technol. 32, 1466–1473. doi:10.1021/es970385u

Francis, A., Dodge, C., 1998. Remediation of soils and wastes contaminated with uranium and toxic metals. Environ. Sci. Technol. 32, 3993–3998. doi:10.1021/es9803310

Garbarino, J.R., Bednar, A.J., Rutherford, D.W., Beyer, R.S., Wershaw, R.L., 2003. Environmental fate of roxarsone in poultry litter. I. Degradation of roxarsone during composting. Environ. Sci. Technol. 37, 1509–1514.

Gavrilescu, M., Pavel, L.V., Cretescu, I., 2009. Characterization and remediation of soils contaminated with uranium. J. Hazard. Mater. 163, 475–510. doi:10.1016/j.jhazmat.2008.07.103

Genz, A., Kornmüller, A., Jekel, M., 2004. Advanced phosphorus removal from membrane filtrates by adsorption on activated aluminium oxide and granulated ferric hydroxide. Water Res. 38, 3523–30. doi:10.1016/j.watres.2004.06.006

Goh, K.-H., Lim, T.-T., Dong, Z., 2008. Application of layered double hydroxides for removal of oxyanions: a review. Water Res. 42, 1343–68. doi:10.1016/j.watres.2007.10.043

Gong, Y., Liu, Y., Xiong, Z., Kaback, D., Zhao, D., 2012. Immobilization of mercury in field soil and sediment using carboxymethyl cellulose stabilized iron sulfide nanoparticles. Nanotechnology 23, 294007. doi:10.1088/0957-4484/23/29/294007

Gong, Y., Liu, Y., Xiong, Z., Zhao, D., 2014. Immobilization of mercury by carboxymethyl cellulose stabilized iron sulfide nanoparticles: reaction mechanisms and effects of stabilizer and water chemistry. Environ. Sci. Technol. 48, 3986–3994. doi:10.1021/es404418a

Gonzalez, C.M., Hernandez, J., Parsons, J.G., Gardea-Torresdey, J.L., 2010. A study of the removal of selenite and selenate from aqueous solutions using a magnetic iron/manganese oxide nanomaterial and ICP-MS. Microchem. J. 96, 324–329. doi:10.1016/j.microc.2010.05.005

Gonzalez, C.M., Hernandez, J., Peralta-Videa, J.R., Botez, C.E., Parsons, J.G., Gardea-Torresdey, J.L., 2012. Sorption kinetic study of selenite and selenate onto a high and low pressure aged iron oxide nanomaterial. J. Hazard. Mater. 211-212, 138–45. doi:10.1016/j.jhazmat.2011.08.023

Gu, B., Liang, L., Dickey, M.J., Yin, X., Dai, S., 1998. Reductive precipitation of uranium(VI) by zero-valent iron. Environ. Sci. Technol. 32, 3366–3373. doi:10.1021/es980010o

Gu, B., Wu, W., Ginder-Vogel, M., 2005. Bioreduction of uranium in a contaminated soil column. Enviromental Sci. Technol. 39, 4841–4847. doi:10.1021/es050011y

Hamilton, S.J., 2004. Review of selenium toxicity in the aquatic food chain. Sci. Total Environ. 326, 1–31. doi:10.1016/j.scitotenv.2004.01.019

Haudin, C.S., Renault, P., Hallaire, V., Leclerc-Cessac, E., Staunton, S., 2007. Effect of aeration on mobility of selenium in columns of aggregated soil as influenced by straw amendment and tomato plant growth. Geoderma 141, 98–110. doi:10.1016/j.geoderma.2007.05.005

He, F., Zhang, M., Qian, T., Zhao, D., 2009. Transport of carboxymethyl cellulose stabilized iron nanoparticles in porous media: column experiments and modeling. J. Colloid Interface Sci. 334, 96–102. doi:10.1016/j.jcis.2009.02.058

He, F., Zhao, D., 2005. Preparation and characterization of a new class of starch-stabilized bimetallic nanoparticles for degradation of chlorinated hydrocarbons in water. Environ. Sci. Technol. 39, 3314–20. doi:10.1021/es048743y

He, F., Zhao, D., 2007. Manipulating the size and dispersibility of zerovalent iron nanoparticles by use of carboxymethyl cellulose stabilizers. Environ. Sci. Technol. 41, 6216–6221. doi:10.1021/es0705543

He, F., Zhao, D., 2008. Hydrodechlorination of trichloroethene using stabilized Fe-Pd nanoparticles: Reaction mechanism and effects of stabilizers, catalysts and reaction conditions. Appl. Catal. B Environ. 84, 533–540. doi:10.1016/j.apcatb.2008.05.008

He, F., Zhao, D., Liu, J., Roberts, C.B., 2007. Stabilization of Fe-Pd nanoparticles with sodium carboxymethyl cellulose for enhanced transport and dechlorination of trichloroethylene in soil and groundwater. Ind. Eng. Chem. Res. 46, 29–34.

He, F., Zhao, D., Paul, C., 2010. Field assessment of carboxymethyl cellulose stabilized iron nanoparticles for in situ destruction of chlorinated solvents in source zones. Water Res. 44, 2360–70. doi:10.1016/j.watres.2009.12.041

He, Z., Minteer, S.D., Angenent, L.T., 2005. Electricity Generation from Artificial Wastewater Using an Upflow Microbial Fuel Cell. Environ. Sci. Technol. 39, 5262–5267. doi:10.1021/es0502876

He, Z., Senwo, Z.N., Mankolo, R.N., Honeycutt, C.W., 2006. Phosphorus fractions in poultry litter characterized by sequential fractionation coupled with phosphatase hydrolysis 4, 304–312.

Hee, S.M., Komlos, J., Jaffé, P.R., 2007. Uranium reoxidation in previously bioreduced sediment by dissolved oxygen and nitrate. Environ. Sci. Technol. 41, 4587–4592. doi:10.1021/es063063b

Hileman, B., 2007. Arsenic In Chicken Production. Chem. Eng. News 85, 34–35.

Ho, Y.S., 2006. Review of second-order models for adsorption systems. J. Hazard. Mater. 136, 681–9. doi:10.1016/j.jhazmat.2005.12.043

Ho, Y.S., McKay, G., 2009. Application of Kinetic Models to the Sorption of Copper(II) on to Peat. Adsorpt. Sci. Technol. 20, 797–815. doi:10.1260/026361702321104282

Hu, J., Tong, Z., Hu, Z., Chen, G., Chen, T., 2012. Adsorption of roxarsone from aqueous solution by multi-walled carbon nanotubes. J. Colloid Interface Sci. 377, 355–61. doi:10.1016/j.jcis.2012.03.064

Hu, Y., Li, Q., Lee, B., Jun, Y., 2013. Aluminum affects heterogeneous Fe(III) (Hydr)oxide nucleation, growth, and ostwald ripening. Environ. Sci. Technol. doi:dx.doi.org/10.1021/es403777w

Huff, W.E., Malone, G.W., Chaloupka, G.W., 1984. Effect of litter treatment on broiler performance and certain litter quality parameters. Poult. Sci. 63, 2167–2171. doi:10.3382/ps.0632167

Hunger, S., Cho, H., Sims, J.T., Sparks, D.L., 2004. Direct speciation of phosphorus in alum-amended poultry litter: solid-state 31P NMR investigation. Environ. Sci. Technol. 38, 674–681. doi:10.1021/es034755s

Hyun, S.P., Davis, J. a., Sun, K., Hayes, K.F., 2012. Uranium(VI) reduction by iron(II) monosulfide mackinawite. Environ. Sci. Technol. 46, 3369–3376. doi:10.1021/es203786p

Igwe, J.C., Nnorom, I.C., Gbaruko, B.C., 2005. Kinetics of radionuclides and heavy metals behaviour in soils : Implications for plant growth 4, 1541–1547.

Jackson, B.P., Bertsch, P.M., 2001. Determination of arsenic speciation in poultry wastes by IC-ICP-MS. Environ. Sci. Technol. 35, 4868–73.

Jackson, B.P., Bertsch, P.M., Cabrera, M.L., Camberato, J.J., Seaman, J.C., Wood, C.W., 1999. Trace element speciation in poultry litter. J. Environ. Qual. 32, 535–40.

Jackson, B.P., Ranville, J.F., Bertsch, P.M., Sowder, A.G., 2005. Characterization of Colloidal and Humic-Bound Ni and U in the "Dissolved" Fraction of Contaminated Sediment Extracts. Environ. Sci. Technol. 39, 2478–2485. doi:10.1021/es0485208

Jackson, B.P., Seaman, J.C., Bertsch, P.M., 2006. Fate of arsenic compounds in poultry litter upon land application. Chemosphere 65, 2028–34. doi:10.1016/j.chemosphere.2006.06.065

Jovanovic, S. V, Pan, P., Wong, L., 2012. Bioaccessibility of uranium in soil samples from Port Hope, Ontario, Canada. Environ. Sci. Technol. 46, 9012–8. doi:10.1021/es3021217

Kelleher, B., Leahy, J., Henihan, A., O'Dwyer, T., Sutton, D., Leahy, M., 2002. Advances in poultry litter disposal technology – a review. Bioresour. Technol. 83, 27–36. doi:10.1016/S0960-8524(01)00133-X

Kelley, M.E., Brauning, S.E., Schoof, R.A., Ruby, M. V, 2002. Assessing Oral Bioavailability of Metals in Soil. Battelle Press, 505 King Avenue, Columbus, OH 43201-2693, USA.

Kepner, R.L.J., Pratt, J.R., 1994. Use of fluorochromes for direct enumeration of total bacteria in environmental samples: past and present. Microbiol. Mol. Biol. Rev. 58, 603–615.

Klimkova, S., Cernik, M., Lacinova, L., Filip, J., Jancik, D., Zboril, R., 2011. Zero-valent iron nanoparticles in treatment of acid mine water from in situ uranium leaching. Chemosphere 82, 1178–84. doi:10.1016/j.chemosphere.2010.11.075

Kocur, C.M., Chowdhury, A.I., Sakulchaicharoen, N., Boparai, H.K., Weber, K.P., Sharma, P., Krol, M.M., Austrins, L., Peace, C., Sleep, B.E., O'Carroll, D.M., 2014. Characterization of nZVI mobility in a field scale test. Environ. Sci. Technol. 48, 2862–2869. doi:10.1021/es4044209

Li, H., Xin, H., Liang, Y., Burns, R.T., 2008. Reduction of ammonia emissions from stored laying hen manure through topical application of zeolite, Al+Clear, Ferix-3, or poultry litter treatment. J. Appl. Poult. Res. 17, 421–431. doi:10.3382/japr.2007-00076

Li, X., Wu, J., Liao, J., Zhang, D., Yang, J., Feng, Y., Zeng, J., Wen, W., Yang, Y., Tang, J., Liu, N., 2013. Adsorption and desorption of uranium (VI) in aerated zone soil. J. Environ. Radioact. 115, 143–50. doi:10.1016/j.jenvrad.2012.08.006

Liang, L., Yang, W., Guan, X., Li, J., Xu, Z., Wu, J., Huang, Y., Zhang, X., 2013. Kinetics and mechanisms of pH-dependent selenite removal by zero valent iron. Water Res. 47, 5846–55. doi:10.1016/j.watres.2013.07.011

Liang, Q., Zhao, D., Qian, T., Freeland, K., Feng, Y., 2012. Effects of stabilizers and water chemistry on arsenate sorption by polysaccharide-stabilized magnetite nanoparticles. Ind. Eng. Chem. Res. 51, 2407–2418. doi:10.1021/ie201801d

Liu, R., Frost, R.L., Martens, W.N., 2009. Absorption of the selenite anion from aqueous solutions by thermally activated layered double hydroxide. Water Res. 43, 1323–9. doi:10.1016/j.watres.2008.12.030

Liu, R., Zhao, D., 2007a. In situ immobilization of Cu(II) in soils using a new class of iron phosphate nanoparticles. Chemosphere 68, 1867–76. doi:10.1016/j.chemosphere.2007.03.010

Liu, R., Zhao, D., 2007b. Reducing leachability and bioaccessibility of lead in soils using a new class of stabilized iron phosphate nanoparticles. Water Res. 41, 2491–502. doi:10.1016/j.watres.2007.03.026

Long, F., Gong, J.L., Zeng, G.M., Chen, L., Wang, X.Y., Deng, J.H., Niu, Q.Y., Zhang, H.Y., Zhang, X.R., 2011. Removal of phosphate from aqueous solution by magnetic Fe–Zr binary oxide. Chem. Eng. J. 171, 448–455. doi:10.1016/j.cej.2011.03.102

Lorentzen, E.M.L., Kingston, H.M., 1996. Comparison of microwave-assisted and conventional leaching using EPA method 3050B. Anal. Chem. 68, 4316–4320. doi:10.1021/ac960553l

Lovely, D.R., Philips, E.J.P., Gorby, Y.A., Landa, E.R., 1991. Microbial reduction of uranium. Nature 350, 413–416.

Loyo, R.L.D.A., Nikitenko, S.I., Scheinost, A.C., Simonoff, M., 2008. Immobilization of selenite on Fe3O4 and Fe/Fe3C ultrasmall particles. Environ. Sci. Technol. 42, 2451–6. doi:10.1021/es702579w

Lǚ, J., Liu, H., Liu, R., Zhao, X., Sun, L., Qu, J., 2013. Adsorptive removal of phosphate by a nanostructured Fe–Al–Mn trimetal oxide adsorbent. Powder Technol. 233, 146–154. doi:10.1016/j.powtec.2012.08.024

Luengo, C., Brigante, M., Antelo, J., Avena, M., 2006. Kinetics of phosphate adsorption on goethite: Comparing batch adsorption and ATR-IR measurements. J. Colloid Interface Sci. 300, 511–518. doi:10.1016/j.jcis.2006.04.015

Machida, M., Kikuchi, Y., Aikawa, M., Tatsumoto, H., 2004. Kinetics of adsorption and desorption of Pb(II) in aqueous solution on activated carbon by two-site adsorption model. Colloids Surfaces A Physicochem. Eng. Asp. 240, 179–186. doi:10.1016/j.colsurfa.2004.04.046

Maier, K.J., Foe, C.G., Knight, A.W., 1993. Comparative toxicity of selenate, selenite, seleno-DL-cystine to Daphnia magna. Environ. Toxicol. Chem. 12, 755–763. doi:10.1002/etc.5620120417

Maity, D., Agrawal, D.C., 2007. Synthesis of iron oxide nanoparticles under oxidizing environment and their stabilization in aqueous and non-aqueous media. J. Magn. Magn. Mater. 308, 46–55. doi:10.1016/j.jmmm.2006.05.001

Martínez, M., Giménez, J., de Pablo, J., Rovira, M., Duro, L., 2006. Sorption of selenium(IV) and selenium(VI) onto magnetite. Appl. Surf. Sci. 252, 3767–3773. doi:10.1016/j.apsusc.2005.05.067

Mavrov, V., Stamenov, S., Todorova, E., Chmiel, H., Erwe, T., 2006. New hybrid electrocoagulation membrane process for removing selenium from industrial wastewater. Desalination 201, 290–296. doi:10.1016/j.desal.2006.06.005

Mclean, J.E., Bledsoe, B.E., 1992. Ground Water Issue Behavior of Metals in Soils. EPA/540/S-92/018.

Mishra, R.R., Prajapati, S., Das, J., Dangar, T.K., Das, N., Thatoi, H., 2011. Reduction of selenite to red elemental selenium by moderately halotolerant Bacillus megaterium strains isolated from Bhitarkanika mangrove soil and characterization of reduced product. Chemosphere 84, 1231–7. doi:10.1016/j.chemosphere.2011.05.025

Missana, T., Alonso, U., Scheinost, a. C., Granizo, N., García-Gutiérrez, M., 2009. Selenite retention by nanocrystalline magnetite: Role of adsorption, reduction and dissolution/co-precipitation processes. Geochim. Cosmochim. Acta 73, 6205–6217. doi:10.1016/j.gca.2009.07.005

Moore, P.A., Daniel, T.C., Gilmour, J.T., Shreve, B.R., Edwards, D.R., Wood, B.H., 1998. Decreasing metal runoff from poultry litter with aluminum sulfate. J. Environ. Qual. 27, 92–99. doi:10.2134/jeq1998.00472425002700010014x

Moore, P.A., Miller, D.M., 1994. Decreasing phosphorus solubility in poultry litter with aluminum, calcium, and iron amendments. J. Environ. Qual. 23, 325–330. doi:10.2134/jeq1994.00472425002300020016x

Morrison, J.L., 1967. Distribution of Arsenic from Poultry Litter in Broiler Chickens, Soil, and Crops 1965–1967.

Moyes, L.N., Parkman, R.H., Charnock, J.M., Vaughan, D.J., Livens, F.R., Hughes, C.R., Braithwaite, A., 2000. Uranium Uptake from Aqueous Solution by Interaction with Goethite, Lepidocrocite, Muscovite, and Mackinawite: An X-ray Absorption Spectroscopy Study. Environ. Sci. Technol. 34, 1062–1068. doi:10.1021/es990703k

Mulligan, C.N., Yong, R.N., Gibbs, B.F., 2001. Remediation technologies for metal-contaminated soils and groundwater: an evaluation. Eng. Geol. 60, 193–207. doi:10.1016/S0013-7952(00)00101-0

Noubactep, C., Meinrath, G., Dietrich, P., Merkel, B., 2003. Mitigating uranium in groundwater: Prospects and limitations. Environ. Sci. Technol. 37, 4304–4308. doi:10.1021/es034296v

O'Loughlin, E.J., Kelly, S.D., Cook, R.E., Csencsits, R., Kemner, K.M., 2003. Reduction of Uranium(VI) by Mixed Iron(II)/Iron(III) Hydroxide (Green Rust): Formation of UO2 Nanoparticles. Environ. Sci. Technol. 37, 721–727. doi:10.1021/es0208409

Oguz, E., 2004. Removal of phosphate from aqueous solution with blast furnace slag. J. Hazard. Mater. 114, 131–7. doi:10.1016/j.jhazmat.2004.07.010

Onken, B.M., Hossner, L.R., 1996. Determination of Arsenic Species in Soil Solution under Flooded Conditions. Soil Sci Soc Am J 60, 1385–1392.

Parida, K., Gorai, B., Das, N., Rao, S., 1997. Studies on ferric oxide hydroxides. J. Colloid Interface Sci. 185, 355–62. doi:10.1006/jcis.1996.4522

Peak, D., 2006. Adsorption mechanisms of selenium oxyanions at the aluminum oxide/water interface. J. Colloid Interface Sci. 303, 337–45. doi:10.1016/j.jcis.2006.08.014

Perrin, S., Pijolat, M., Valdivieso, F., Soustelle, M., 2001. Kinetic study of the effect of a sudden change in temperature during the reduction of U3O8 into UO2 by hydrogen. Solid State Ionics 141-142, 109–115. doi:10.1016/S0167-2738(01)00729-9

Phillips, E.P., Landa, E., Lovley, D., 1995. Remediation of uranium contaminated soils with bicarbonate extraction and microbial U(VI) reduction. J. Ind. Microbiol. 14, 203–207. doi:10.1007/BF01569928

PIJOLAT, M., 1997. Reduction of uranium oxide U3O8 to UO2 by hydrogen. Solid State Ionics 101-103, 931–935. doi:10.1016/S0167-2738(97)00385-8

Polyzopoulos, N.A., Keramidas, V.Z., Pavlatou, A., 1986. On the limitations of the simplified Elovich equation in describing the kinetics of phosphate sorption and release from soils. J. Soil Sci. 37, 81–87. doi:10.1111/j.1365-2389.1986.tb00009.x

Popescu, I.-C., Filip, P., Humelnicu, D., Humelnicu, I., Scott, T.B., Crane, R.A., 2013. Removal of uranium (VI) from aqueous systems by nanoscale zero-valent iron particles suspended in carboxy-methyl cellulose. J. Nucl. Mater. 443, 250–255. doi:10.1016/j.jnucmat.2013.07.018

Rai, D., Felmy, a. R., Ryan, J.L., 1990. Uranium (IV) hydrolysis constants and solubility product of U02.xH2O(am). Inorg. Chem. 29, 260–264. doi:10.1021/ic00327a022

Rao, G.R., Mishra, B.G., 2005. A comparative UV−vis-diffuse reflectance study on the location and interaction of cerium ions in Al- and Zr-pillared montmorillonite clays. Mater. Chem. Phys. 89, 110–115. doi:10.1016/j.matchemphys.2004.08.037

Raven, K.P., Jain, A., Loeppert, R.H., 1998. Arsenite and Arsenate Adsorption on Ferrihydrite: Kinetics, Equilibrium, and Adsorption Envelopes. Environ. Sci. Technol. 32, 344–349. doi:10.1021/es970421p

Riba, O., Scott, T.B., Vala Ragnarsdottir, K., Allen, G.C., 2008. Reaction mechanism of uranyl in the presence of zero-valent iron nanoparticles. Geochim. Cosmochim. Acta 72, 4047–4057. doi:10.1016/j.gca.2008.04.041

Ristić, M., De Grave, E., Musić, S., Popović, S., Orehovec, Z., 2007. Transformation of low crystalline ferrihydrite to α-Fe2O3 in the solid state. J. Mol. Struct. 834-836, 454–460. doi:10.1016/j.molstruc.2006.10.016

Rowland, R.C., Stephens, D.W., Waddell, B., Naftz, D.L., 2003. Selenium contamination and remediation at Stewart Lake saterfowl management area and Ashley Creek, Middle Green River Basin, Utah. USGS Fact Sheet FS–031–03.

Savitzky, A., Golay, M.J.E., 1964. Smoothing and Differentiation of Data by Simplified Least Squares Procedures. Anal. Chem. 36, 1627–1639. doi:10.1021/ac60214a047

Scofield, J.H., 1973. Lawrence Livermore Laboratory Report No. UCRL-51326, unpublished.

Scott, T.B., Allen, G.C., Heard, P.J., Randell, M.G., 2005. Reduction of U(VI) to U(IV) on the surface of magnetite. Geochim. Cosmochim. Acta 69, 5639–5646. doi:10.1016/j.gca.2005.07.003

Skorupa, J.P., 1998. Selenium poisoning of fish and wildlife in nature: lessons from twelve real-world examples, in: WT, F., RA, E. (Eds.), Environmental Chemistry of Selenium. Marcel Dekker, New York, pp. 315–354.

Smith, V.H., Tilman, G.D., Nekola, J.C., 1999. Eutrophication: impacts of excess nutrient inputs on freshwater, marine, and terrestrial ecosystems. Environ. Pollut. 100, 179–196. doi:10.1016/S0269-7491(99)00091-3

Spallholz, J.E., Hoffman, D.J., 2002. Selenium toxicity: cause and effects in aquatic birds. Aquat. Toxicol. 57, 27–37. doi:10.1016/S0166-445X(01)00268-5

Stolz, J.F., Perera, E., Kilonzo, B., Kail, B., Crable, B., Fisher, E., Ranganathan, M., Wormer, L., Basu, P., 2007. Biotransformation of 3-nitro-4-hydroxybenzene arsonic acid (roxarsone) and release of inorganic arsenic by Clostridium species. Environ. Sci. Technol. 41, 818–23.

Szlachta, M., Gerda, V., Chubar, N., 2012. Adsorption of arsenite and selenite using an inorganic ion exchanger based on Fe-Mn hydrous oxide. J. Colloid Interface Sci. 365, 213–21. doi:10.1016/j.jcis.2011.09.023

Torres, J., Pintos, V., Domínguez, S., Kremer, C., Kremer, E., 2010. Selenite and selenate speciation in natural waters: interaction with divalent metal ions. J. Solution Chem. 39, 1–10. doi:10.1007/s10953-009-9491-3

Trussell, R.R., Trussell, A., Kreft, P., 1980. Selenium removal from ground water using activated alumina. U.S. Environmental Protection Agency, Number: 600280153.

Tufenkji, N., Elimelech, M., 2004. Deviation from the classical colloid filtration theory in the presence of repulsive DLVO interactions. Langmuir 20, 10818–28. doi:10.1021/la0486638

UNSC, 1993. United Nations Scientific Committee on the Effects of Atomic Radiation. Sources and effects of ionizing radiation: Report to the General Assembly, with Scientific Annexes. United Nations. ISBN 92-1-142200-0.

USDA, 2014. Broiler production by state, 2013. [WWW Document]. URL http://www.nass.usda.gov/Charts_and_Maps/Poultry/brlmap.asp

USEIA, 2014. Domestic Uranium Production Report – Quarterly, - 4th Quarter 2013 [WWW Document]. URL http://www.eia.gov/uranium/production/quarterly/

USEPA, 1996. Acid digestion of sediments, sludges, and soils, Method 3050B, in Wastes-Hazardous Waste-Test methods. Washington, DC.

USEPA, 2009. National primary drinking water regulations, EPA 816-F-09-004.

USEPA, 2011. Drinking water contaminants: List of contaminants & their MCLs. [WWW Document]. URL http://water.epa.gov/drink/contaminants/index.cfm#List. Accessed 8 February 2011.

USFDA, 2011. Questions and Answers Regarding 3-Nitro (Roxarsone).

USGS, 2008. Selenium in Counties of the Conterminous States.

Voegelin, A., Hug, S.J., 2003. Catalyzed oxidation of arsenic(III) by hydrogen peroxide on the surface of ferrihydrite: an in situ ATR-FTIR study. Environ. Sci. Technol. 37, 972–978. doi:10.1021/es025845k

Wan, J., Tokunaga, T.K., Brodie, E., Wang, Z., Zheng, Z., Herman, D., Hazen, T.C., Firestone, M.K., Sutton, S.R., 2005. Reoxidation of Bioreduced Uranium under Reducing Conditions. Environ. Sci. Technol. 39, 6162–6169. doi:10.1021/es048236g

Wang, Y., Frutschi, M., Suvorova, E. Phrommavanh, V. Descostes, M., Osman, A.A.A., Geipel, G., Bernier-Latmani, R., 2013. Mobile uranium(IV)-bearing colloids in a mining-impacted wetland. Nat. Commun. doi:10.1038/ncomms3942

Wersin, P., Jr, M.F.H., Persson, P.E.R., Redden, G., Leckie, J., Harris, D.W., Stanford, G., 1994. Interaction between aqueous uranium (VI) and sulfide minerals: Spectroscopic evidence for sorption and reduction. Geochim. Cosmochim. Acta 58, 2829–2843.

WNA, 2014. World Uranium Mining Production [WWW Document]. URL http://www.world-nuclear.org/info/Nuclear-Fuel-Cycle/Mining-of-Uranium/World-Uranium-Mining-Production/

Wood, B.H., Wood, C.W., Yoo, K.H., Yoon, K.S., Delaneya, D.P., 1996. Nutrient accumulation and nitrate leaching under broiler litter amended corn fields. Commun. Soil Sci. Plant Anal. 27, 2875–2894. doi:10.1080/00103629609369747

Wu, D., Zhang, B., Li, C., Zhang, Z., Kong, H., 2006. Simultaneous removal of ammonium and phosphate by zeolite synthesized from fly ash as influenced by salt treatment. J. Colloid Interface Sci. 304, 300–6. doi:10.1016/j.jcis.2006.09.011

Wu, W., Carley, J., Gentry, T., Ginder-Vogel, M. a, Fienen, M., Mehlhorn, T., Yan, H., Caroll, S., Pace, M.N., Nyman, J., Luo, J., Gentile, M.E., Fields, M.W., Hickey, R.F., Gu, B., Watson, D., Cirpka, O. a, Zhou, J., Fendorf, S., Kitanidis, P.K., Jardine, P.M., Criddle, C.S., 2006. Pilot-scale in situ bioremedation of uranium in a highly contaminated aquifer. 2. Reduction of u(VI) and geochemical control of u(VI) bioavailability. Environ. Sci. Technol. 40, 3986–95.

Xie, S., Zhang, C., Zhou, X., Yang, J., Zhang, X., Wang, J., 2009. Removal of uranium (VI) from aqueous solution by adsorption of hematite. J. Environ. Radioact. 100, 162–6. doi:10.1016/j.jenvrad.2008.09.008

Xie, W., Liang, Q., Qian, T., Zhao, D., 2015. Immobilization of selenite in soil and groundwater using stabilized Fe-Mn binary oxide nanoparticles. Water Res. 70, 485–494. doi:10.1016/j.watres.2014.12.028

Xu, Y., Zhao, D., 2007. Reductive immobilization of chromate in water and soil using stabilized iron nanoparticles. Water Res. 41, 2101–8. doi:10.1016/j.watres.2007.02.037

Yan, L., Xu, Y., Yu, H., Xin, X., Wei, Q., Du, B., 2010. Adsorption of phosphate from aqueous solution by hydroxy-aluminum, hydroxy-iron and hydroxy-iron-aluminum pillared bentonites. J. Hazard. Mater. 179, 244–50. doi:10.1016/j.jhazmat.2010.02.086

Yan, S., Hua, B., Bao, Z., Yang, J., Liu, C., Deng, B., 2010. Uranium(VI) removal by nanoscale zerovalent iron in anoxic batch systems. Environ. Sci. Technol. 44, 7783–9. doi:10.1021/es9036308

Zeng, L., Li, X., Liu, J., 2004. Adsorptive removal of phosphate from aqueous solutions using iron oxide tailings. Water Res. 38, 1318–26. doi:10.1016/j.watres.2003.12.009

Zhang, G., Liu, H., Liu, R., Qu, J., 2009. Removal of phosphate from water by a Fe-Mn binary oxide adsorbent. J. Colloid Interface Sci. 335, 168–74. doi:10.1016/j.jcis.2009.03.019

Zhang, G., Qu, J., Liu, H., Liu, R., Li, G., 2007a. Removal mechanism of As(III) by a novel Fe-Mn binary oxide adsorbent: oxidation and sorption. Environ. Sci. Technol. 41, 4613–9. doi:10.1021/es063010u

Zhang, G., Qu, J., Liu, H., Liu, R., Wu, R., 2007b. Preparation and evaluation of a novel Fe-Mn binary oxide adsorbent for effective arsenite removal. Water Res. 41, 1921–8. doi:10.1016/j.watres.2007.02.009

Zhang, Y., Yang, M., Dou, X.M., He, H., Wang, D.S., 2005. Arsenate adsorption on an Fe-Ce bimetal oxide adsorbent: role of surface properties. Environ. Sci. Technol. 39, 7246–53. doi:10.1021/es050775d

Zhao, D., Sengupta, A.K., 1998. Ultimate removal of phosphate from wastewater using a new class of polymeric ion exchangers. Water Res. 32, 1613–1625. doi:10.1016/S0043-1354(97)00371-0

Zhao, D., Sengupta, A.K., 2000. Ligand separation with a copper(II)-loaded polymeric ligand. Ind. Eng. Chem. Res. 39, 455–462. doi:10.1021/ie990740k

Zhao, D., Yang, X., Zhang, H., Chen, C., Wang, X., 2010. Effect of environmental conditions on Pb(II) adsorption on β-MnO2. Chem. Eng. J. 164, 49–55. doi:10.1016/j.cej.2010.08.014

Zhou, P., Gu, B., 2005. Extraction of oxidized and reduced forms of uranium from contaminated soils: effects of carbonate concentration and pH. Environ. Sci. Technol. 39, 4435–40.

Appendix 1

Removal of Chlorate from Water Using Various Classes of Ion Exchangers

Wenbo Xie[a,b], Rebecca Clay[a], and Dongye Zhao[a,c,*]

[a] *Environmental Engineering Program, Department of Civil Engineering, Auburn University, Auburn, AL 36849, USA*

[b] *College of Fisheries and Life Science, Shanghai Ocean University, Shanghai, 201306, PR China*

[c] *Institute of Environmental Science, Taiyuan University of Science and Technology, Taiyuan, Shanxi 030024, PR China*

*Corresponding author. Phone: 334-844-6277; Fax: 334-844-6290; E-mail: zhaodon@auburn.edu

Abstract

Chlorate, an oxyanion associated with various forms of chlorine disinfection, is a likely candidate for future U.S. regulation in drinking water. The primary route of environmental exposure to chlorate is through drinking water disinfection, and specifically through disinfection with bulk sodium hypochlorite. While future regulatory thresholds are unknown, the U.S. EPA has established a chlorate Health Reference Level (HRL) of 210 μg/L. There are numerous mechanisms for chlorate formation, but it is usually a very fast reaction. Furthermore, chlorate levels are inherently tied to chlorite and perchlorate, other disinfection byproducts currently regulated or pending national regulation. Bench-scale testing results are presented for five classes of ion exchange resins and for synthesized ZVI particles, for chlorate removal with an initial concentration of 1,000 μg/L. The kinetics of both technologies are compared. Ultimately both show promise for effective and rapid chlorate removal. Ion exchange resins performed effectively in drinking water; ZVI performed effectively in brine solutions. The challenges of each approach and limitations of the bench-scale testing, which require further evaluation, are summarized in this paper.

Keywords

Chlorate, Drinking water, Sorption, Ion exchange resin, ZVI

Appendix 2

Oxidation of Three Alkylated PAHs by Surface Level Ozone: Effects of Dispersant

Wenbo Xie[a,b] and Dongye Zhao[a,c,*]

[a] *Environmental Engineering Program, Department of Civil Engineering, Auburn University, Auburn, AL 36849, USA*

[b] *College of Fisheries and Life Science, Shanghai Ocean University, Shanghai, 201306, PR China*

[c] *Institute of Environmental Science, Taiyuan University of Science and Technology, Taiyuan, Shanxi 030024, PR China*

*Corresponding author. Phone: 334-844-6277; Fax: 334-844-6290; E-mail: zhaodon@auburn.edu

Abstract

This work presented the oxidation of three alkylated PAHs (i.e., 1-methylnaphthalene, 1-methyfluorene, and 9, 10-dimethylanthracene) by surface level ozone (86-200 ppb) in seawater and the effects of a popular oil dispersant (Corexit EC9500A) on the ozonation. The volatilization and ozonation rates of PAHs in the seawater were compared under same experiment conditions using the first-order kinetic model and the trend was observed as: 1-methylnaphthalene > 1-methyfluorene > and 9, 10-dimethylanthracene. The ozonation of PAHs favored alkaline pH. The presence of dispersant enhanced the ozonation of PAHs in all cases. Mechanistic studies indicated that direct ozonation by ozone molecule was the dominant oxidation mechanism in the absence of dispersant, and the presence of dispersant could increase the oxidation of PAHs by increasing the activity of indirect ozonation (i.e., hydroxyl radicals). The degradation pathways of the PAHs were also studied in this paper. To our knowledge, this is the first study of PAHs ozonation by surface level ozone.

Keywords

Ozonation, Alkylated PAHs, Surface level ozone, Dispersant, Mechanism

Appendix 3

**ELSEVIER LICENSE
TERMS AND CONDITIONS**

Jul 09, 2015

This is a License Agreement between Wenbo Xie ("You") and Elsevier ("Elsevier") provided by Copyright Clearance Center ("CCC"). The license consists of your order details, the terms and conditions provided by Elsevier, and the payment terms and conditions.

All payments must be made in full to CCC. For payment instructions, please see information listed at the bottom of this form.

Supplier	Elsevier Limited The Boulevard,Langford Lane Kidlington,Oxford,OX5 1GB,UK
Registered Company Number	1982084
Customer name	Wenbo Xie
Customer address	Auburn University
	AUBURN UNIVERSITY, AL 36849
License number	3665140335597
License date	Jul 09, 2015
Licensed content publisher	Elsevier
Licensed content publication	Water Research
Licensed content title	Immobilization of selenite in soil and groundwater using stabilized Fe–Mn binary oxide nanoparticles
Licensed content author	Wenbo Xie,Qiqi Liang,Tianwei Qian,Dongye Zhao
Licensed content date	1 March 2015
Licensed content volume number	70
Licensed content issue number	n/a
Number of pages	10
Start Page	485
End Page	494
Type of Use	reuse in a thesis/dissertation
Portion	full article
Format	both print and electronic
Are you the author of this Elsevier article?	Yes
Will you be translating?	No
Title of your thesis/dissertation	Removal or Immobilization of Radionuclides and Trace-metals in Water, Soil and Poultry Litter Using Stabilized Nanoparticles